# THE DEFORMATION AND BREAKUP OF LIQUID DROPS IN AN EXTENSIONAL FLOW FIELD, AND THE INSTABILITY OF STATIONARY AND EXTENDING LIQUID THREADS

---

An Abstract of a Thesis

Presented to

the Faculty of the Department of Chemical Engineering

University of Houston

---

In Partial Fulfillment

of the Requirements for the Degree

Master of Science in Chemical Engineering

---

by

Kuo-Liang Yu

December, 1974

ACKNOWLEDGEMENTS

I would like to express my sincere gratitude to my adviser, Dr. Raymond W. Flumerfelt, for his consistent guidance, support, and encouragement throughout the whole course of this thesis, especially for his patience in reading and verifying the first draft of this thesis. The gratitudes are extended to other committee in the oral presentation of this thesis for the enthusiasm and generosity in giving their valuable suggestions.

Sincere acknowledgements are also due to Mr. Roy M. Priest and Mr. Payne for their suggestion and assistance in constructing the experimental apparatus.

A very special gratitude should be given to my mother and my wife for their sacrifice, patience, and incomparable spiritual support which have made the completion of this thesis possible.

Finally, I am very glad to dedicate this thesis to my mother and my wife with all my love.

ABSTRACT

This work involves an experimental investigation of the deformation and breakup of liquid drops as well as the instability of liquid threads (both Newtonian and viscoelastic) in an extensional flow field.

For Newtonian systems, it is found that Taylor's first order theory works quite well over a wider range of deformation than expected, and Chaffey and Brenner's second order theory does not provide a better approximation than Taylor's theory. It is also concluded that Barthes and Acrivos theory is good for systems with viscosity ratio, defined as $\lambda = \eta_D/\eta_C$ (where $\eta_D$ and $\eta_C$ are the viscosities of dispersed phase and continuous phase), $\lambda \geqslant 0.7$, but fails to describe deformation for systems with small $\lambda$. The pointed end phenomenon associated with Newtonian drops with $\lambda \leqslant 0.5$ was also observed for viscoelastic drops, however in the latter it was observed when $\lambda \leqslant 11.2$.

The breakup criterion for Newtonian drops is established and expressed in terms of two dimensionless groups: $E_C = \bar{G}_C a \eta_C/\sigma$ and $\lambda = \eta_D/\eta_C$, where $\eta_D$ and $\eta_C$ are the dispersed and the continuous viscosities, $\bar{G}_C/2$ is the extensional rate at breakup, a is the drop radius and $\sigma$ is the interfacial tension. The range of viscosity ratio within which drop breakup can occur in a plane hyperbolic flow field is wider than that in a simple shear flow field, and the ratio of $E_C$ in plane hyperbolic flow fields and $E_C$ in simple shear flow fields is only about 1/3 at $\lambda = 1$, and becomes smaller as $\lambda$ takes values different from 1. As for the breakup of viscoelastic drops, $E_C$ is found to increase with Deborah number up to about 10, and

then level off gradually as Deborah number increases further.

The bounds of validity of four limiting equations of Tomotika's general theory for stationary liquid threads have been obtained in terms of the appropriate dimensionless groups. These criteria provide bounds for applying the limiting equations of Rayleigh and Tomotika.

The instability of stationary Newtonian threads is found to follow Tomotika's theory quite well, and that of stationary viscoelastic threads deviate from the Newtonian systems in a way which seems to confirm qualitatively with Lee's theory on viscoelastic threads.

The instability criterion, in terms of $E_{DPC} = C d_{DP} \eta_C / \sigma$ (where C is the extensional rate and $d_{DP}$ is the broken drop diameter) and the viscosity ratio, of an extending Newtonian thread is also established, and it is found that the system with small $\lambda$ is more unstable than the system with high $\lambda$ .

The value of $E_{DPC}$ in case of an extending viscoelastic thread is again found to increase almost linearly with Deborah number, and the slope depends on the viscosity ratio; the smaller the viscosity ratio, the steeper the slope.

The measurements of the relative varicosity amplitude, $\delta/a$, at various times before breakup reveal that the viscoelastic thread (both stationary and extending) is more unstable than the Newtonian thread with same viscosity ratio, interfacial properties, and kinematic conditions.

## TABLE OF CONTENTS

| CHAPTER | | PAGE |
|---|---|---|

LIST OF FIGURES

FIGURE PAGE

## LIST OF TABLES

# CHAPTER I

## INTRODUCTION

A characteristic response of all real fluids is the irreversible deformation resulting from the application of an even infinitely small stress. In multiphase systems, besides the dynamic stresses arising from inertial and viscous interactions between the phases, we also have interfacial forces arising from the non-zero interfacial tension between the phases. Interfacial tension usually tends to resist the increase of contact area between different immiscible phases. The interaction of these dynamic and interfacial forces plays a very significant role in dispersion processes of immiscible fluids. Practically, such processes arise in the atomization of fuel in internal combustion engines, aeration operations during fermentation, emulsification processes, as well as in the fiber spinning of polymer melts, etc.

The basic concerns in these problems are:

(1) What are the possible physical processes which may cause the drop (or the thread) to break up?

(2) How do these physical processes proceed, and how do fluid properties affect the nature of the dispersion resulting from these processes?

Due to the importance of breakup of drops and threads in many essential processes, it has captured the interests of scientists and techonologists in various fiels for many decades.

Despite this, the complexity and uncertainty of these processes still prevent convincing and sufficiently accurate results to be obtained. Such results will be forthcoming only after we understand single droplet(and thread) deformation and breakup in certain flow field.

The dispersion of one immiscible fluid in another usually begins with two originally irregular bulky fluids. The disintegration process may occur only when the dynamic stresses induced by certain devices are large enough to overcome the static force of interfacial tension which always resists deformation and dispersion by attempting to maintain minimum contact area between the fluids. However, once the drop is extended into a thread, the interfacial tension is the agent promoting the breakup via capillary forces.

As the disintegration process goes on, more and more individual drops are formed, and the drop size is gradually decreased. In addition, the inertial forces diminish, and the interfacial and viscous forces become dominant. Further, the drops tend to become more regular in shape and the nature of the flow fields causing the deformation and breakup can be clearly identified. In viscous systems, it is these latter stages of dispersion which are of principal interest since they govern the ultimate size and distribution of the droplets obtained.

The eventual equilibrium drop size depends not only on the physical properties of the fluid system, but also on the flow conditions, i.e., flow type, deformation rate, etc.. According to

Hinze's analysis (17), the flow patterns which may cause drop breakup can be classified as:

(1) Parallel flow

(2) Couette flow

(3) Plane hyperbolic flow

(4) Biaxial hyperbolic flow

(5) Rotational flow

The flow field of any dispersion device can always be characterized as one or a combination of these five elementary patterns. To date, only Couette, parallel, and plane (uniaxial) hyperbolic flow have been extensively studied with respect to deformation and breakup of drops.

G. I. Taylor (34) first initiated the study of drop deformation and breakup in viscous systems in 1934. Besides an experimental investigation of the critical shear rate at breakup, he derived the first equation relating the deformation of a drop to the physical properties of fluids and the shear rate of flow field. Taylor's theory was limited to small deformations and conditions of negligible inertial effects. This pioneering work has been modified by a number of investigators— Chaffey and Brenner ( 5), Cox ( 7), and Barthes and Acrivos( 8 ), among the others. However, their works still can not explain the breakup process at large deformation.

Most of the earlier studies were mainly concerned with Newtonian systems, especially in simple shear (or Couette) flow fields. However, the plane hyperbolic flow field has been shown experimentally to be a prefered flow type in dispersion devices, particularly with systems with either high of low viscosity ratios. It is the purpose of this work to conduct an experimental investigation of the deformation and breakup of liquid drops in plane hyperbolic flow fields, and the instability of stationary and extending liquid threads. Both Newtonian and viscoelastic fluids will be studied.

# CHAPTER 2

# THEORETICAL BACKGROUND

## 2-1. General Remarks

Increased viscosity and non-Newtonian effects such as visco-elasticity and shear dependent viscosity, are well-known phenomena of dispersions, or emulsions when these systems undergo a hydrodynamic flow. Most of these phenomena result from the interaction of the deformable and non-deformable particles which make up the dispersion. From the point of view of hydrodynamics, the increased viscosity of a dispersion may be considered as a consequence of the perturbation of the continuous phase flow field around the suspended particles or liquid drops. The degree of perturbation which leads to an increase rate of energy dissipation, of course, will be closely related to the shape of particles present. Experimentally, it has been found that the viscosity of suspensions is affected by factors such as: the shape, size, internal flexibility, and ease of deformation of the dispersed phase. Thus it is important to obtain more precise information on the deformation of drops in various flow fields. Such information is essential for the development of theories to accurately describe the rheological behavior of disperse systems.

Considerable theoretical and experimental efforts have been devoted to the study of drop deformation and breakup in simple shear flows, beginning with G. I. Taylor's original small deformation theory. Among these works, of particular importance are:

The thorough study of Rumscheidt and Mason ( 28 ), who studied the deformation, circulation, and breakup of liquid droplets both in plane hyperbolic and Couette flow fields; the theoretical analysis of Chaffey and Brenner, which extended Taylor's theory to a second order approximation in the deformation parameter; and the transient analysis of Cox ( 7) who studied the time effect on the deformation and circulation. The most recent development in this area is that due to Acrivos ( 8) who derived the time dependent equation for deformation and also presented a theoretical way to predict approximate conditions for breakup.

We now review the important aspects of these studies in the next section.

## 2-2 Deformation of a Single Droplet

### 2-2-1 Previous Theoretical Studies

The two flow fields as chosen by G. I. Taylor in his studies on the deformation and breakup of liquid droplets can be written as:

Plane hyperbolic flow: $$V_x = \frac{\bar{G}}{2}x, \quad V_y = -\frac{\bar{G}}{2}y, \quad V_z = 0 \qquad (2\text{-}1)$$

Uniform shear flow: $$V_x' = \bar{G}y', \quad V_y' = V_z' = 0 \qquad (2\text{-}2)$$

Where $\bar{G}$ is the magnitude of the rate of strain in flow field. The first flow field is irrotational, and the second is rotational. As pointed out by Taylor (34), and Batrok and Mason, if the coordinate axes X and Y of the plane hyperbolic flow field are rotated with a constant angular speed $\bar{G}/2$, and if the coordinate axes X' and Y' of the uniform laminar shear flow field lie instantaneously at $45^o$ to

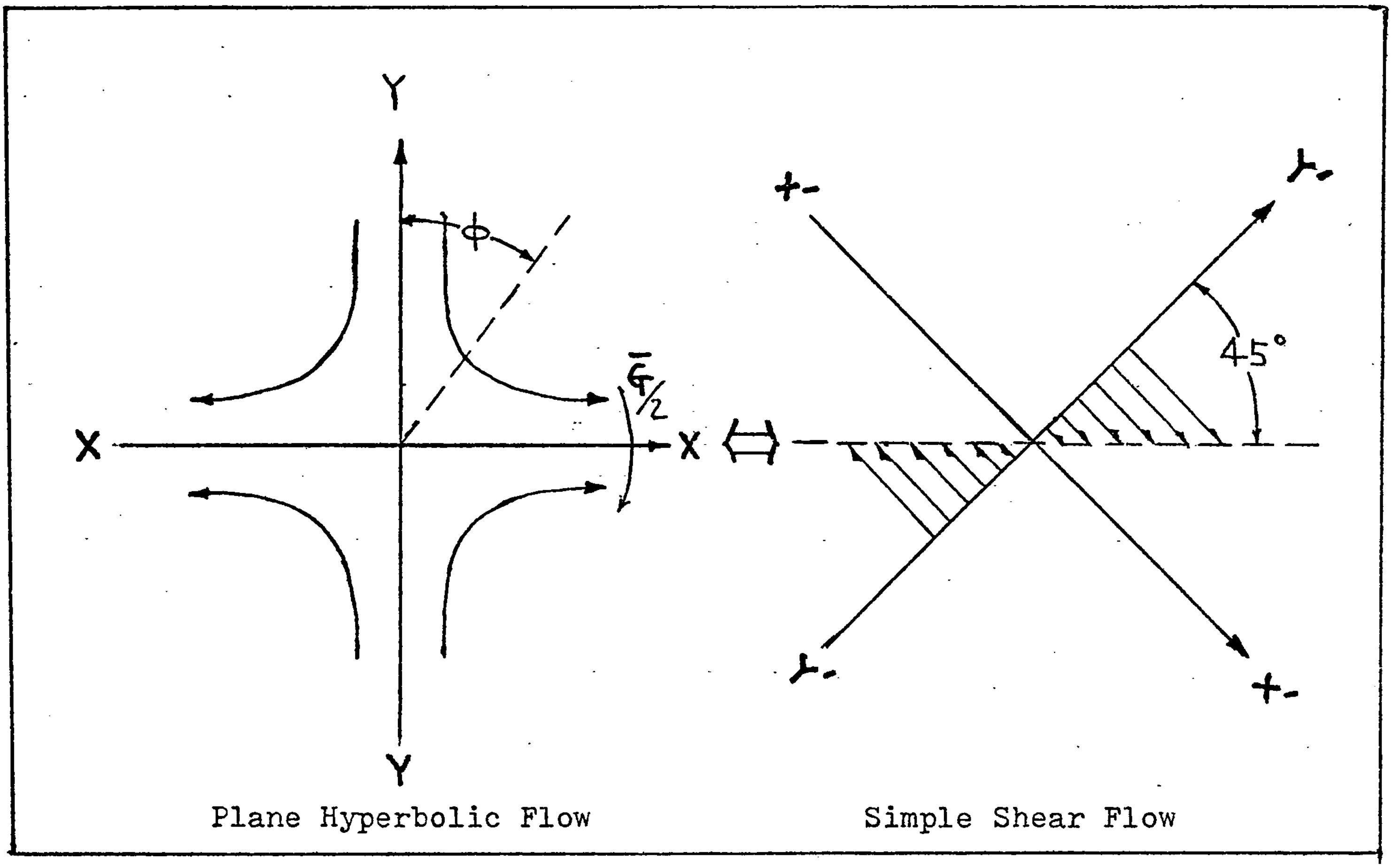


Figure 2-1. Coordinate Transformation of Plane Hyperbolic Flow to Simple Shear Flow by Rotation of Axes

axes X and Y, then the two flow fields become identical at that moment. The situation of transformation is shown on Fig. 2-1. In this instance, the coordinates of these two flow fields are related by:

$$X' = 1/\sqrt{2}(X + Y)$$

$$Y' = 1/\sqrt{2}(X - Y)$$

$$\phi' = \phi - \pi/4$$

Here the identity of these two fields is instantaneously only. Therefore, effects which depend only on the instantaneous distribution of velocity and are not affected by a rotation of the whole system will be identical in the two fields; this applies to internal circulation in an undeformed fluid drops. On the other hand, effects which depend both on the instantaneous distribution and on the time sequence of distribution of velocity will be very different in the two. This occurs when fluid drops suffer large deformations. The significance of these remarks has been demonstrated by Taylor in his original paper.

When a neutrally bouyant liquid drop is placed in the center (or stagnant) point of a plane hyperbolic flow field, the disturbance to the fluid motion surrounding this droplet will generate a stress field, which can be discomposed into tangential and normal components acting on the drop surface. In the case of a liquid drop whose interface is not contaminated by any impurity or surfactant, the tangential stresses are continuously transmitted across the interface, so that a velocity gradient will be developed inside the drop. The normal stresses, on the other hand, are discontinuous at the interface and will generate a pressure difference which will be counterbalanced by the capillary pressure due to the interfacial tension. The drop, therefore, assumes a shape which balances the forces associated with the normal stresses and capillary pressure.

As we know, the difficulties in an analytical formulation of such a problem are almost insurmountable, partly because the correct boundary conditions are not always known, and partly because the interdependence of drop shape and velocity distribution is unseparable. Taylor initiated the first attempt to make an approximate analytical formulation of this problem. In his hydrodynamical analysis, Taylor made the following assumptions:

(1) There is no slip at the surface of the drop (velocity components are continuous across the interface).

(2) The drop is only slightly deformed from its spherical equilibrium shape.

(3) The tangential stress parallel to the surface is continuous at the surface of the drop so that any film which may exist between the two liquids merely transmits tangential stress from one fluid to the other.

(4) The normal stress is discontinuous, and the difference is balanced by capillary pressure, $\sigma(1/R_1 + 1/R_2)$.

Where $\sigma$ is interfacial tension and $R_1$ and $R_2$ are the principal radii of surface curvature.

By using Lamb's general solution to the Navier-Stokes equation for steady creeping flow, Taylor derived the velocity and pressure distribution both in the drop and in the suspending fluid. From these results, the respective normal stresses acting at the surface were obtained, and expressed as:

$$P_{rr} = 5/2\ \bar{G}\ \eta_c(\lambda+8/5)/(\lambda+1)\ \cos 2\phi \qquad \text{outside drop} \qquad (2\text{-}3)$$

$$P'_{rr} = 9/4\ \bar{G}\ \eta_c(\lambda/(\lambda+1))\ \cos 2\phi \qquad \text{inside drop} \qquad (2\text{-}4)$$

With a resulting pressure difference across the interface given by:

$$\Delta P_N = P'_{rr} - P_{rr} = -4\ \bar{G}\eta_c(19\lambda+16)/(16\lambda+16)\ \cos 2\phi \qquad (2\text{-}5)$$

Where: $\eta_c$: viscosity of continuous phase

$\lambda$: the ratio of viscosity of drop and outside fluid,

$\Delta P_N$: normal stress difference of inside and outside fluid

$\phi$: polar angle of spherical coordinate (Refer to Fig. 2-1)

From Eq. (2-5), it follows that $\Delta P_N<0$ when $-\pi/4 < \phi < \pi/4$, and the drop will be subjected to compressive stresses which tend to contract the drop; and that $\Delta P_N>0$ when $\pi/4 < \phi < 3\pi/4$, and the drop will be subjected to tensile stresses which tend to extend it. In addition, it can also be seen that $\Delta P_N$ has its maximum and minimum values when $\phi = \pi/2$ (or $3\pi/2$), and 0 (or $\pi$) respectively. Based on these considerations, the shape of the deformed drop is that given in Figure 2-2.

Then boundary condition (4) gives

$$\sigma(1/R_1 + 1/R_2) = P'_{rr} - P_{rr} + \text{constant} \qquad (2\text{-}6)$$

or $$\sigma(1/R_1 + 1/R_2) = -4\bar{G}\eta_c(19\lambda+ 16)/(16\lambda+ 16)\ \cos 2\phi + \text{constant}$$

It can be seen from Eq. (2-6) that it is necessary to find the shape of a nearly spherical drop for which the variation in $(1/R_1 + 1/R_2)$ is proportional to $\cos 2\phi$. Taylor has verified that for the surface whose equation is

$$r = a(1-D_I\cos 2\phi) \qquad (2\text{-}7)$$

$1/R_1+1/R_2$ will be proportional to $\cos 2\phi$, and can be expressed as:

(2-8)

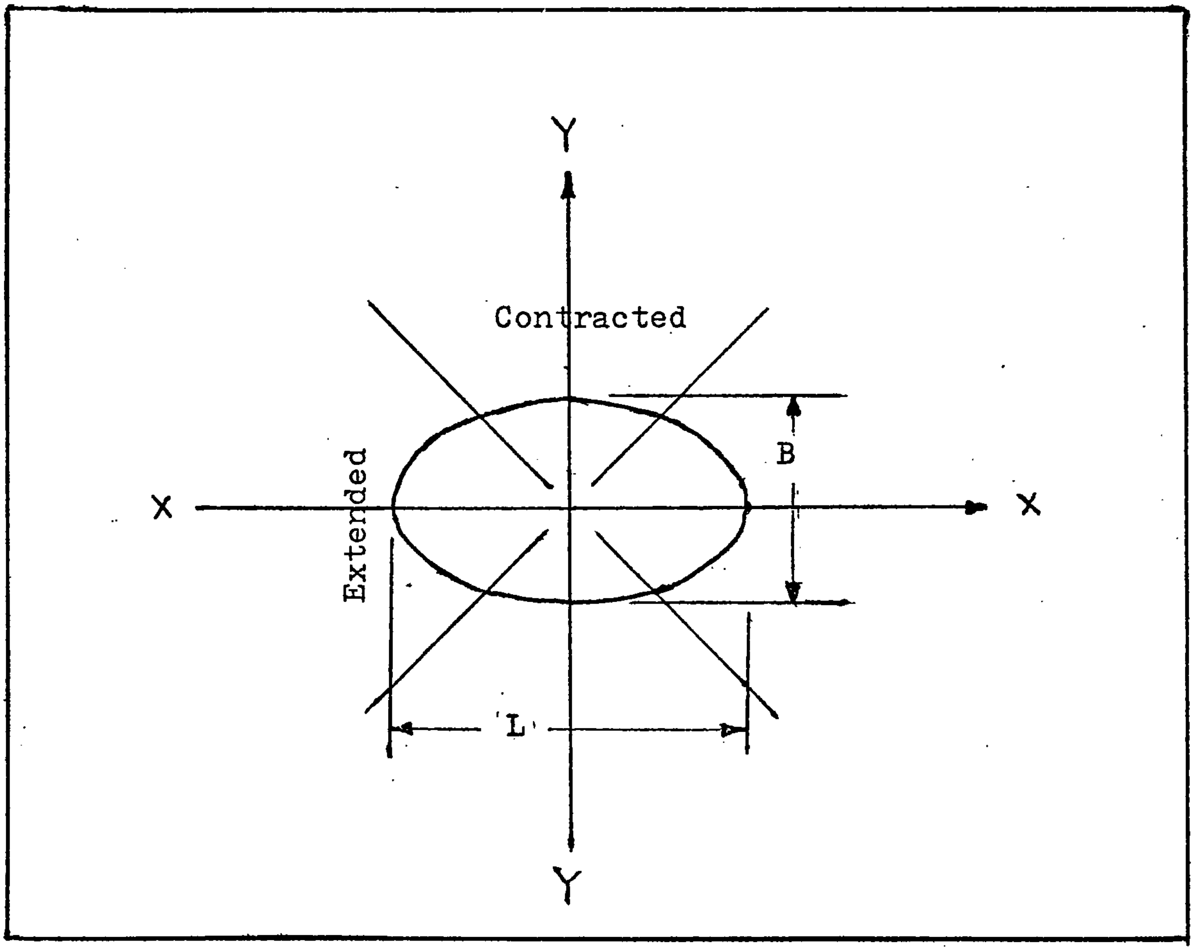


Figure 2-2. The Shape of A Deformed Drop and Its Parameters

$$1/R_1+1/R_2 = 2/a\ (1 - 2D_I\cos 2\phi) \qquad (2\text{-}8)$$

Here $D_I$ is the deformation parameter in the equatorial X-Y plane. For small deformation, it can be shown that

$$D_I = D = (L - B)/(L + B) \qquad (2\text{-}9)$$

Where L and B are the principal axes of the deformed ellipsoid drop.

By combining Eqs. (2-6) and (2-8), and equating the coefficients of $\cos 2\phi$, Taylor finally obtained the following equation:

$$D_I = (19\lambda + 16)/(16\lambda + 16)\ \bar{G}\eta_C a/\sigma \qquad (2\text{-}10)$$

Equation (2-10) reveals that for nearly spherical drops, the deformation parameter, $D_I$ defined by Eq. (2-9), is proportional to a non-dimensional group, $E = \bar{G}\eta_C a/\sigma$, which is a ratio of viscous forces, $\eta_C\bar{G}$, to interfacial tension forces, $\sigma/a$. The constant of proportionality, $(19\lambda+ 16)/(16\lambda+ 16)$, varies from 1 to 1.875 when $\lambda$ changes from 0 to $\infty$.

It should be noted that Equation (2-10) stemmed from the velocity field associated with a spherical drop, or rather a zero order velocity field in $D_I$. In order to obtain the drop deformation with accuracy to second order in $D_I$, it is necessary to know the fluid velocity both outside and inside the drop to first order in $D_I$. Chaffey and Brenner made such an effort and derived the first order velocity field and from this they found the equation giving the drop shape to second order in $D_I$ for both uniform shear field and plane hyperbolic field. Their equation for the plane hyperbolic field is: (in XY plane):

$$r/a = 1-D_I\cos 2\phi + D_I^2\left\{H'+(H/4)\cos 4\phi\right\} + O(D_I^3) \qquad (2\text{-}11)$$

Where $D_I = \bar{G}a\,\eta_C/\sigma\ (19\lambda + 16)/(16\lambda + 16)$

$$H = 2(1171\lambda + 656)/(19\lambda + 16)/27$$

$$H' = (8383\lambda^2 + 12543\lambda + 3728)/\left[(\lambda+1)(19\lambda + 16)\right]/630$$

According to Equation (2-9), the experimentally observed parameter $D = (L-B)/(L+B)$ is related to $D_I$ by

$$D = (L-B)/(L+B) = D_I/\left[1+D_I^2(H'+H/4)\right] \qquad (2\text{-}12)$$

In the limit $D_I \rightarrow 0$, this equation can be simplified to Taylor's first order equation, i.e., Equation (2-10). However, after comparison with experimental data in a uniform shear flow field, Turner and Chaffey in 1969 concluded that the applicable range of Chaffey and Brenner's second order theory is not significantly beyond that of Taylor's first order theory.

In 1969 Cox developed a first order theory expanding in term of $\epsilon$ , a small parameter representing the magnitude order of deformation, to determine the transient shape of a fluid drop in both simple shear and plane hyperbolic flow field. For steady state, his equation reduced to Equation (2-10) for plane hyperbolic flow field.

The most recent theoretical work on the deformation and breakup of drops is due to Barthes and Acrivos ( 8 ). These investigators expanded the solution to the creeping flow equations in powers of E', a small parameter representing the tendency of the drop to deform. They carried out the expansion solution to second order in E'. Further, they applied the linear stability theory to predict the onset of burst.

As shown by Frankel and Acrivos ( 12) in 1970, the surface of the drop in a system of axes moving with the center of the particle is defined by

$$r = 1+3E'F_{lm}\left(\frac{x_l x_m}{r^2}\right) + E'^2\left(\frac{-6}{5}F_{lm}F_{lm}+105F_{lmpq}\frac{x_l x_m x_p x_q}{r^4}\right) + 0(3) \tag{2-13}$$

where $r = (x_l x_l)^{\frac{1}{2}}$, and $E' = \bar{G}a\eta_c/2\sigma$.

The tensor $F_{ij}$ and $F_{ijlm}$ are chosen to be symmetric with respect to any permutation of their indices and to have zero contraction. Their expressions will depend on the dynamic behavior of the system, i.e., on the type of the undisturbed creeping flow field.

For a plane hyperbolic flow field, Barthes and Acrivos derived the following expression for D

$$D = \frac{3\,E'\bar{D} + 105\,E'^2 D_{1111}}{2 + 3\,E'\bar{S} + E'^2\left(18\bar{S}^2/5 + 6\bar{D}^2/5 + 105\bar{S}_{1111}\right)} \tag{2-14}$$

where $\bar{S} = F_{11} + F_{22}$, $\quad \bar{D} = F_{11} - F_{22}$

$$S_{1111} = -\frac{99}{35}\frac{b_1}{b_o}\bar{D} - \frac{b_2}{70b_o}(81\bar{S}^2 + 57\bar{D}^2)$$

$$D_{1111} = -\frac{+3}{35}\frac{b_1}{b_o}\bar{S} - \frac{9}{7}\frac{b_2}{b_o}\bar{S}\bar{D}$$

Here $\bar{S}$ and $\bar{D}$ are determined from the following equations at steady state,

$$a_1\bar{S} + \frac{E'}{3}\left[a_2\bar{D}-a_3(3\bar{S}^2-\bar{D}^2)/2\right] + E'^2\bar{S}\left[c_3(3\bar{S}^2+\bar{D}^2)/2 + \bar{D}(c_4+c_6/3) + c_7/3 + 2c_5\right] = 0$$

$$a_1\bar{D} + 2a_o + E'\bar{S}(a_2+a_3\bar{D}) + E'^2\left[(2c_1+c_3\bar{D})(3\bar{S}^2+\bar{D}^2)/2 + c_4\bar{D}^2 + c_6(\bar{S}^2+\bar{D}^2)/2 + \bar{D}(2c_2+c_7+2c_5)\right] = 0 \tag{2-15}$$

The coefficient $a_o,\ldots a_9,\ b_o,b_1,b_2,c_1,\ldots,c_7$, are known rational functions of $\lambda$, and their expression are given in Appendix I .

Solving numerically Equation (2-15) for various values of $E'$, we are able to construct the prediction curve, $D_I$ vs. $E'$. The comparison with experimental data will be shown in Chapter 4.

Before ending this section, we would like to point out the differences between these theoretical works. There are various perturbation approaches to the solution of this problem: 1) expansion in terms of a drop deformation parameter, $\epsilon$, 2) expansion in terms of dimensionless group $E = \overline{G}a\eta_c/\sigma$ , 3) expansion in terms of $\lambda$ . Taylor, Chaffey and Brenner, and Barthes and Acrivos used E as the expansion parameter; Taylor also used $\lambda$. On the other hand, Cox obtained a solution expanding in terms of $\epsilon$ , by assuming only the drop deformation be small and of order $\epsilon$, where $\epsilon << 1$.

2-2-2. Dimensional Approach For Viscoelastic Fluids

All of the equations described so far are only applicable to Newtonian systems, and the results have been expressed in terms of $D_I$, E, and viscosity ratio, $\eta_D/\eta_c$. However, for a viscoelastic drop, some additional groups are expected to arise in these problems which are due to the complex rheological behavior of the fluid.

To date, theories for the deformation of non-Newtonian drops are not available. Nevertherless, a dimensional analysis can be used to identify the important characteristic groups once the rheological equation of state is specified. For this purpose, the modified form of the Bird-Carreau (1968) model was chosen to characterize the fluid rheological properties. According to this theory, the constitutive equation is expressed as

$$\tau_{ij} = -\int_{-\infty}^{t} \bar{m}[t-t', \mathrm{II}(t')]\left[\left(1+\frac{\epsilon}{2}\right)\bar{\Gamma}_{ij}(t') - \left(\frac{\epsilon}{2}\right) g^{ir}(x)\, g^{is}(x)\, \Gamma_{rs}(t')\right] dt' \qquad (2\text{-}16)$$

with memory function as:

$$\bar{m}(t-t', \mathrm{II}(t')) = \sum_{p=1}^{\infty} \frac{\eta_p}{\lambda_{2p}^2} \frac{e^{-(t-t')/\lambda_{2p}}}{1+\frac{1}{2}\lambda_{1p}^2\, \mathrm{II}(t')} \qquad (2\text{-}17)$$

and finite strain tensor as:

$$\bar{\Gamma}_{ij}(t') = -g^{ij}(x) + \left(\partial x^i/\partial x'^m\right)\left(\partial x^j/\partial x'^n\right) g^{mn}(x') \qquad (2\text{-}18)$$

$$\Gamma_{ij}(t') = g_{ij}(x) - \left(\partial x'^m/\partial x^i\right)\left(\partial x'^n/\partial x^j\right) g_{mn}(x') \qquad (2\text{-}19)$$

Where $x_i$, $x_i'$ : material coordinate of fluid element at time t and t' respectively

$g^{ij}$, $g_{ij}$ : contravariant and covariant components of the metric tensor

II(t): second invariant of the rate of strain tensor

The material constants $\eta_p$, $\lambda_{1p}$, and $\lambda_{2p}$ are related empirically to other five parameters, which can be determined from simple viscometric data. These parameters are defined by

$$\eta_p = \eta_o \frac{\lambda_{1p}}{\sum_{k=1}^{\infty} \lambda_{1k}} \quad , \; \lambda_{1p} = \lambda_1 (2/(p+1))^{\alpha_1}, \;\; \lambda_{2p} = \lambda_2 (2/(p+1))^{\alpha_2} \tag{2-20}$$

where $\eta_o$: zero shear viscosity

$\lambda_1$, $\lambda_2$: time constants

$\alpha_1$, $\alpha_2$: slope parameters

Therefore, for a viscoelastic fluid drop in a plane hyperbolic flow field of a Newtonian fluid, the physical parameters occuring in the problem are the extensional rate $\bar{G}/2$ (of the undisturbed flow), the initial (undeformed) radius a of the drop, the interfacial tension $\sigma$, the viscosity of continuous fluid $\eta_c$, and the five parameters of drop fluid, $\eta_{o}$, $\lambda_1$, $\lambda_2$, $\alpha_1$, $\alpha_2$. Here we assume a neutrally buoyant drop. Six dimensionless groups can be formed from these quantities: $Ga\eta_c/\sigma$, $\eta_{o}/\eta_c$, $\lambda_1\bar{G}$, $\lambda_1/\lambda_2$, $\alpha_1$, $\alpha_2$. The deformation is then

$$D \doteq \mathcal{D}\,(\bar{G}a\eta_c/\sigma \;\; , \;\; \eta_{o}/\eta_c, \; \lambda_1\bar{G}, \; \lambda_1/\lambda_2, \; \alpha_1, \; \alpha_2) \tag{2-21}$$

As reported by MacDonald, Carreau, and Bird, the ratios $\lambda_1/\lambda_2$, $\alpha_1/\alpha_2$ are more or less constant for a large number of viscoelastic fluids. Assuming this to be the case, we can simplify Equation (2-21) into:

$$D = \mathcal{D}\,(\bar{G}a\,\eta_c/\sigma, \;\; \eta_{o}/\eta_c, \;\; \lambda_1\sigma/a\eta_c \; , \; \alpha_1) \tag{2-22}$$

This is the equation which will be used to analyze the experimental data of viscoelastic fluid drop in Newtonian fluids. For a Newtonian drop, $\lambda_1 = 0$, $\alpha_1 = 1$, Equation (2-22) becomes

$$D = \mathcal{D}(\bar{G}a\eta_c/\sigma \quad , \lambda ) \qquad (2\text{-}23)$$

Comparing with Equations (2-10) and (2-12), we find that the latter result is consistent with the theoretical relations given previously.

In the case of a viscoelastic drop, the deformation depends not only on E, $\lambda$, and $\alpha_1$, but also on $\lambda_1\sigma/a\eta_c = T$. Physically this group $\lambda_1\sigma/a\eta_c$ can be considered as the ratio between the characteristic time $\lambda_1$ of the viscoelastic fluid making up the drop and a $\eta_c/\sigma$, a characteristic relaxation time of the drop under deformation.

## 2-3. Breakup Of A Deformed Drop and The Deformation At Burst

The deformation of a suspended drop will increase gradually and attain an equilibrium state, when the extension rate of the continuous phase is increased until a critical value $\bar{G}_c/2$ is reached, at which point the drop will break. For Newtonian fluids, this critical value is a function of the viscosity ratio, $\lambda$, with the following important properties:

if $\bar{G} < \bar{G}_c$ stable deformation obtained

if $\bar{G} > \bar{G}_c$ continuous deformation and breakup

To date, almost no theoretical equation exists to predict the critical shearing rate for a given fluid system (both Newtonian and non-Newtonian). However, an interpretation of this phenomenon can be obtained simply by using dimensional analysis. Here the critical extension rate at which breakup of a deformed drop occurs can be expressed as a function of all the physical parameters occuring in the problem, i.e.,

$$\bar{G}_c = \bar{G}_c(\rho_c, \rho_D, \eta_c, \eta_D, a, \sigma) \qquad (2\text{-}24\text{-}a)$$

for a Newtonian drop in a Newtonian continuous phase, and

$$\bar{G}_c = \bar{G}_c(\eta_c, \eta_{oD}, \rho_c, \rho_D, a, \lambda_1, \lambda_2, \alpha_1, \alpha_2, \sigma) \qquad (2\text{-}24\text{-}b)$$

for viscoelastic drop in a Newtonian continuous phase. By applying dimensional analysis, the above two equation can be rewritten as:

$$E_c = \bar{G}_c a \eta_c/\sigma = E_c(\eta_D/\eta_c, \rho_D/\rho_c, \rho_c a^2 \bar{G}_c/\eta_c) \qquad (2\text{-}25\text{-}a)$$

and $$E_c = E_c(\eta_{oD}/\eta_c, \rho_D/\rho_c, \rho_c a^2 \bar{G}_c/\eta_c, \bar{G}_c \lambda_1, \lambda_1/\lambda_2, \alpha_1, \alpha_1/\alpha_2) \qquad (2\text{-}25\text{-}b)$$

Here, the Bird-Carreau model is again used to characterize the properties of the viscoelastic material. Neglecting inertial effects and gravity forces (a neutrally buoyant drop), and making use of the constant ratio, $\lambda_1/\lambda_2$, $\alpha_1/\alpha_2$, as reported by MacDonald etc., we can simplify Equations (2-25-a) and (2-25-b) into

$$E_c = E_c(\eta_D/\eta_c) \qquad (2\text{-}26\text{-}a)$$

$$E_c = E_c(\eta_{oD}/\eta_c, \bar{G}_c \lambda_1, \alpha_1) \qquad (2\text{-}26\text{-}b)$$

where $E_c = \bar{G}_c a \eta_c/\sigma$. $\bar{G}_c \lambda_1$ is the "Deborah number", which, similar to the T dimensionless group in the correlation for VE drop deformation, presents the ratio of $\lambda_1$, the characteristic time of the VE fluid, and $1/\bar{G}_c$, the characteristic time of the flow field.

Equation (2-26-b) will give Equation (2-26-a) as a special case when $\lambda_1 = 0$ and $\alpha_1 = 1$, i.e., when the drop is Newtonian.

G. I. Taylor interpreted the critical condition of breakup as the point when the maximum value of $\Delta P_N$ distributed over the drop surface tending to disrupt the drop exceeds the force, due to surface tension, tending to hold it together. Based upon this definition, and assuming that Equation (2-5) holds, Taylor indicated that the drop will burst when

$$4\bar{G}\,\eta_c \frac{(19\lambda + 16)}{(16\lambda + 16)} > 2\sigma/a \tag{2-27}$$

Further, if Equation (2-10) is used in this equation we obtain the critical deformation, i.e., the deformation at which the drop begins to break. This is given by

$$D_I \geqslant 1/2 \tag{2-28}$$

In using these last two results, it must be kept in mind that they are based on a small deformation theory.

# CHAPTER 3

## EXPERIMENTAL APPARATUS, MATERIALS, AND PROCEDURES

### 3-1. Experimental Apparatus

Two four-roll devices, one built by W. K. Lee during his Ph. D. work, the other built during this study, were alternatively used to produce the plane hyperbolic flow field required in this experimental investigation. We will term these two devices respectively as "modified four-roll device" (MFRD, built by W.K. Lee), and "four-roll device" (FRD, built in this study). The MFRD was built with the four rolls mounted on the corners of a $4 \times 3$-inch rectangle in order to obtain the best approximation to an uniaxial extensional flow field along the X-axis. According to the theoretical analysis of Lee (20), the flow field produced by this device can also be expressed approximately by Equation (2-1) for the area around the stagnation point, i.e., X=0, Y=0. The details relating to the construction of the MFRD was explained in Lee's dissertation.

The four-roll device built in this study is similar to the MFRD, with a change in the driving machanism and the location of the rollers. It consists of four identical plexi-glass cylinders, $1\frac{1}{2}$" diameter and $3\frac{1}{2}$" high, which were mounted at the corners of $4 \times 4$ inch rectangle, as shown in Figure 3-1. These cylinders are immersed in the continuous phase, which was floated on a heavier low viscosity fluid and contained in a $13 \times 13 \times 4\frac{1}{2}$ inch plexi-glass box with a removable circular cover at the top. Each cylinder was mounted in the box with a teflon bearing installed in the top plate to hold the upper end in position, and with a sealed ball bearing at the bottom plate to support the shaft which extends through the bottom plate and connects

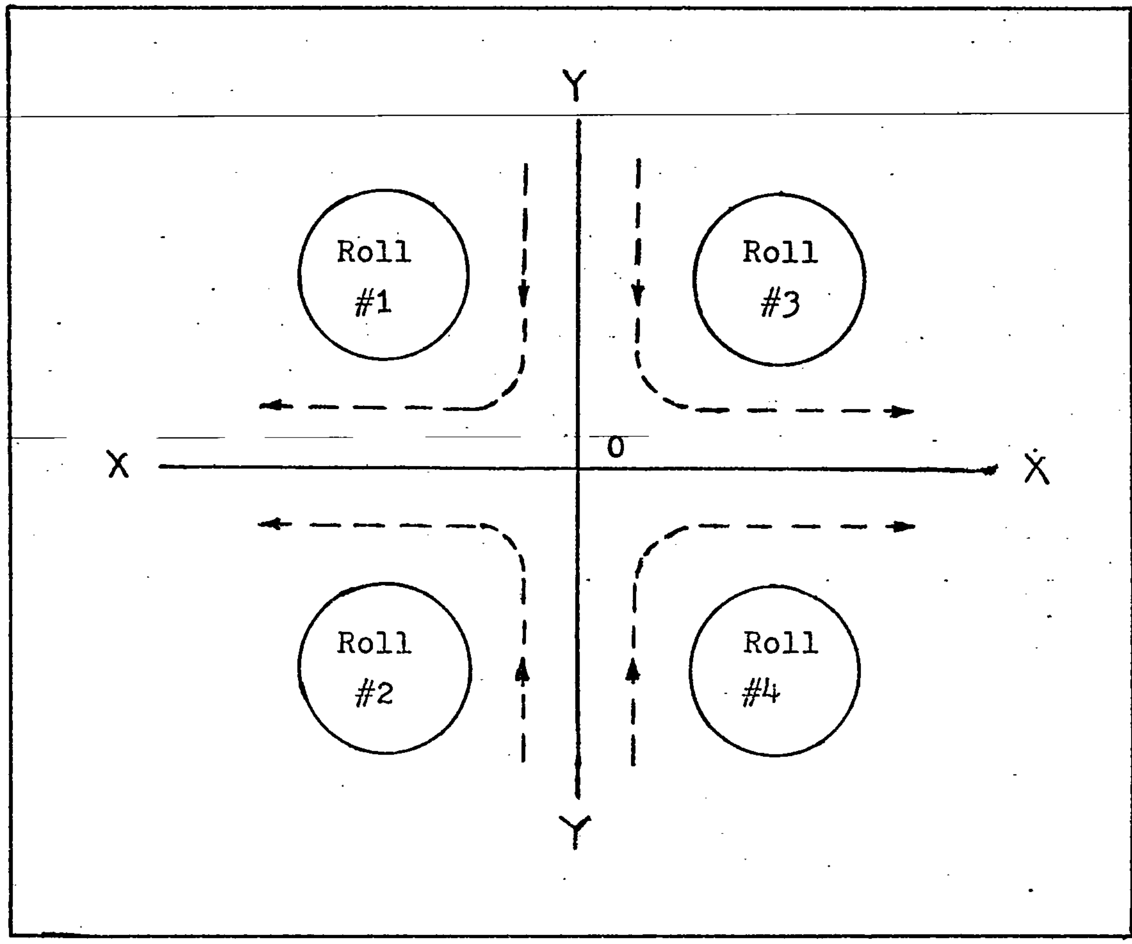


Figure 3-1. The scheme of Four-Roll Apparatus

to the drive system below (see Figure 3-2, 3-3).

Figure 3-1 shows schematically the FRD built here to experimentally examine the drop behavior. The four rolls are driven by two separate variable speed motors, one driving rolls one and two and the second deriving rolls three and four. The flow field produced is a plane hyperbolic flow field in which the velocity components in the X and Y directions are given by:

$$V_x = \bar{G}X/2, \quad V_y = -\bar{G}Y/2, \quad V_z = 0. \tag{2-1}$$

Where $\bar{G}/2$ is the extension rate.

Photographs of the four-roll apparatus are shown in Figures 3-2 and 3-3. As shown, the four rollers are driven by two motors mounted behind the bottom plate of the box. Here a no-slip plastic belt and gear pulley system is used in the drive mechanism. The speed of these two variable drives are controlled by an electric controller in which two speed adjustments are possible, one regulating the speed of both motors together, the other regulating the speed of one motor relative to the other. By adjusting these two control knobs , we could easily match the motor speeds and control the drop at the stagnation point. The speeds of the motors are determined directly from the reading shown on the digital voltmeter which is connected to the outputs of two tachometers installed inside the motors. The actual roll speed and the meter reading are related by

$W$ (RPM) = 1.75×volt for 100-1 ratio gear box

$W$ (RPM) = 17.5×volt for 10-1 ratio gear box

for both tachometers.

According to W. K. Lee (20), the extension rate, $\bar{G}/2$, in the four-roll device should be equal to a constant times the roller speed. However, we found that the accuracy of this statement depends on the

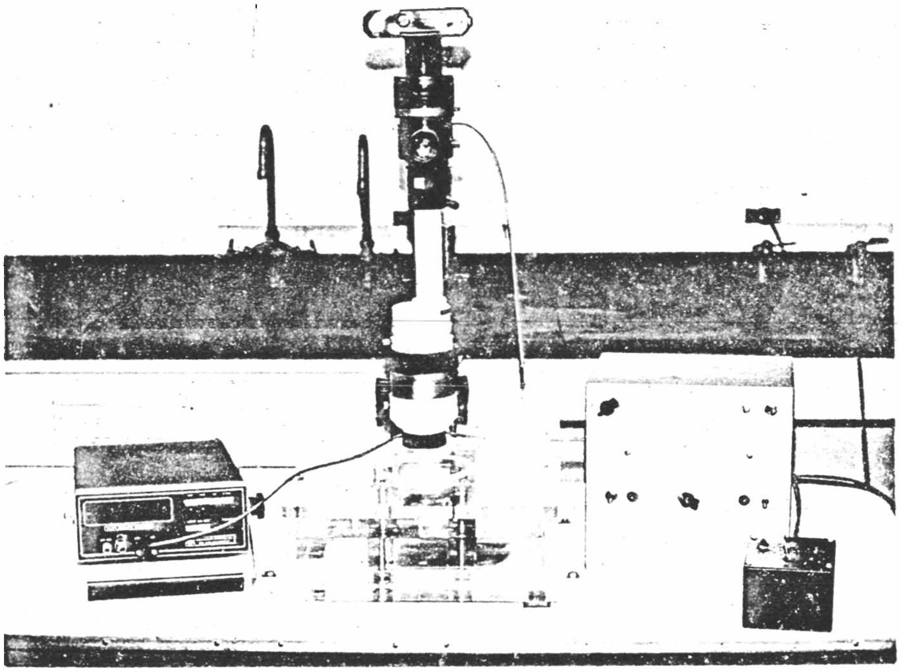

Figure 3-2. The Four-Roll Apparatus (Front View)

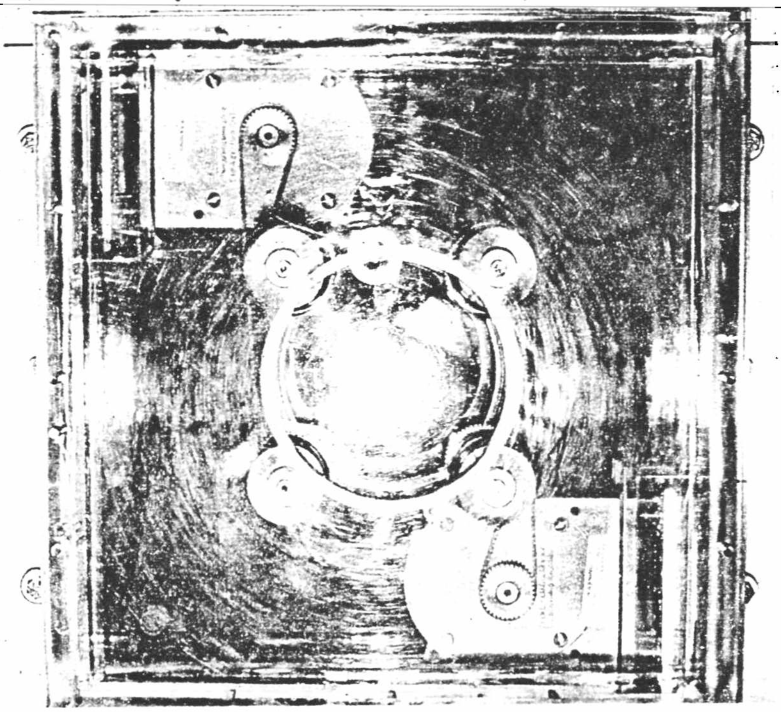

Figure 3-3. The Four-Roll Apparatus (Top View)

viscosity of the fluid used as the continuous phase. Two series of velocity measurements of tracer particles dispersed in two different continuous phase (80% glycerine solution (low viscosity) and Dow Corning Oil 510 with $\eta_C$= 300 poise) were carried out to establish the relation between W and $\bar{G}$. The velocity fields corresponding to different roller speeds were determined from motion picture of the movement of aluminium tracer particles in the fluid. Also, small air bubbles were used for the same purpose. The extension rate, $\bar{G}/2$ for each roller speed was calculated from the following equations:

$$\bar{G} = 2\ln(X_2/X_1)/(t_2-t_1) \qquad (3\text{-}2\text{-}a)$$

$$\bar{G} = -2\ln(Y_2/Y_1)/(t_2-t_1) \qquad (3\text{-}2\text{-}b)$$

By measuring the time elapsed for a particle to move between two different X (or Y) positions, we could determine $\bar{G}/2$ for each roller speed. The accuracy of Equation (2-1) in describing the flow field near the stagnant (observation) point O in Figure 3-1 is confirmed from such experiments (see data in Appendix II). The results are plotted in Figures 3-4 and 3-5 for the 80% glycerine solution and the silicone oil ( $\eta_C$= 300 poise), respectively.

The data for the glycerine solution deviates from a straight line as W reaches about 15 RPM and higher. On the other hand, the data tor the silicone oil fall approximately on a straight line for roller speeds up to 50 RPM. The deviation from a straight line, we believe, is due to the increasing inertial effects as the speed is increased. Since the viscosity of the silicone oil is about 100 times greater than that of the glycerine solution, it is expected that the linear relation between G and W will hold for roller speeds

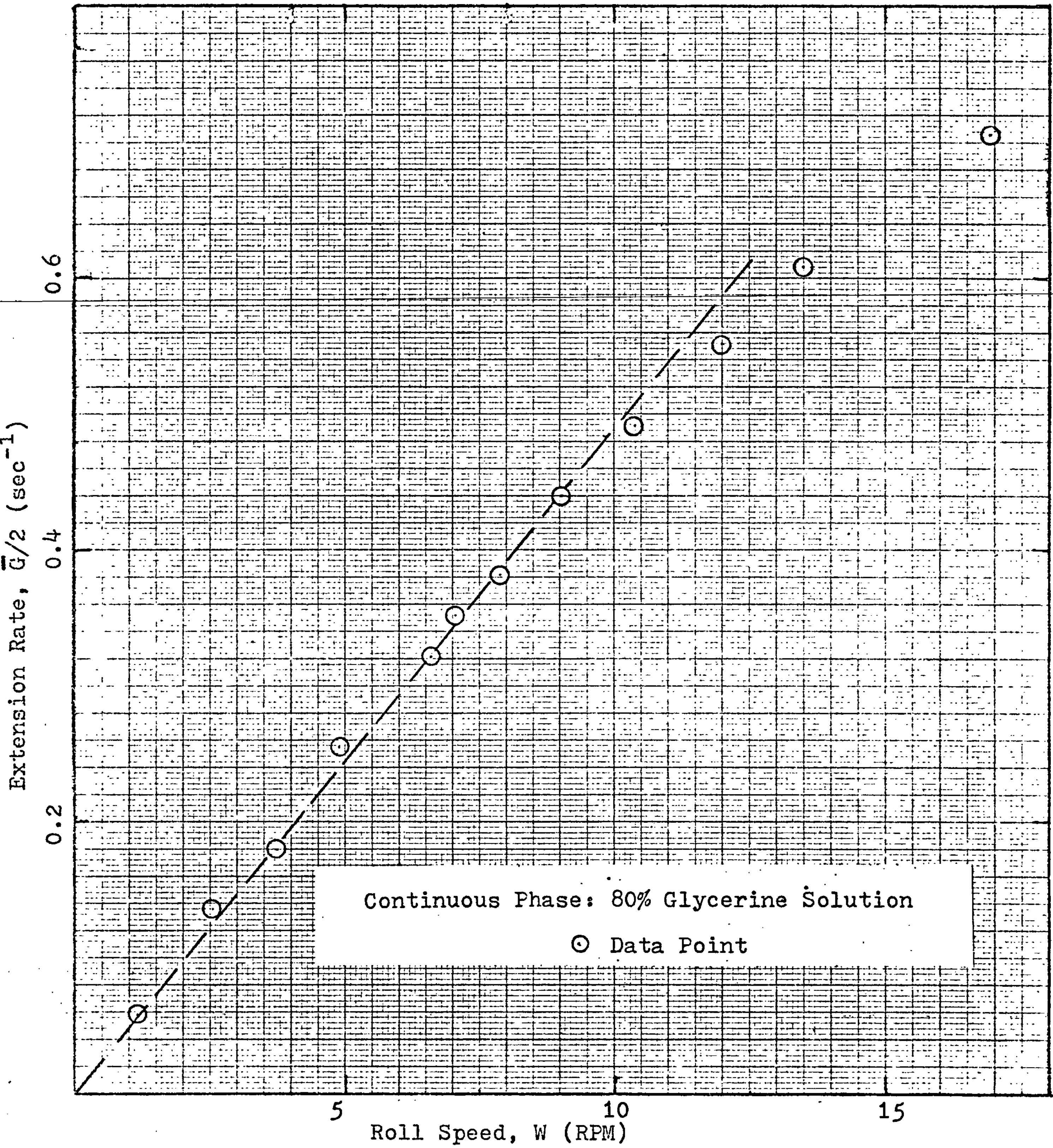


Figure 3-4. Dependence of Extension Rate on The Roll Speed

Continuous Phase: 80% Glycerine Solution

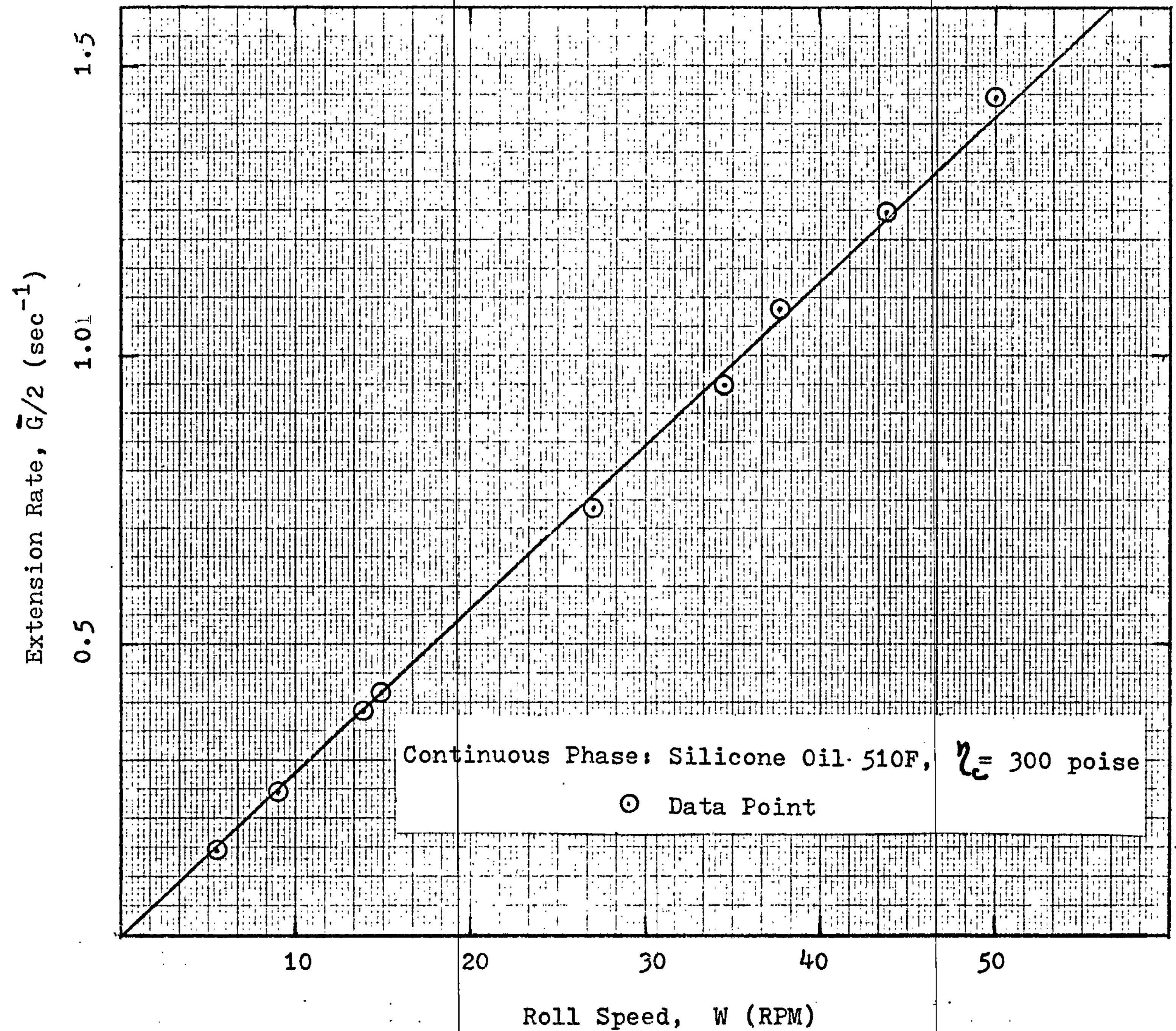


Figure 3-5. Dependence of Extension Rate on The Roll Speed

significantly higher than even the 50 RPM measured here.

In this study, silicone oils with $\eta_c$= 103 poise and 300 poise were used as the continuous phases. The relationships between the roller speed, $W_r$(RPM), and the magnitude of the extension rate, $\bar{G}/2$, are taken as:

$\bar{G}$ (sec$^{-1}$) = 0.0556W Four-roll device (3-3-a)

~~$\bar{G}$ (sec$^{-1}$) = 0.0322W Modified four-roll device (3-3-b)~~

Equation (3-3-b) was derived and experimentally verified by Lee in his dissertation (20). Extension rates from 0.0048 sec$^{-1}$ to 21 sec$^{-1}$ can be obtained with the FRD.

The continuous phase was floated on a heavier, low viscosity fluid (a water-glycerine solution) for the purpose of reducing the end effects of bottom wall. The drop was introduced into the continuous phase by injection from a syringe through the circular window at the center of top wall. By regulating the speed of two drive motors, the drop could be adjusted to the center of the apparatus, which was also the stagnation point of the flow field; The behavior of the drop was observed through a Wild-M7 microscope, which gives a magnification up to 124 times. Photographs were taken with a Nikon PFM still camera connected to the microscope.

## 3-2. Material

Tables 3-2-1 to 3-2-3 show the properties of the fluid systems used in this experimental study. Silicone oil 510 and 200 were used as the continuous phase. Various fluids, including glycerine-water solutions, syrup, molasses, and polymer solutions (Separan AP 30 in

Table (3-2-1). Properties of Fluid Systems (Newtonian Systems)

| Continuous Phase: Silicone Oil 200F $\eta_c$ = 103 poise, $\rho_c$ = 0.97 g/c.c. | | | | | |
|---|---|---|---|---|---|
| System | Drop Phase | $\eta_D$ poise | $\lambda = \eta_D/\eta_c$ | $\sigma$ dyne/cm | $\rho_D$ g/c.c. |
| 1 | Molasses | 2828 | 27.46 | 38.8 ** | 1.45 |
| 2 | " | 353 | 3.42 | 34.6 ** | 1.44 |
| 3 | " | 232 | 2.25 | 33.8 ** | 1.43 |
| 4 | " | 72.8 | 0.707 | 33.5 ** | 1.41 |
| 5 | " | 42.5 | 0.413 | 35.0 ** | 1.40 |
| 6 | " | 30.7 | 0.298 | 37.0 ** | 1.39 |
| 7 | Syrup | 8.8 | 0.085 | 33.7 * | 1.36 |
| 8 | " | 3.4 | 0.033 | 32.0 * | 1.34 |
| 9 | glycerol | 2.59 | 0.025 | 28.5 ** | 1.24 |
| 10 | " | 1.95 | 0.0189 | 29.0 * | 1.24 |
| 11 | " | 0.62 | 0.006 | 26.2 * | 1.22 |

* Drop Deformation Method

** Pendant Drop Method

Table (3-2-2). Properties of Fluid Systems (Newtonian Systems)

| Continuous Phase: Silicone Oil 510F $\eta_c$ = 300 poise, $\rho_c$ = 1.0 g/c.c. | | | | | |
|---|---|---|---|---|---|
| System | Fluid Thread | $\eta_D$ poise | $\lambda = \eta_D/\eta_c$ | $\sigma$ * dyne/cm | $\rho_D$ g/c.c. |
| 12 | Molasses | 2828 | 9.42 | 26.80 * | 1.45 |
| 13 | " | 382 | 12.73 | 28.4 * | 1.44 |
| 14 | " | 232 | 0.77 | 28.5 * | 1.43 |
| 15 | " | 72.8 | 0.24 | 26.5 * | 1.41 |
| 16 | " | 30.7 | 0.10 | 26.0 * | 1.39 |
| 17 | Syrup | 8.8 | 0.03 | 29.5 * | 1.36 |
| 18 | Glycerol | 2.59 | 0.0086 | 20.6 * | 1.24 |

* Drop Deformation Method

Table (3-2-3). Properties of Fluid Systems (Viscoelastic Dispersed Phase)

| Continuous Phase: Silicone Oil 510F $\eta_C$ = 300 poise, $\rho_C$ = 1.0 g/c.c. | | | | | | | | |
|---|---|---|---|---|---|---|---|---|
| Dispersed Phase | $\rho_D$ g/c.c. | $\eta_{oD}$ poise | $\lambda = \eta_D/\eta_C$ | $\lambda_1$ $sec^{-1}$ | $\lambda_{21}$ $sec^{-1}$ | $\alpha_1$ | $\alpha_2$ | $\sigma$ ** dyne/cm |
| 2.0% Sep AP 30 ⁑ | 1.066 | 3364 | 11.2 | 49.5 | 66.5 | 3.04 | 2.71 | 18.5 |
| 1.5% " | 1.058 | 1013 | 3.4 | 35.5 | 30.9 | 2.68 | 2.18 | 22.5 |
| 1.0% " | 1.056 | 381 | 1.27 | 21.0 | 22.0 | 2.56 | 2.10 | 25.0 |
| 0.75% " | 1.056 | 159 | 0.53 | 11.1 | 6.94 | 2.48 | 1.78 | 26.0 |

⁑ In 80-20 Water-Glycerine Solution

** Pendant Drop Method

20-80 glycerine-water solution) were used as the dispersed phase.

The viscosities of the Newtonian fluids were measured with a Weissenberg Rheogoniometer with the temperature controlled at 24.5°C, which was the temperature of the laboratory where the experiments were conducted. The data checked very well with separate measurements using the falling ball method.

The polymer solutions were characterized by the modified Bird-Carreau model (1968), involving 5 parameters, i.e., $\eta_o$, $\lambda_1$, $\lambda_2$, $\alpha_1$, $\alpha_2$. The physical interpretation of these parameters has been explained in the last chapter. This model was used successfully by Flumerfelt (10) in a study of drop breakup of viscoelastic fluids in a simple shear field.

In order to characterize all five material parameters, viscosity-shear rate and normal stress-shear rate data were obtained with the Weissenberg Rheogoniometer with the temperature controlled at 24.5°C. Generally, the lowest shear rate obtainable with this equipment is not low enough to determine $\eta_o$. Consequently, the zero-shear viscosities, $\eta_o$, of the polymer solution were all measured with the falling ball tests with different diameter balls (31). The parameters were then determined by a computer fitting of the B-C model to experimental data. These data and the predicted curves are plotted in Figures (3-6) and (3-7); the fitted parameters are shown in Table (3-2-3).

The interfacial tensions for the Newtonian systems were measured by the drop deformation method (assuming Taylor's Equation (2-10) holds when $D_I$ is small). In checking with pendant drop data obtained as a function of contact time of the phases, it was found

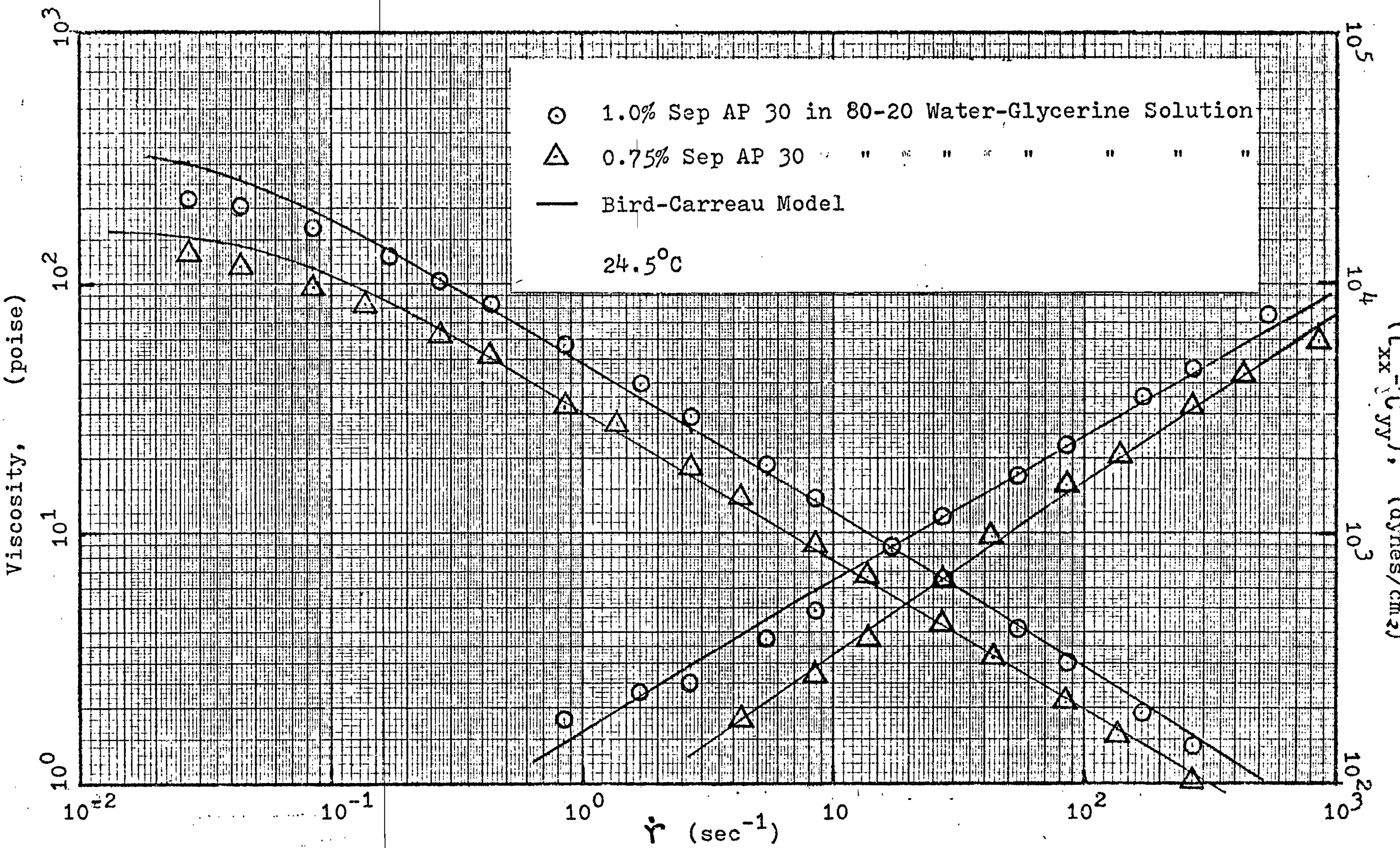


Figure 3-6. Viscosity and Normal Stress Data for Sep AP 30 Solutions

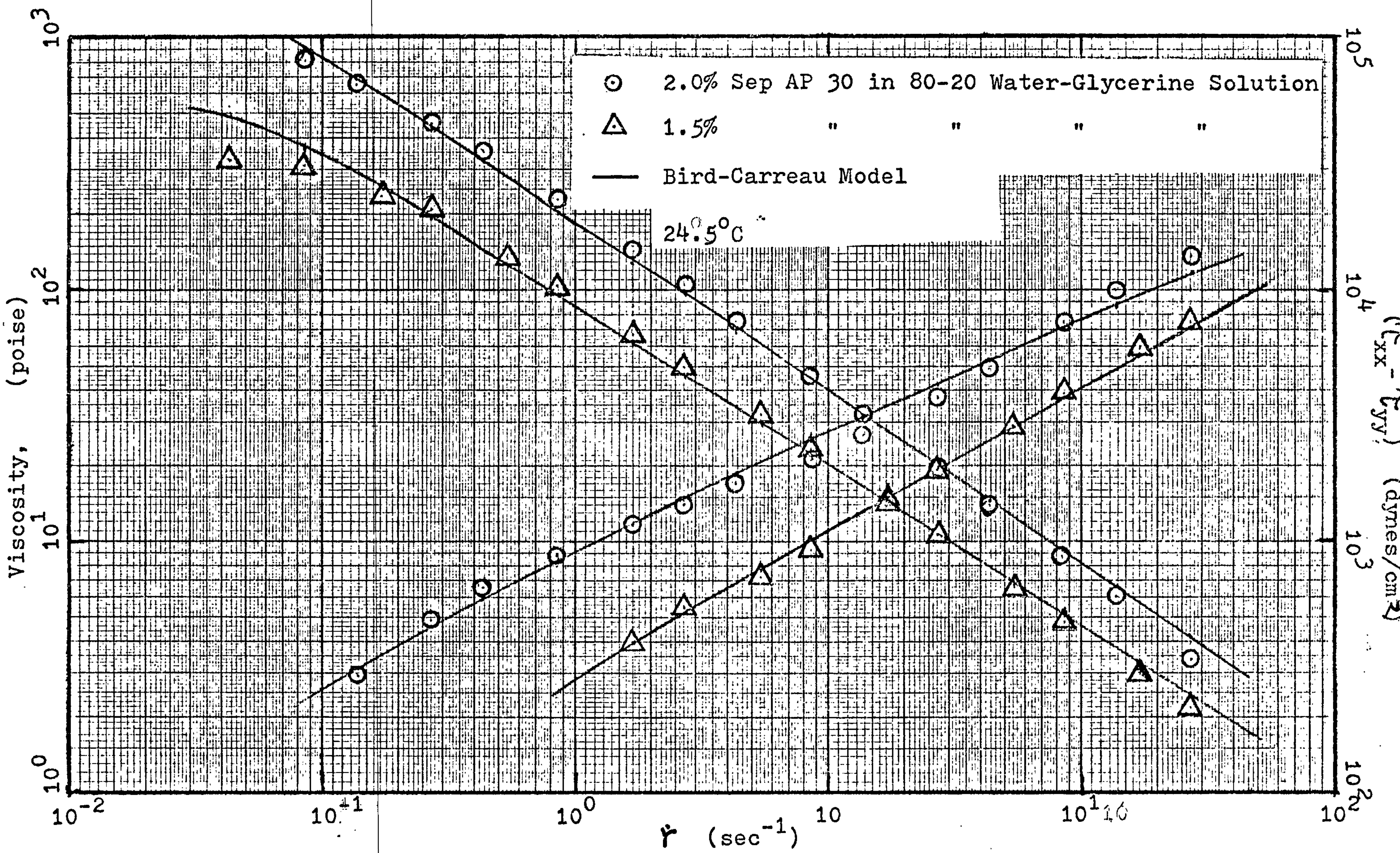


Figure 3-7. Viscosity and Normal Stress Data
For Sep AP 30 Solutions

that the initial contact time value of $\sigma$ should be used, in stead of the final equilibrium value of $\sigma$ (as $t_c \sim \infty$) in the calculation of the dimensionless group $E = \bar{G}a\eta_c/\sigma$ . The reliability of the deformation method, based on Taylor's theory of small deformation, has been established by Rumscheidt and Mason (28).

For the non-Newtonian systems, the interfacial tensions at various contact times were also measured. The interfacial tension value used will be dependent on the contact time of the drop innersed in continuous phase. The $\sigma$ - t data are shown in Figure 3-8. The value corresponding to initial(5 min)contact time was used in the work here. The use of the latter was based on the estimated time which the drops spent in the continuous phase before the breakup experiment was completed.

3-3. Experimental Procedures

Figure 3-9 shows schematically the arrangement of the apparatus used to experimentally examine the drop behavior. The microscope and camera (still or motion) were mounted above the center of apparatus. A lamp was put below the bottom plate to provide the proper illumination. With this arrangement, the drop could be viewed from the top or side. The initial drop size were measured with a cathetometer when $\bar{G} = 0$.

After locating the drop at the center of the apparatus, with the roller speeds being such that $\bar{G} < \bar{G}_c$, the drop was seen to be deformed into a steady ellipsiod shape oriented along X-axis. Every effort was taken to keep the drop at center as long as possible. The drop shape was then photographed with the still camera connected to the

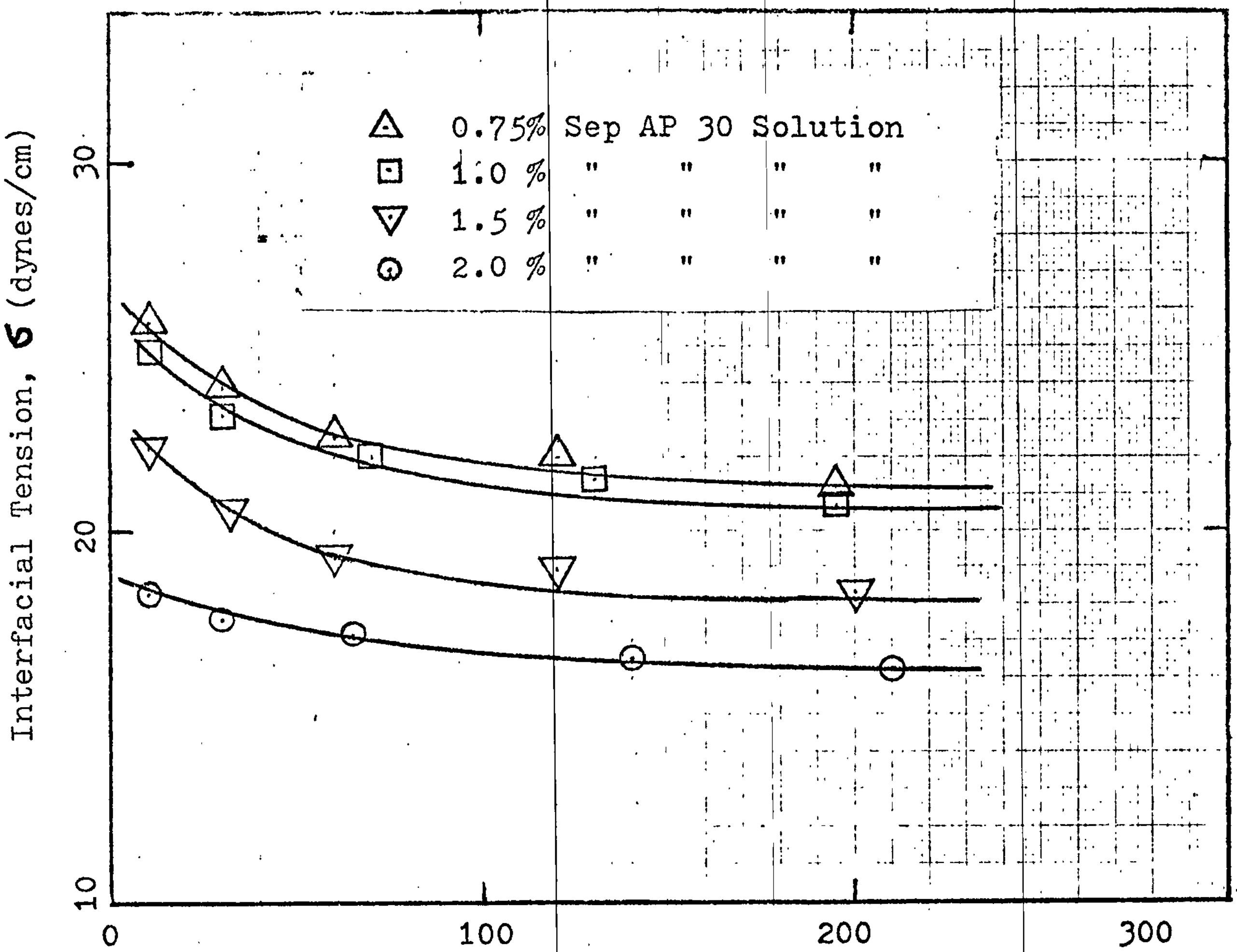


Figure 3-8. Interfacial Tension vs. Contact Time
Sep AP 30 Solution—Silicone Oil 510F

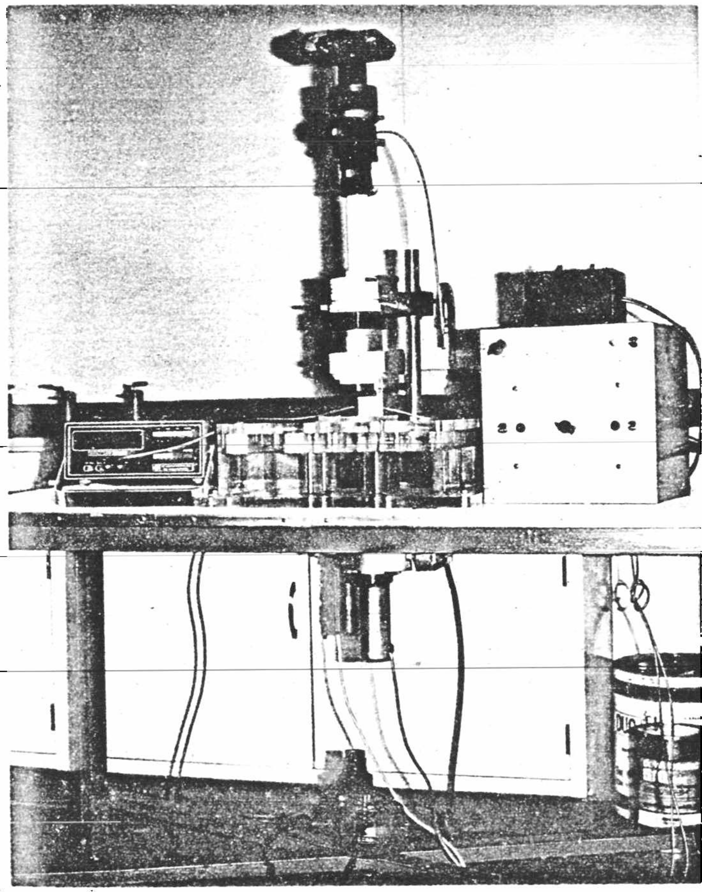

Figure 3-9. The arrangement of Experimental Apparatus

microscope. In Newtonian system, different drop sizes at different extension rates were examined to determine the deformation curves. On the other hand, in non-Newtonian systemm the deformation curves were obtained from measurements on a single drop size only, since, as pointed out in the last chapter, the deformation of viscoelastic drops depends on the T group, which for a given fluid system depends only on the drop size. By holding the diameter constant, we can hold T group constant, and can then determine the deformation as a function of E.

The critical extension rate was determined by inserting a drop into continuous phase, and then gradually increasing the roller speed until the drop became unstable.

# CHAPTER 4

## EXPERIMENTAL RESULTS

### 4-1. Deformation

Drop sizes ranging from 0.05 cm to o.3 cm were used in the experimental study of drop behavior. All Newtonian data were taken with the modified four-roll apparatus (MFRD); the data for the viscoelastic systems were taken with the four-roll apparatus (FRD).

In this section, deformation data for a number of fluid system, both Newtonian and non-Newtonian, will be presented and compared with the theoretical equations of G. I. Taylor, Chaffey and Brenner, and Barthes and Acrivos, in order to check the relative accuracy and range of applicability of these theories. Where possible, the relative effects of the physical properties will be specified and demonstrated.

A drop when suspended in the center of a hyperbolic flow field will be distorted into an ellipsoidal shape when viewed along the Z-axis, and its major axis will be along the X-axis and its minor axis along the Y-axis. In a simple shear field ($V_x = \overline{G}Y$), the major and minor axes are rotated $45^o$ from the orientation in the plane hyperbolic flow field. The deformation defined by Equation (2-9), increases with extension rate, $\overline{G}/2$, until a sharply defined critical value, $\overline{G}_C$, is reached, above which the drop bursts. Different drop deformation and breakup mechanisms were observed with Newtonian systems of different viscosity ratios. When $\overline{G} > \overline{G}_C$ and $\lambda < 0.5$, the ends of the drop drew out into sharp points from which small droplets of disperse phase were released. When $\overline{G} > \overline{G}_C$

and $\lambda > 0.5$, in stead of developing pointed ends, the drop was pulled out into a thread, which increased in length until its diameter reached the order of $10^{-3}$ cm. However there is no sharp boundary between these two cases (Fig. 4-1). The deformation of a viscoelastic drop is similar to that of a Newtonian drop, but the mechanism of bursting into thread is somewhat different. The pointed end phenomenon was also observed in case of viscoelastic drops, however it happened even when $\lambda = 11.2$ (2.0% Sep AP 30 solution), and , instead of releasing droplets from the pointed ends, the drop increased its length until the onset of burst. This is quite different from a Newtonian drop. Figure (4-2). shows the deformation of a viscoelastic drop (2.0% Sep AP 30 solution) under various extension rates up to breakup.

4-1-1. <u>Deformation of Newtonian Drops</u>

Quantitative measurements of deformation of six fluid systems were taken, and the results were represented in terms of the deformation parameter, $D = (L-B)/(L+B)$, and the dimensionless group, E.

Figures (4-3) to (4-8) show the experimental deformation data of six systems. A linear relation between D and E were observed in each case when D small, i.e., at small extension rates. If we assume Taylor's linear equation holds in this region, then the interfacial tension can be determined from the slope of the linear portion by means of Equation (2-10). This method has been shown reliable by Rumscheidt and Mason (1966).

In order to show the reliability of this method, interfacial

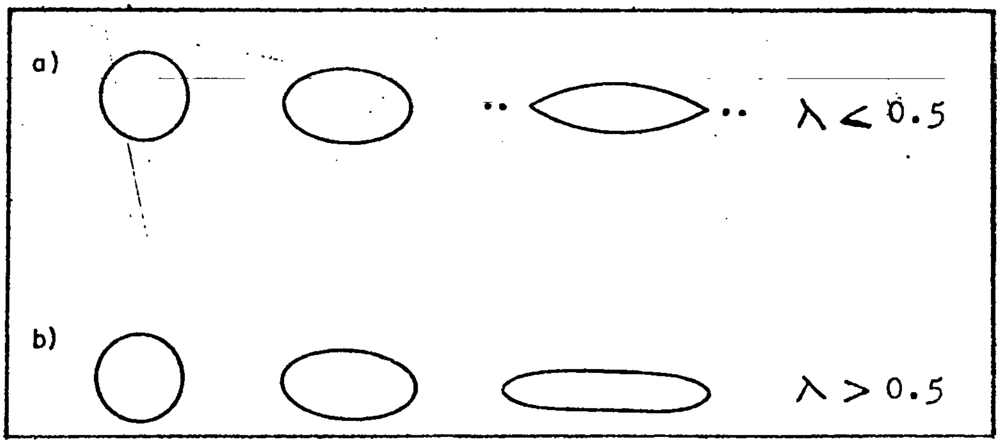


Figure 4-1. Typical Observation of Deformation and Burst of Drops in Plane Hyperbolic Flow Field

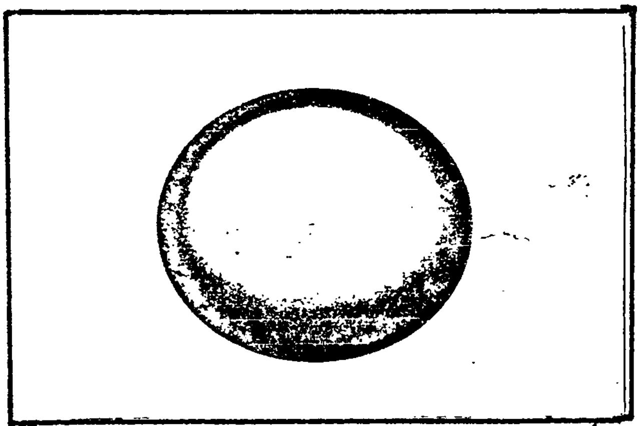

$2a=0.1163$ cm, $\overline{G}/2 = 0.0298 \text{ sec}^{-1}$

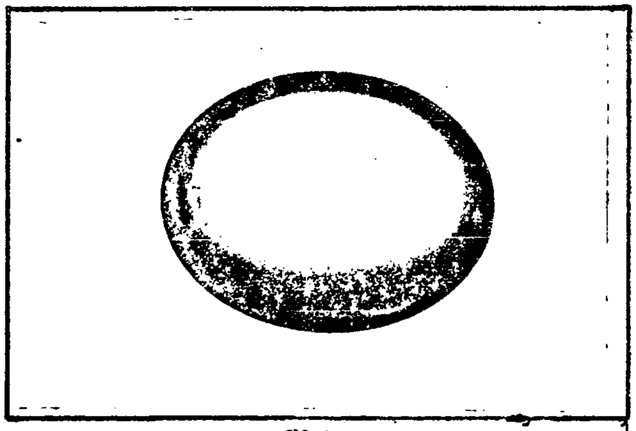

$2a=0.1163$ cm, $\overline{G}/2 = 0.0506 \text{ sec}^{-1}$

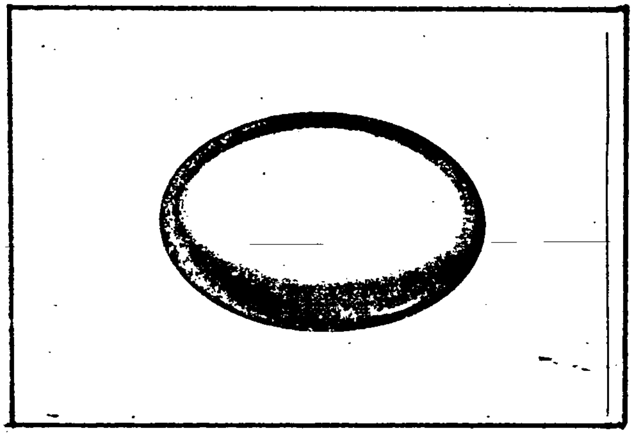

$2a=0.1163$ cm, $\overline{G}/2 = 0.0790 \text{ sec}^{-1}$

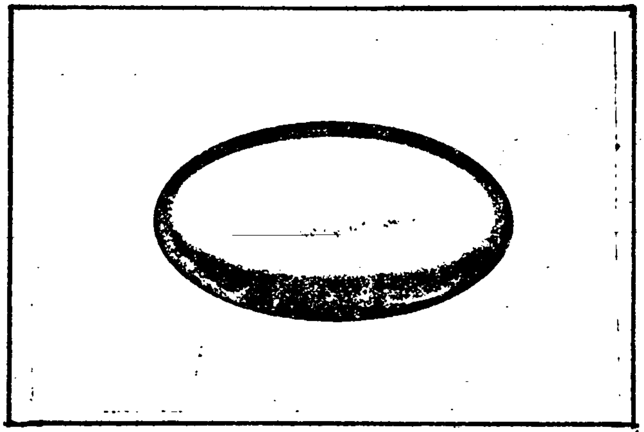

$2a=0.1163$ cm, $\overline{G}/2 = 0.1005 \text{ sec}^{-1}$

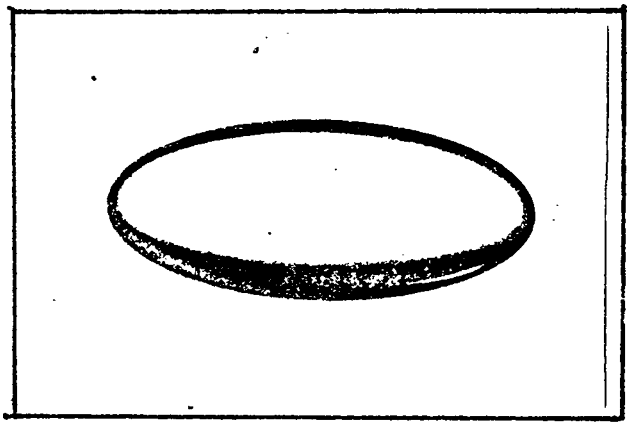

$2a=0.1163$ cm, $\overline{G}/2 = 0.1189 \text{ sec}^{-1}$

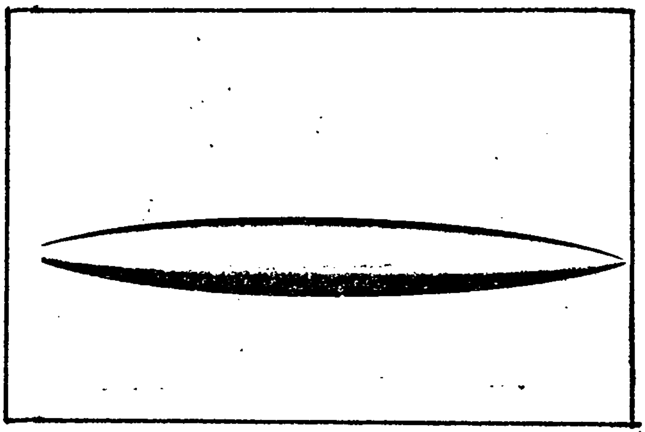

$2a=0.1163$ cm, $\overline{G}/2 = 0.1375 \text{ sec}^{-1}$

Figure 4-2. Deformation of a Viscoelastic Drop at Various Extension Rates up to Breakup (2.0% Sep AP30)

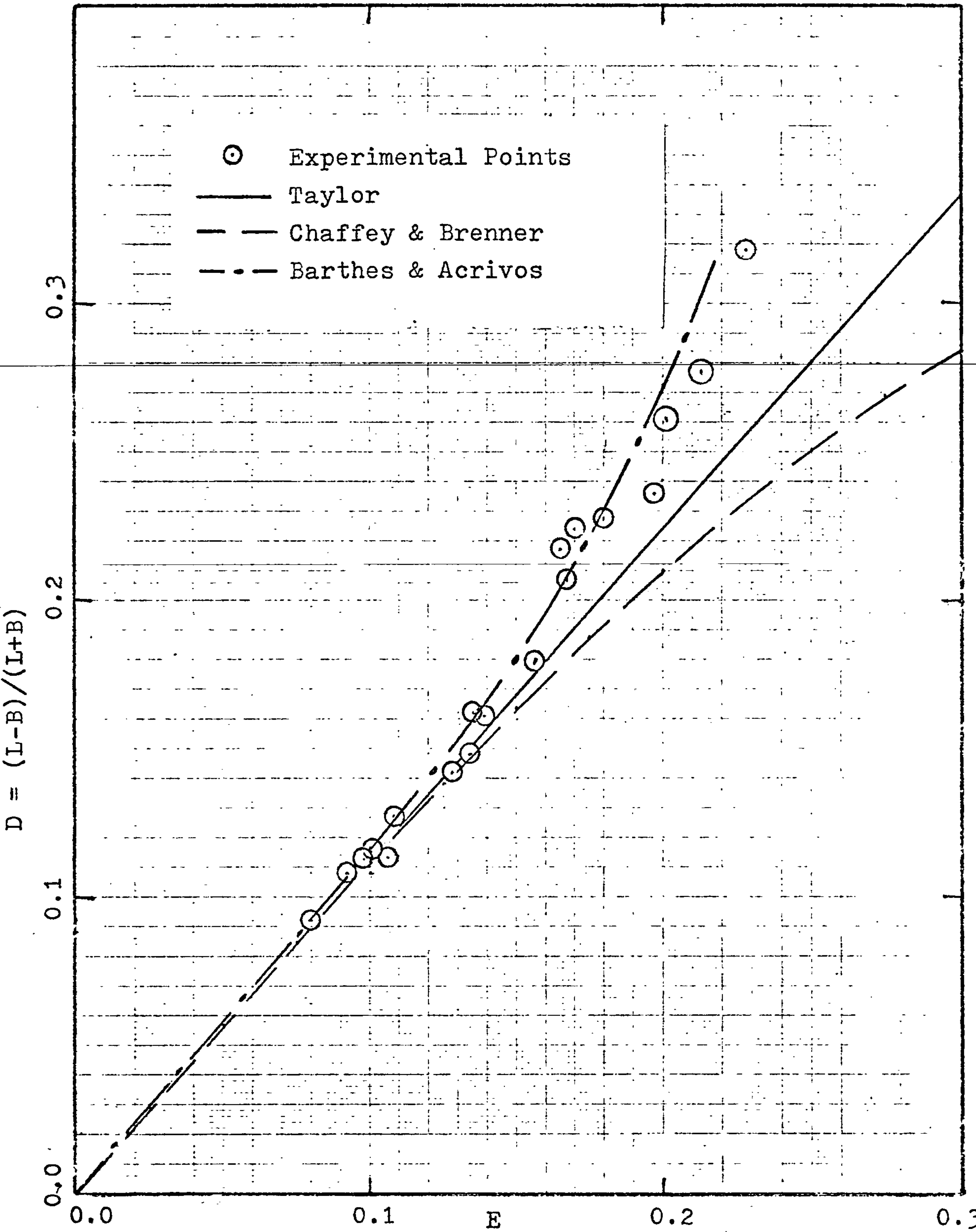


Figure 4-3. Experimental Deformations and Theoretical Lines For Fluid System 2 ($\lambda = 3.42$)

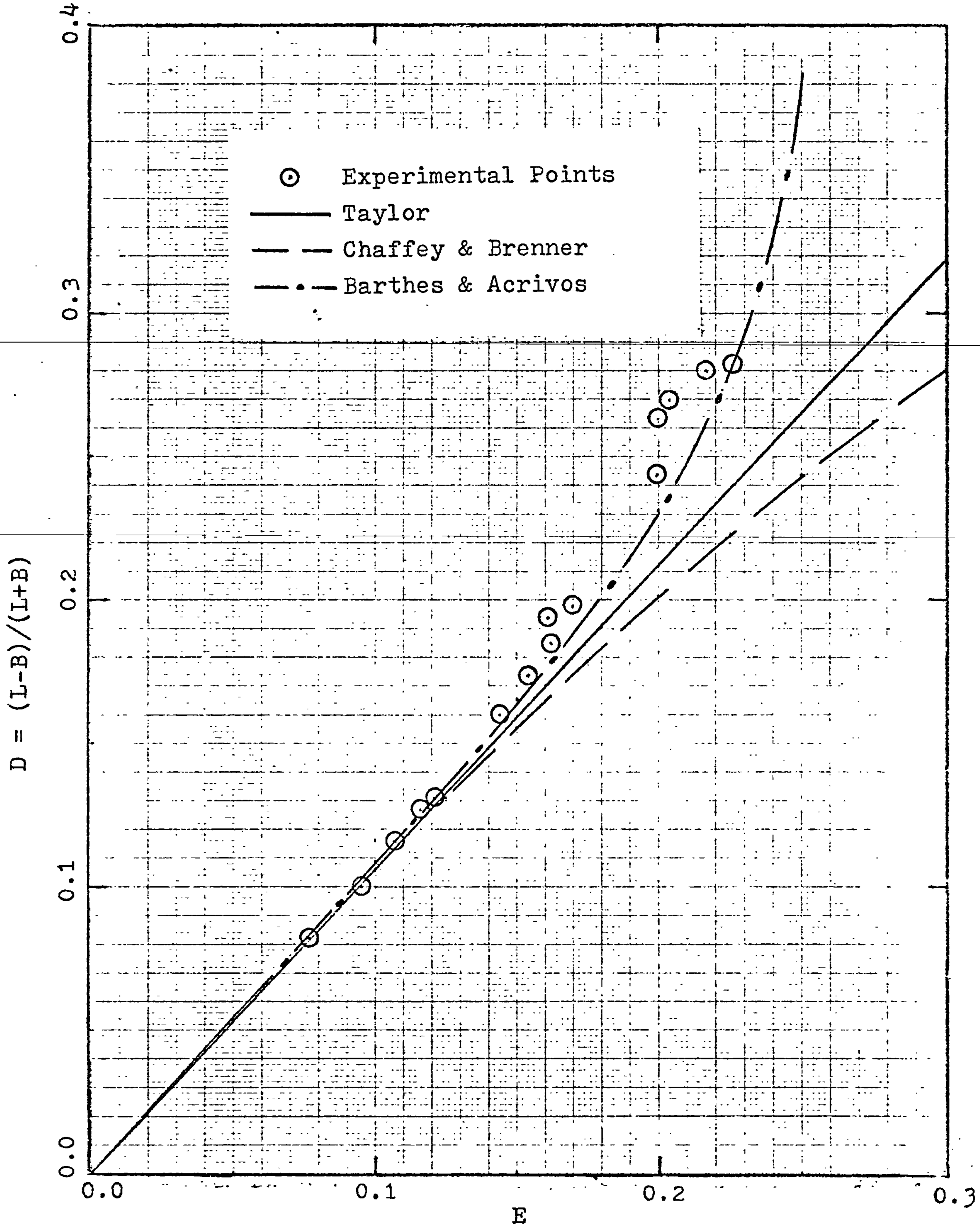


Figure 4-4. Experimental Deformations and Theoretical Lines for Fluid System 4 ( $\lambda$ = 0.707)

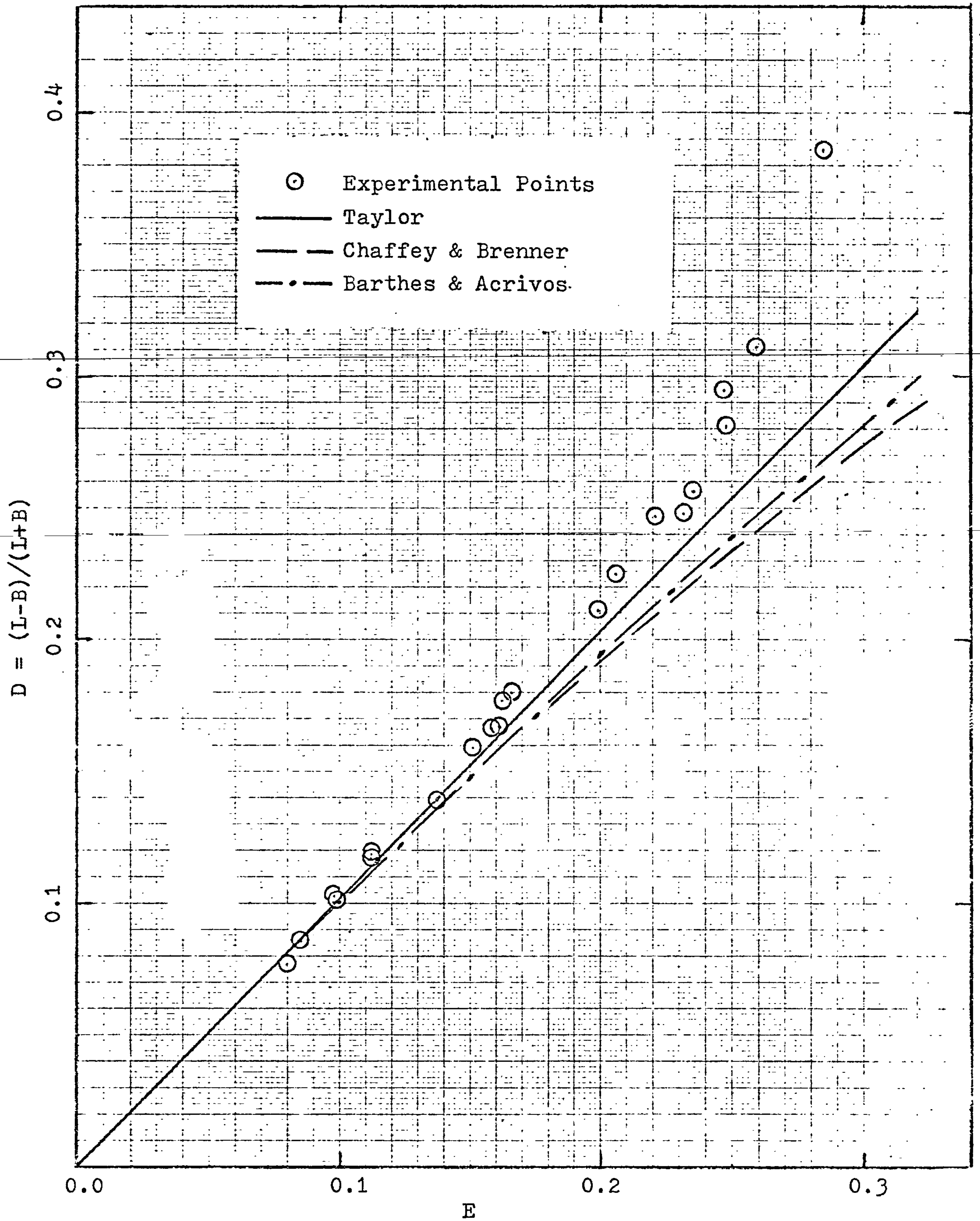


Figure 4-5. Experimental Deformations and Theoretical Lines for Fluid System 7 ( $\lambda$ = 0.085)

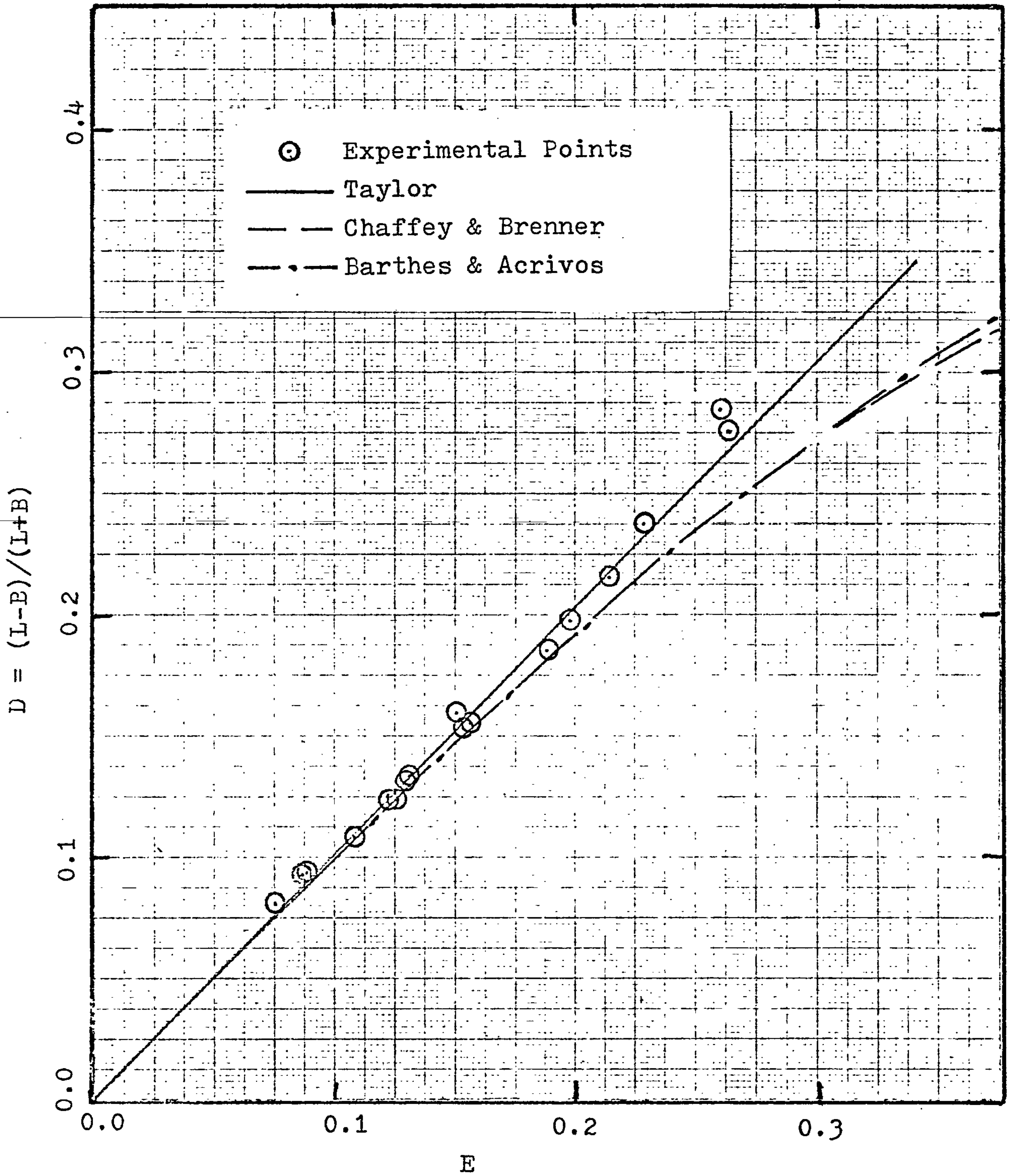


Figure 4-6. Experimental Deformations and Theoretical Lines for Fluid System 8 ( $\lambda$ = 0.033)

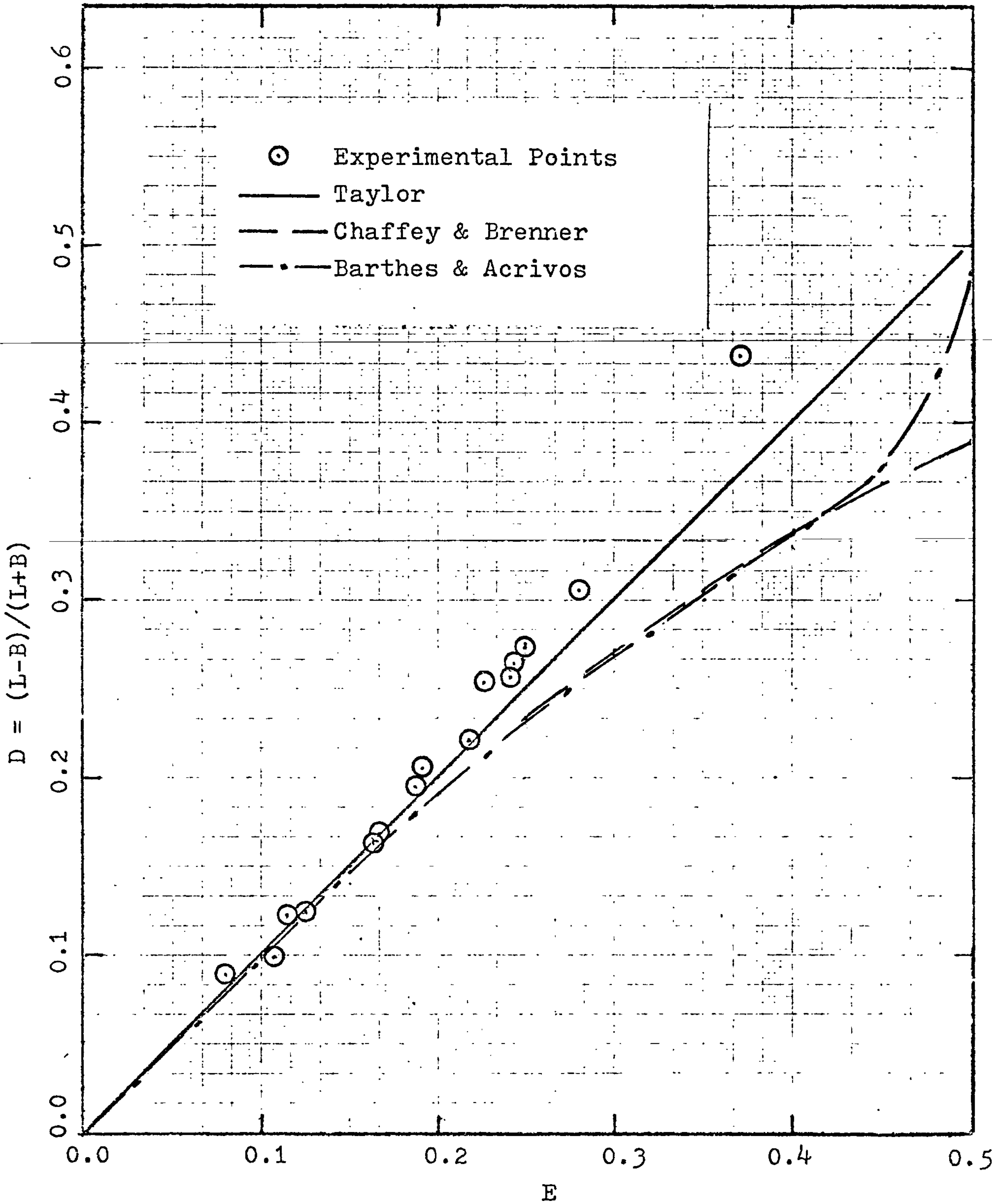


Figure 4-7. Experimental Deformations and Theoretical Lines for Fluid System 10 ( $\lambda$ = 0.0189)

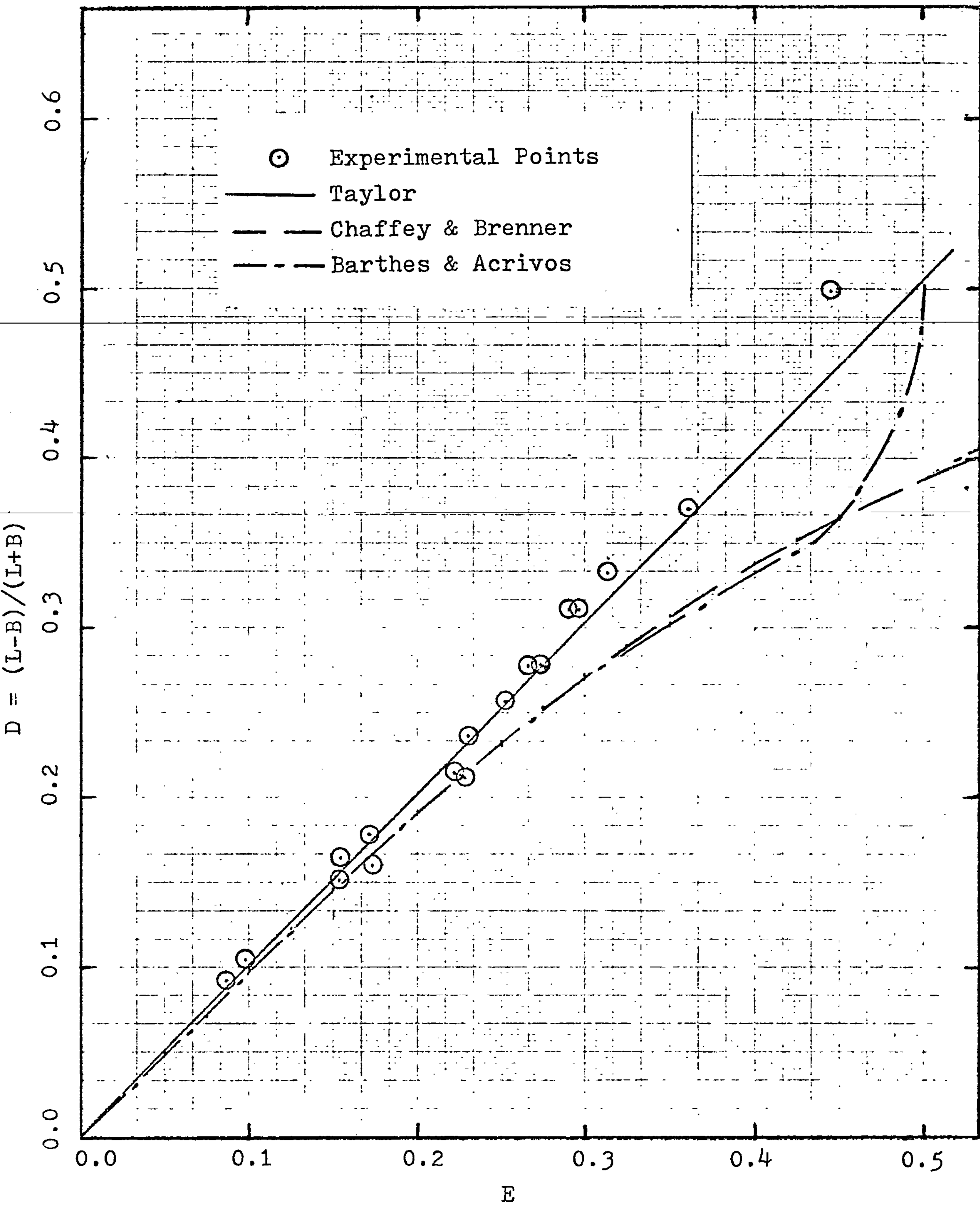


Figure 4-8. Experimental Deformations and Theoretical Lines for Fluid System 11 ( $\lambda = 0.006$)

tensions of two fluid systems at various interphase contact times were measured using the pendant drop method. The drop shape was photographed with the system described in the last chapter. The resulting slides were then projected on a wall to make accurate determinations on drop shape; the magnification was in the order of 60 to 80. The interfacial tension values obtained with the deformation method are shown in Fig. (4-9). As seen, the initial contact values from the pendant drop method agree quite well with those from the deformation method.

The circled dots in Figures (4-3) to (4-8) show the deformation results calculated with the interfacial tensions corresponding to zero contact time. Curves corresponding to Equation (2-10), (2-12), and (2-14) are also shown on each plot. It can be seen that the experimental data match very well with these theoretical curves for small values of E, but deviate away from the curves of Taylor, and of Chaffey and Brenner as E gets higher, and in fact in a reverse trend from that predicted by Chaffey and Brenner. The agreement with Acrivos' theory depends on the fluid systems, i.e., on the viscosity ratios. The agreement is good for systems 2 and 4 ($\lambda$= 3.4 and 0.707). However, the deviations are quite significant for systems 7, 8, 10, and 11, where E can become quite large.

To summarize, the second order theory developed by Chaffey and Brenner does not appear to provide a better approximation than the first order theory of Taylor. Acrivos' theory is quite good when $\lambda \geqslant 0.7$, but completely fails to describe the deformation for systems with small $\lambda$ or alternately, in systems where large E values are required before significant deformation occurs.

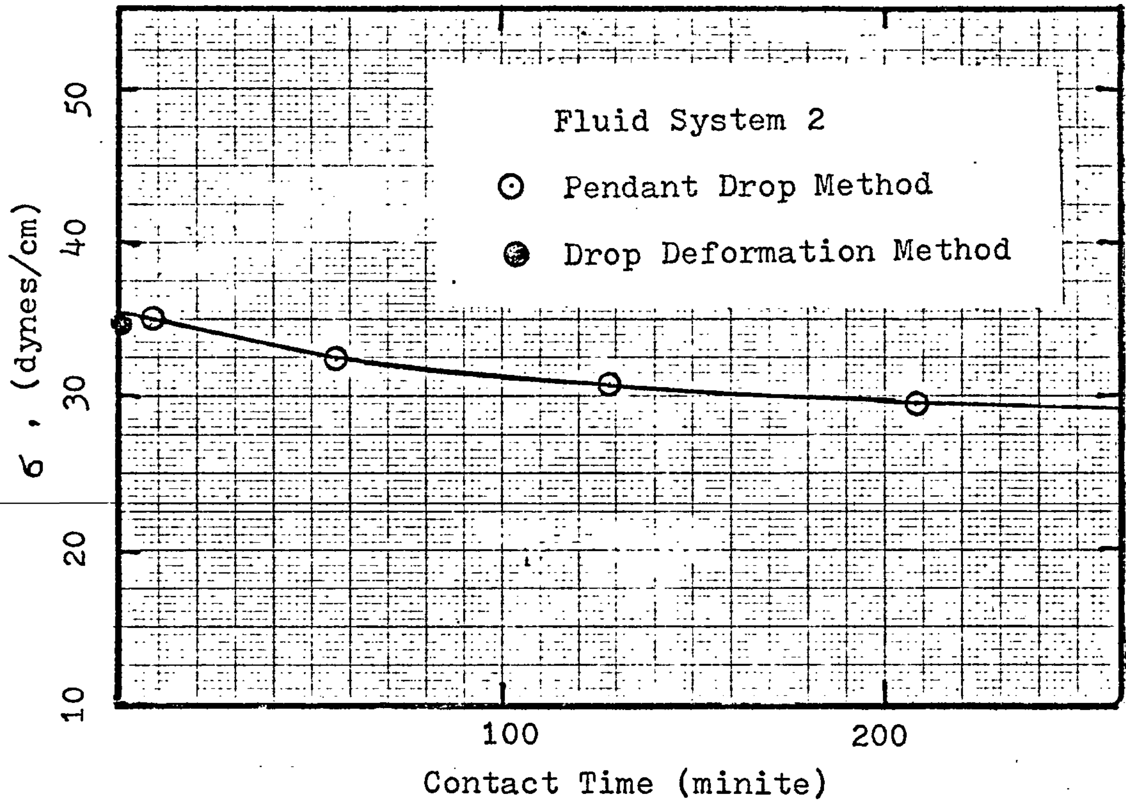


Figure 4-9a. Interfacial Tension vs. Contact Time

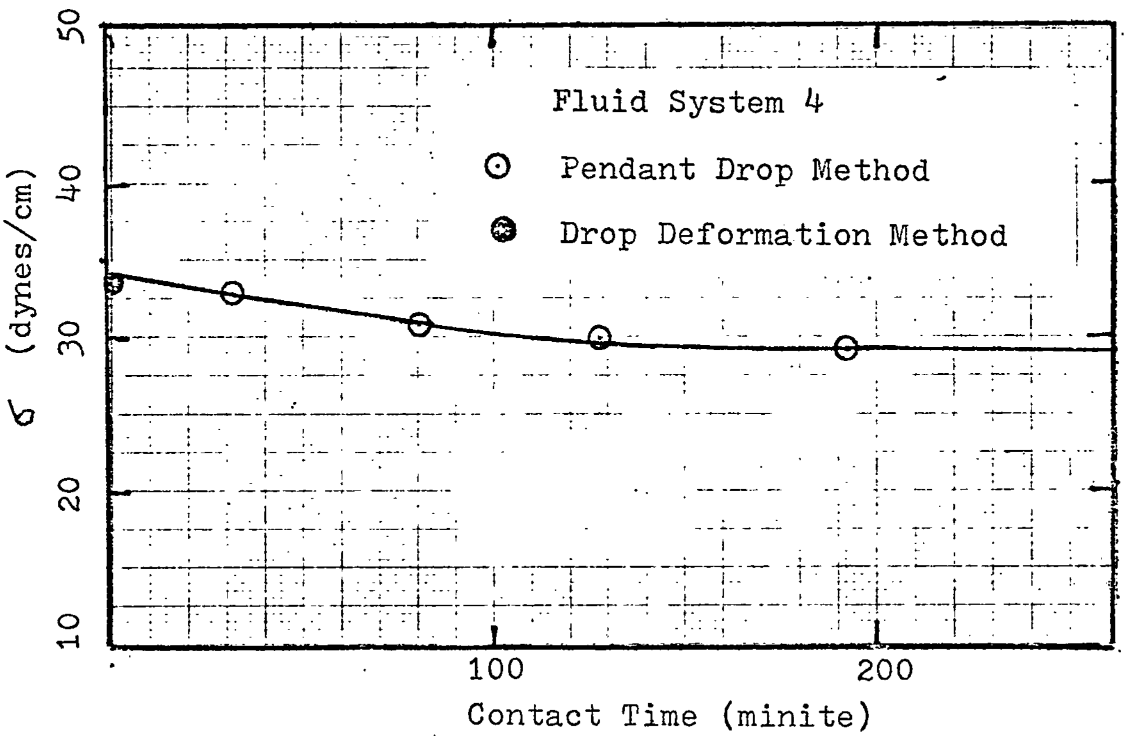


Figure 4-9b. Interfacial Tension vs. Contact Time

It is quite interesting to find that Taylor's Equation (Eq. (2-10)) works fairly well as D goes up to about 0.2 for $\lambda = 3.42$ and about 0.35 for $\lambda = 0.006$, although this theory was derived for small deformation of nearly spherical drops.

There is a steep increase of the deformation group D, which occurs approximately when D = 0.35 $\sim$ 0.55 for $\lambda$ changing from 0.0189 to 3.42, and about 0.6 $\sim$ 0.7 for $\lambda = 0.006$. Therefore, the value $D_c = 0.5$, which was estimated by Taylor is not strictly correct; however, it is surprisingly good considering it results from a small deformation theory.

4-1-2. Deformation of Viscoelastic Drops

No theoretical relation has been derived for the deformation of viscoelastic drops. In this case, we use the dimensionless representations given in Chapter 2. In particular, we have

$$D = D\left(\bar{\xi} a \eta_c / \sigma,\ \eta_{oD}/\eta_c,\ \frac{\lambda_1 \sigma}{a \eta_c},\ \alpha_1\right)$$

For a given fluid system, $\eta_{oD}/\eta_c$, $\alpha_1$ are fixed, and E and $\frac{\sigma\lambda_1}{a\eta_c}$ will depend on the experimental conditions, that is, the extension rate and drop diameter. Consequently, the deformation data for the viscoelastic drop case shall be given with both E and $\frac{\sigma\lambda_1}{a\eta_c}$ specified in each case.

The interfacial tension corresponding to initial contact time was used in each case, and the experimental data are shown on Figures (4-10) to (4-12). In each Figure, two deformation curves with different $\frac{\lambda_1\sigma}{a\eta_c}$ values are shown. It is worthwhile to point out that, in all three fluid systems shown, data with di-

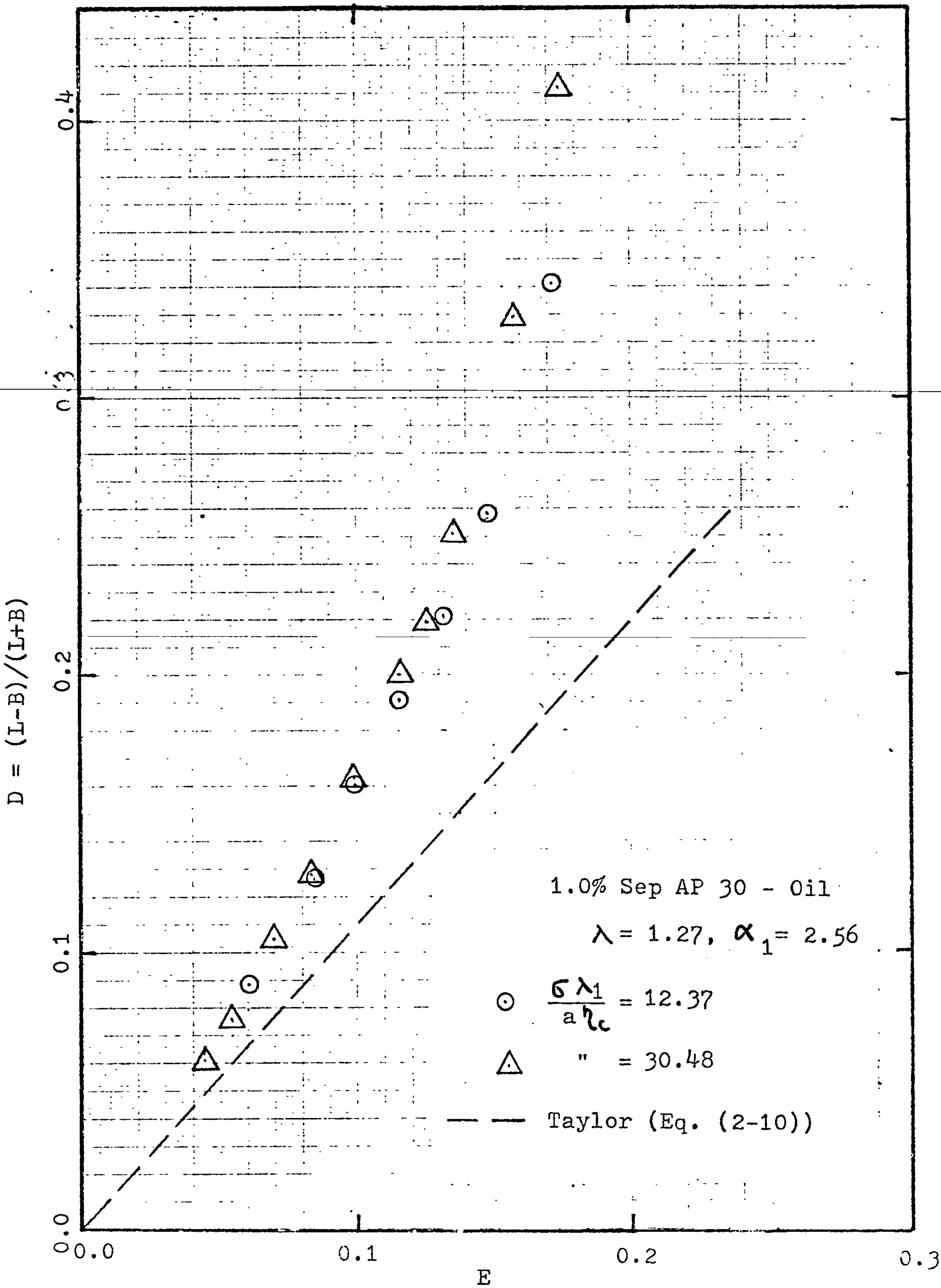


Figure 4-10 Experimental Deformation vs. E for 1.0% Sep AP 30 Solution

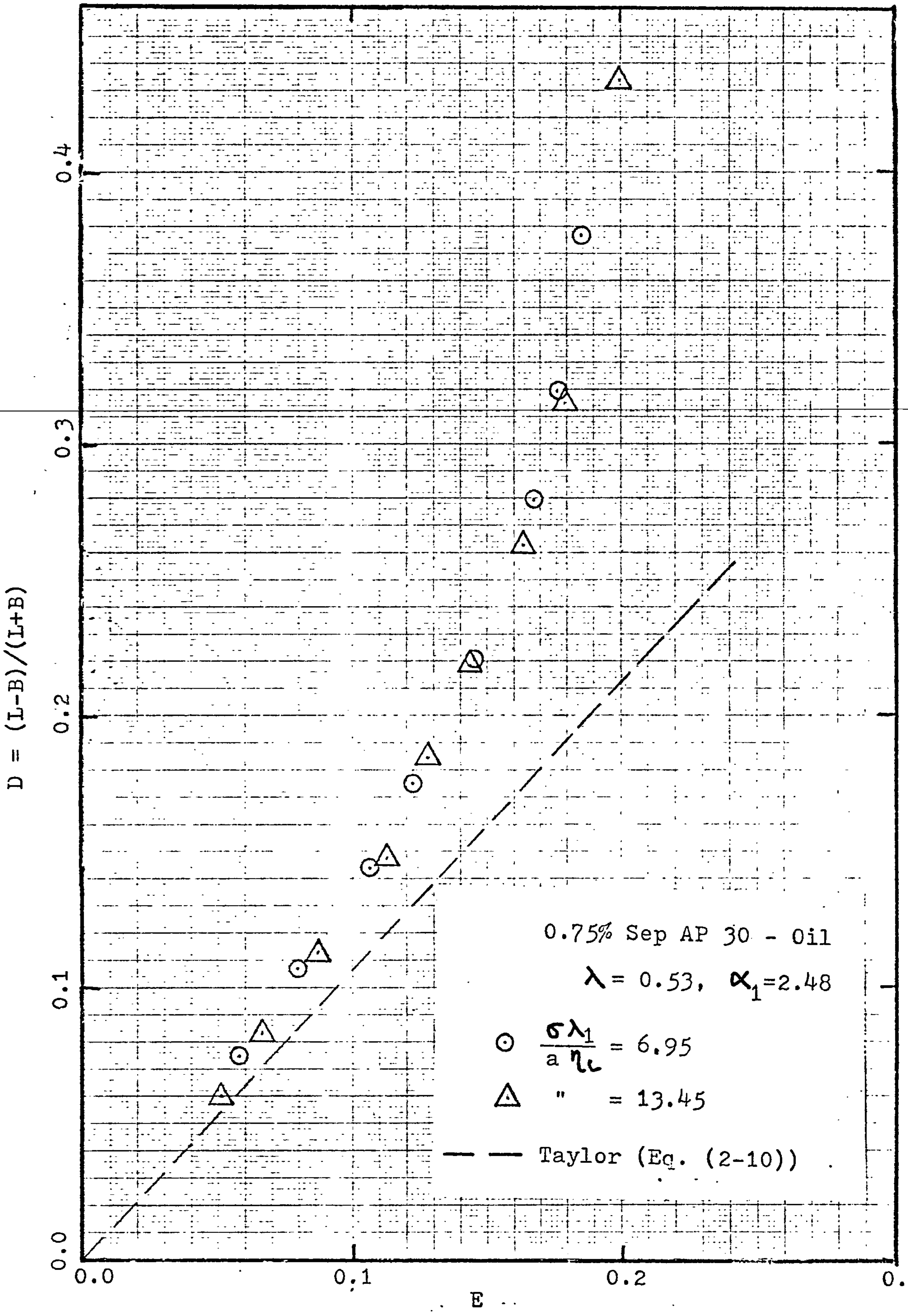


Figure 4-11 Experimental Defortions vs. E

for 0.75% Sep AP 30 Solution

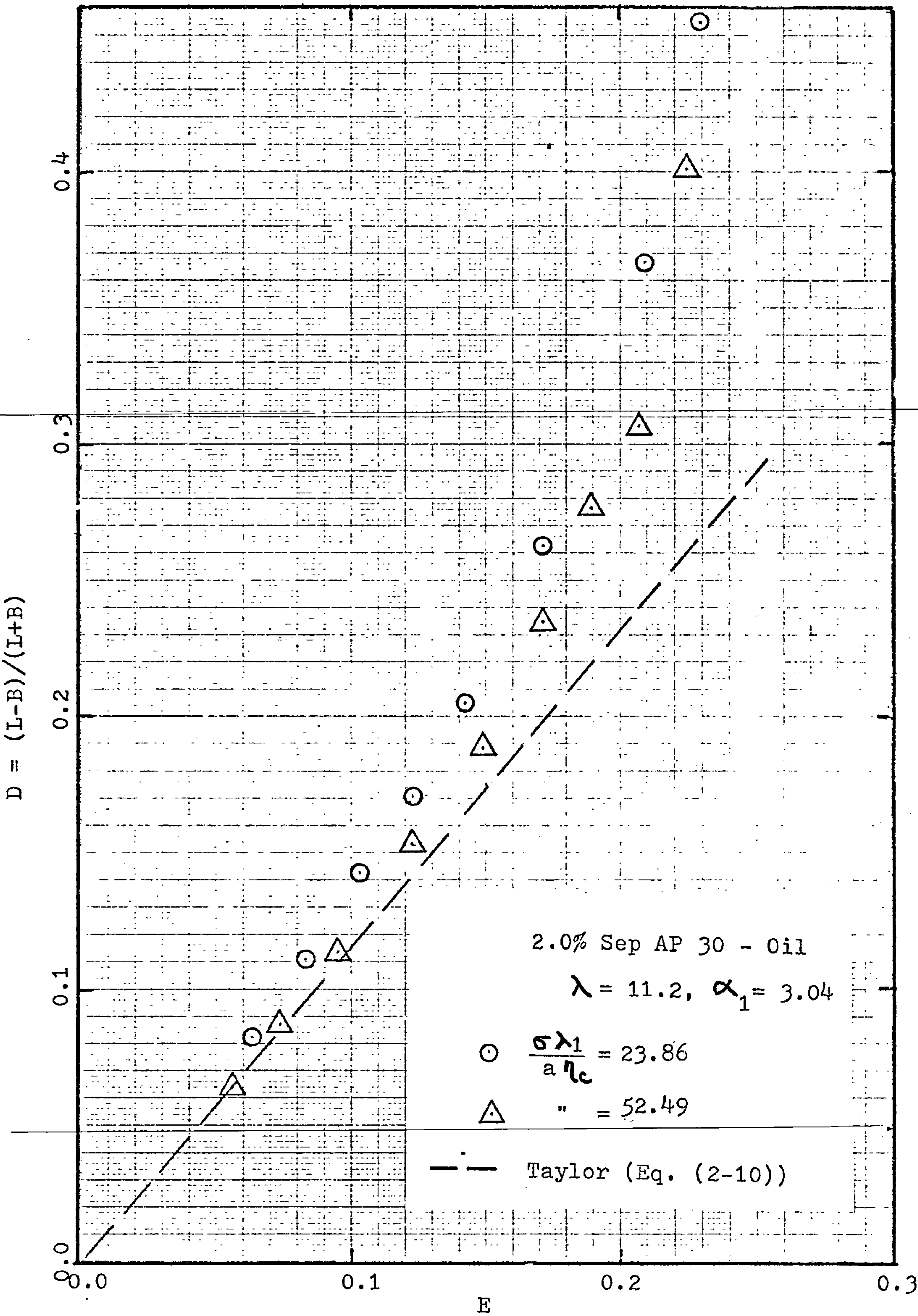


Figure 4-12 Experimental Deformations vs. E
2.0% Sep AP 30 Solution

fferent $\frac{\sigma\lambda_1}{a\eta_c}$ , i.e., with different drop sizes, fall on the same linear line when the dimensionless group, E, is small, especially, for the 0.75% and 1.0% Sep AP 30 solution cases. This seems to indicate that within this range of E, the non-Newtonian effects are negligible. In other words, Taylor's linear equation for Newtonian systems would be applicable in this range, with $\lambda = \eta_{oD}/\eta_C$. With this in mind, Equation (2-10) was also shown in each plot. The comparison between the data and the curve seems to confirm what we expected. As $\bar{G}\eta_c a/\sigma$ gets large, the data , corresponding to different $T' = \frac{\lambda_1\sigma}{a\eta_c}$ values, start to depart slightly from each other in each system. This effect can also be demonstrated in the breakup experiment, as will be shown in the next section. The value of deformation where the breakup process begins is generally in fair agreement with $D_c = \frac{1}{2}$ given by Taylor's analysis for Newtonian systems.

4-2. Drop Breakup Results

4-2-1. Newtonian Systems

It had been shown both theoretically and experimentally that deformation of a Newtonian system depends upon $\lambda$ and E only, and increases sharply as E approaches a certain value. Therefore, for a given fluid system with a fixed viscosity ratio, there must be a critical value of E, say $E_c$, above which the unstable condition in drop deformation will consequently result in breakup of the drop. Remenbering that E is the ratio of viscous forces to interfacial forces, we, therefore, expect that large drop size, high continuous phase viscosity, high extension rate, $\bar{G}/2$, and small interfacial tension, $\sigma$ , will be associated with an easily dispersed system. This can be explained and confirmed with the experimental results which gave an almost constant critical $E_c$ with different drop diameters for given fluid systems. Figure 4-13 shows the constancy of $E_c$ with various combinations of drop sizes for fluid system 4.

All of the breakup results with the 11 fluid systems are given in Table 4-2-1 and plotted in Figure 4-14 in accordance with Equation (2-26-a) in chapter 2. The critical value, $E_c$, shown here for each system is an average value of several experimental data like those illustrated in Figure 4-13. The average percent deviations from the mean value are also shown in the Table, the later being calculated from

$$\Delta E_c \% = \frac{1}{N} \sum \frac{|E_{ci} - E_c|}{E_c}$$

where N is the number of individual experimental points taken, and $E_{ci}$, the critical E corresponding to each point, and $E_c$, the average value of $E_{ci}$.

The results are also plotted in Figure 4-14 on a log-log scale with $E_c$ and $\lambda = \eta_D/\eta_c$ as coordinates. The few data points taken by G. I. Taylor and by Rumscheidt and Mason are also added on this plot. These data fall on a curve, which shows a minimum in $E_c$ at viscosity ratio somewhere between 1 and 2, with a slow increase in $E_c$ as $\lambda$ is decreased from 1 down to 0.006, and a similar slow increase in $E_c$ as $\lambda$ is increased from 2 or up. The minimum value of $E_c$, according to Figure 4-14 is approximately equal to 0.22. In order to compare these data, the corresponding

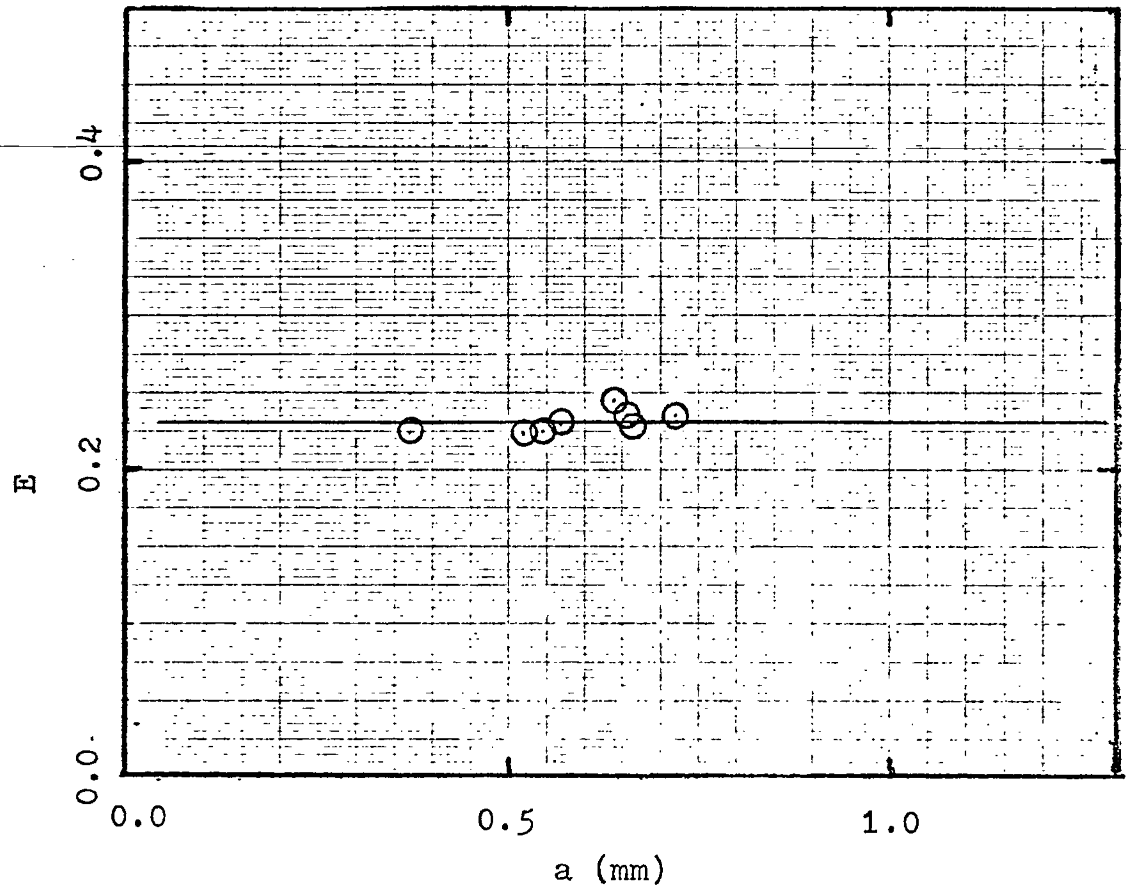


Figure 4-13 Constancy of $E_c$ With Different Drop Radii
Fluid System 3 ( $\lambda$ = 2.25 )

Table 4-2-1. Experimenatal Data of Drop Breakup of Newtonian Fluid Systems

| Fluid System | $\lambda$ | $E_C$ | Deviation % | Range of Diameter (cm) |
|---|---|---|---|---|
| 1 | 27.46 | 0.263 | 2.2 | 0.09-0.14 |
| 2 | 3.42 | 0.241 | 2.0 | 0.10-0.15 |
| 3 | 2.25 | 0.233 | 2.8 | 0.07-0.14 |
| 4 | 0.707 | 0.249 | 2.5 | 0.11-0.16 |
| 5 | 0.413 | 0.237 | 1.8 | 0.12-0.17 |
| 6 | 0.298 | 0.243 | 2.3 | 0.11-0.18 |
| 7 | 0.085 | 0.326 | 1.6 | 0.12-0.16 |
| 8 | 0.033 | 0.362 | 1.7 | 0.13-0.18 |
| 9 | 0.025 | 0.430 | 2.5 | 0.11-0.20 |
| 10 | 0.0146 | 0.445 | 1.9 | 0.13-0.18 |
| 11 | 0.0060 | 0.493 | 1.1 | 0.13-0.22 |

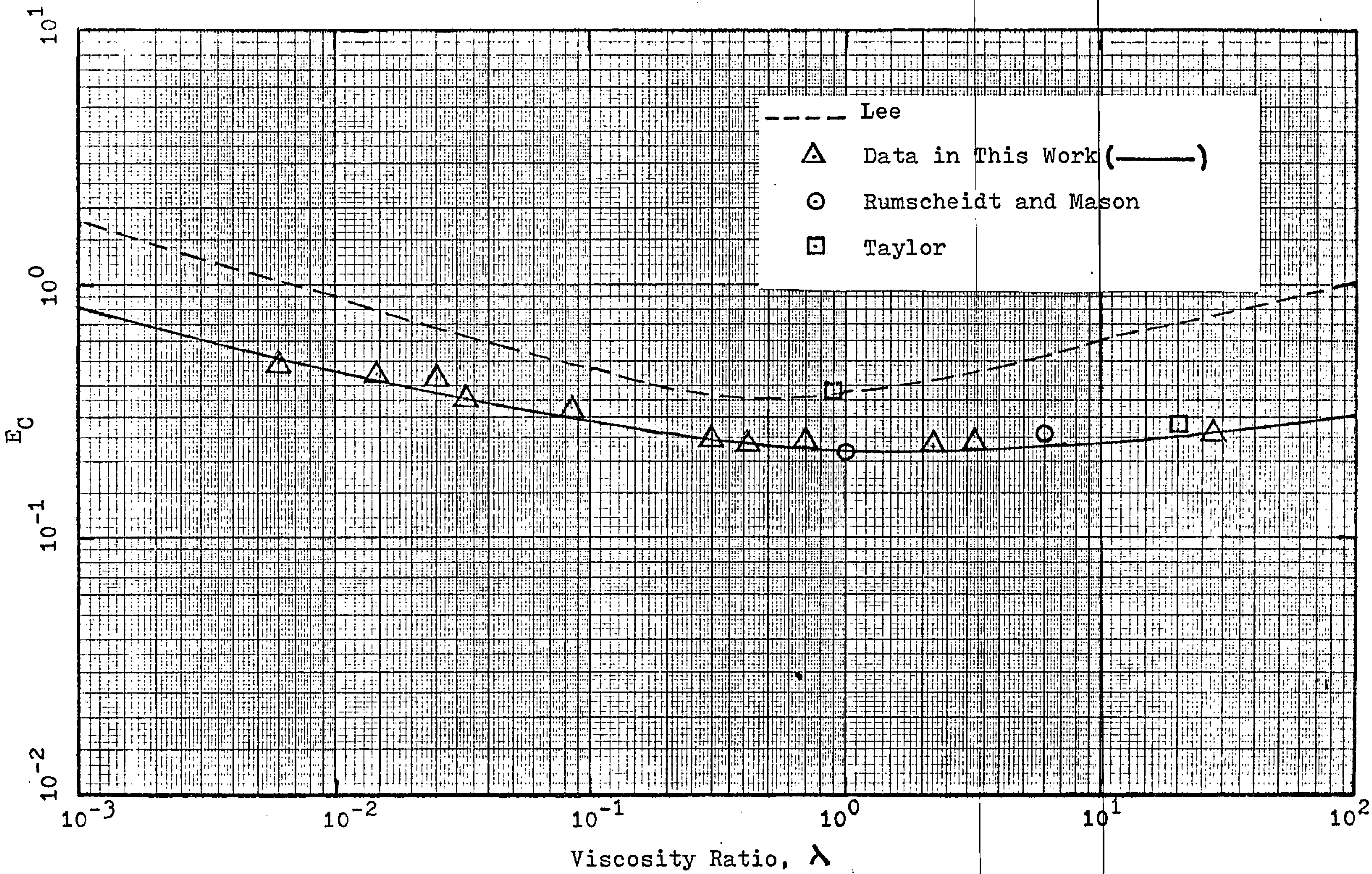


Figure 4-14. Effect of Viscosity Ratio On $E_C$ Required for Drop Breakup in Plane Hyperbolic Flow Field

experimental curve obtained by W. K. Lee (1972) is also shown in Figure 4-14. Lee's data fall onto an envelope curve above that obtained in this study, and show a minimum $E_c$ (about 0.35) at the range of $\lambda$ from 0.1 to 1, with higher increase rate in $E_c$ at both high and low ends of $\lambda$. This difference, I believe, is due to the end effect, since Lee did not float his quite high viscosity (100 ~ 300 poise) continuous phase on a heavier low viscosity fluid to reduce the wall effect caused by the bottom plate.

Similar experimental data, but in a simple shear flow field, has been reported by several investigators. A comparison is shown in Figure 4-15. It is interesting to note that the minimum value of $E_c$ in a plane hyperbolic flow field is only one-third of that (about 0.6) observed in a simple shear field, and that there is a limitation of the range of $\eta_D/\eta_C$ for possible drop breakup in simple shear fields ($\lambda <$ 3.5). The ratio of $E_c$ in a plane hyperbolic flow field to that in rotational flow field becomes even smaller as the viscosity ratio, $\lambda$, moves away from the minimum point (about $\lambda$ =1) in either direction. Thus, for same magnitudes of G, the plane hyperbolic flow field seems to be more effective in drop breakup and dispersion than the simple shear field.

### 4-2-2. Viscoelastic Systems (VE Drop Phase - Newtonian Continuous Phase)

The relation for $E_c$ in this case in quite different to that for Newtonian systems. In accordance with the analysis in chapter 2, the breakup data on viscoelastic systems can be described by:

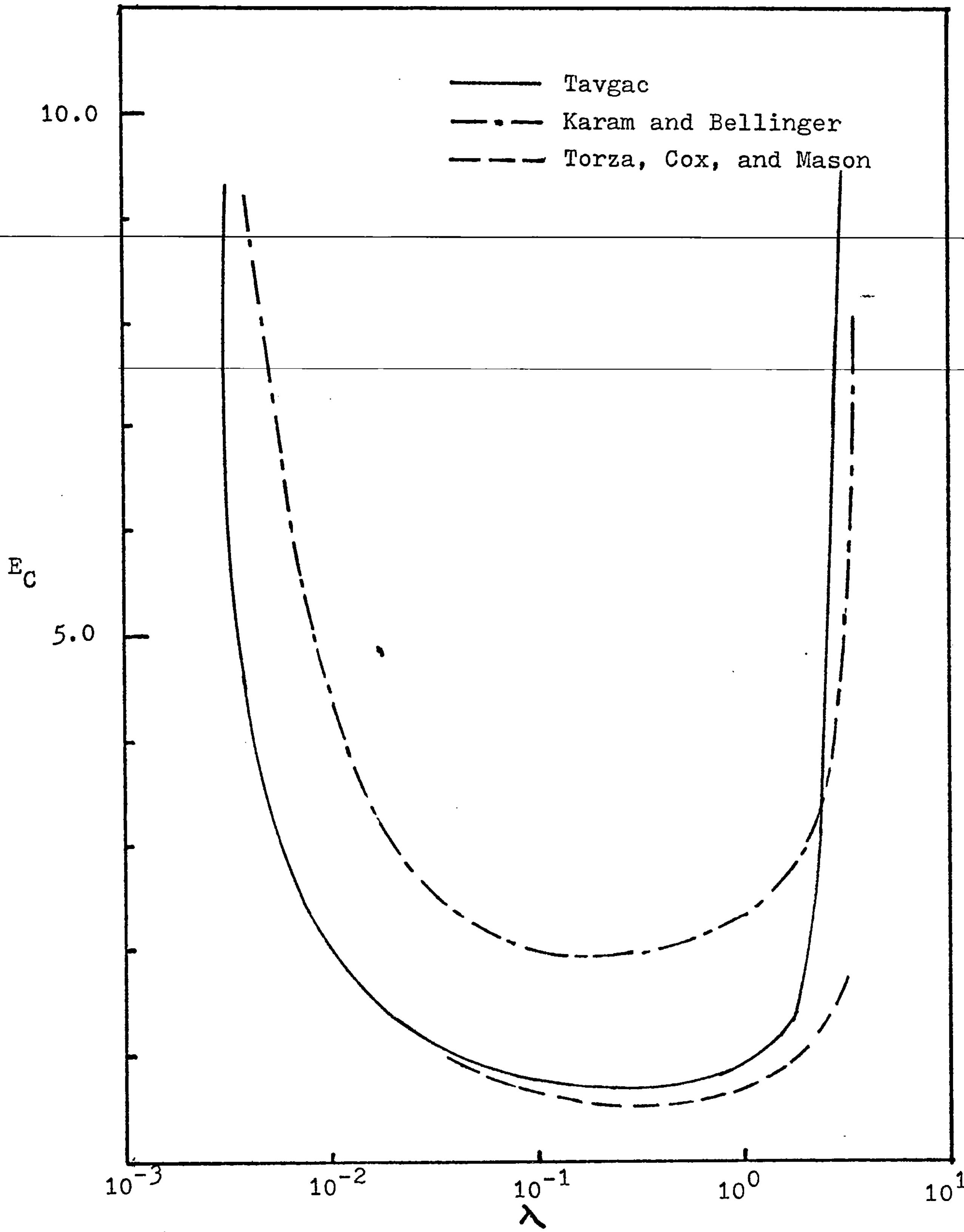


Figure 4-15. Effect of Viscosity Ratio on $E_c$ Required for Drop Breakup in Simple Shear Flow Field

$$E_c = E_c\left( \eta_{oD}/\eta_c ,\ C_c \lambda_1 ,\ \alpha_1 \right) \qquad (2\text{-}26\text{-}b)$$

where $C_c = \bar{G}_c/2$. Here the Bird-Carreau model was used to characterize the polymer solutions.

Four fluid systems were examined here (see Table 3-2-3 for physical properties), and the results are shown in Figures 4-16 to 4-19.. The curves for each system were constructed by taking data with different drop sizes. It is quite interesting to find that the critical value of E increases almost linearly with Deborah number, up to about De = 10, and then goes gradually into an asymptotic constant value as De increases further. This can be seen from these figures, especially in the cases involving the 1.5% and 2.0% Sep AP 30 solutions, where De values up to 22 were obtained.

Similar experimental data in a simple shear flow field have also been reported by Tavgac in 1972. However, in his experiments, the linear increase of $E_c$ with De was observed over the full range of De number studied, about $2 < De < 250$.

Thus, the plane hyperbolic flow field seems to be attractive in the design of dispersion devices for VE materials in view of the leveling off of $E_c$ as De gets large, since this may give a smaller $E_c = \bar{G}_c a \eta_c/\sigma$ which means a smaller drop size can be obtained for a given $\bar{G}_c$.

If we extropolate the linear portion of $E_c$ vs. De to De = 0, we will obtain a limiting value of $E_c$, which should be equal to that of Newtonian system with $\lambda = \eta_{oD}/\eta_c$. As shown on these figures, the extropolated values of $E_c$ for the 1.5% and

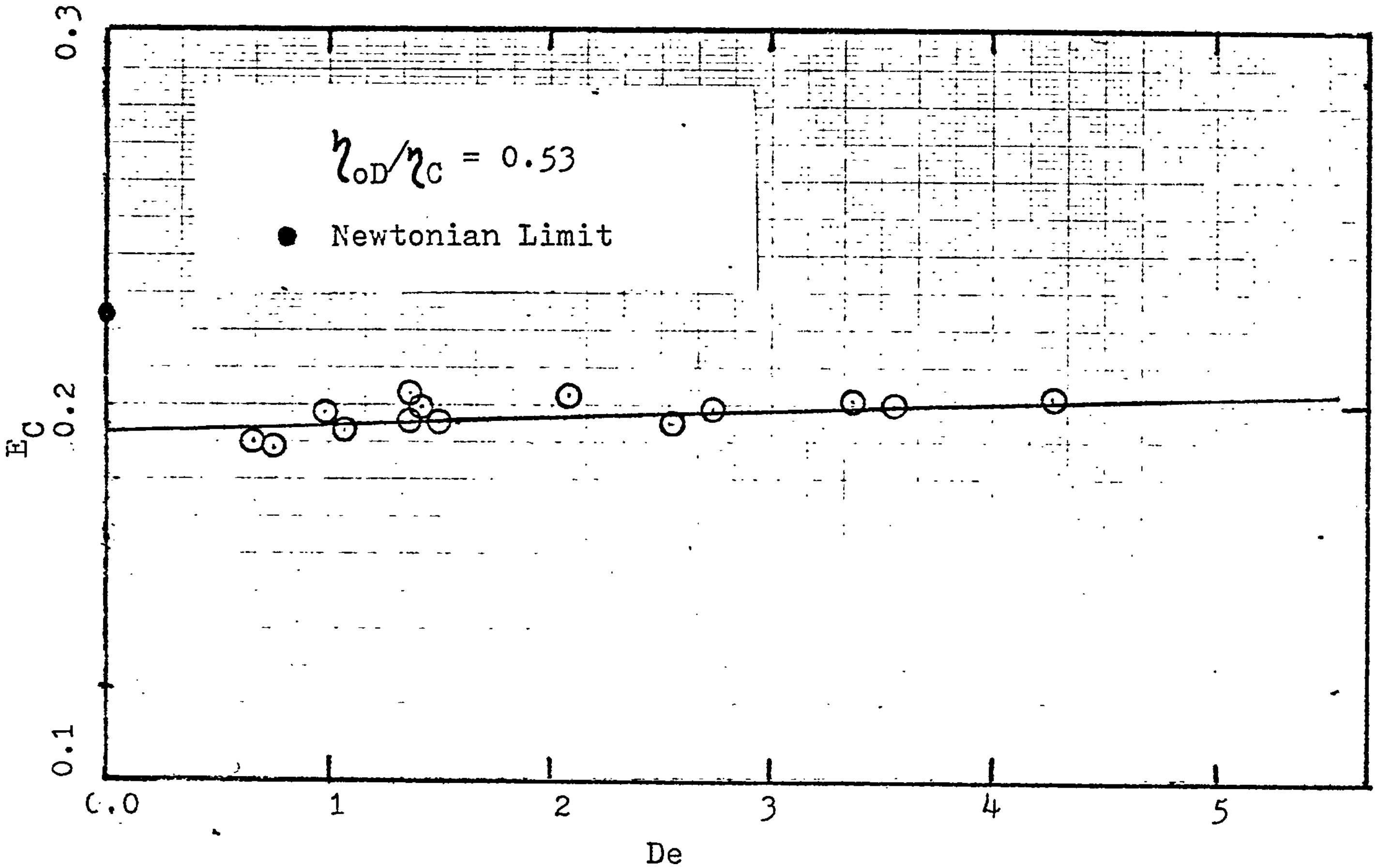


Figure 4-16. Effect of Deborah Number on $E_C$ Required for Breakup of 0.75% Sep AP 30 Drop - Silicone Oil

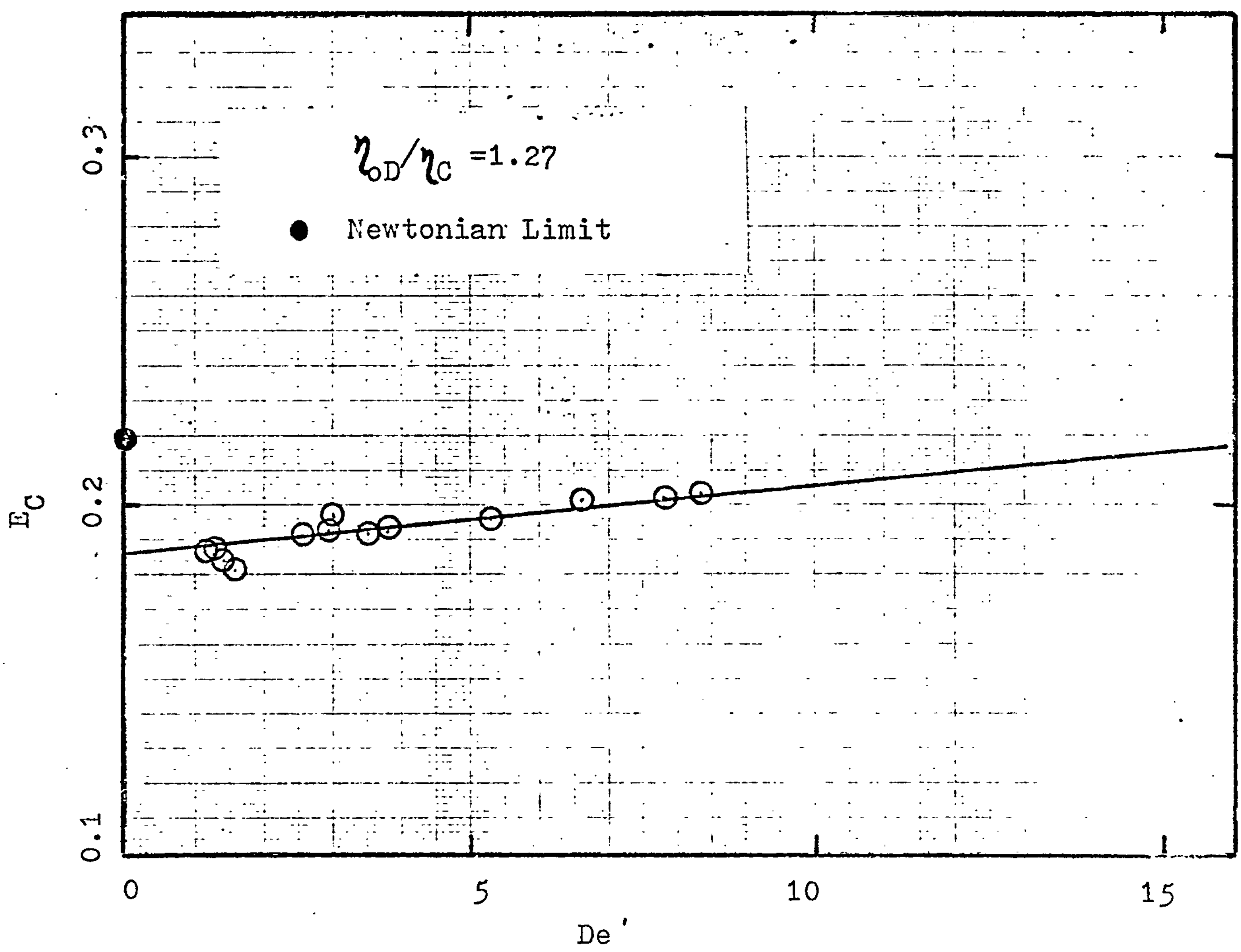


Figure 4-17. Effect of Deborah Number on $E_C$ Required for Breakup of 1.0% Sep AP 30 Drop - Silicone Oil

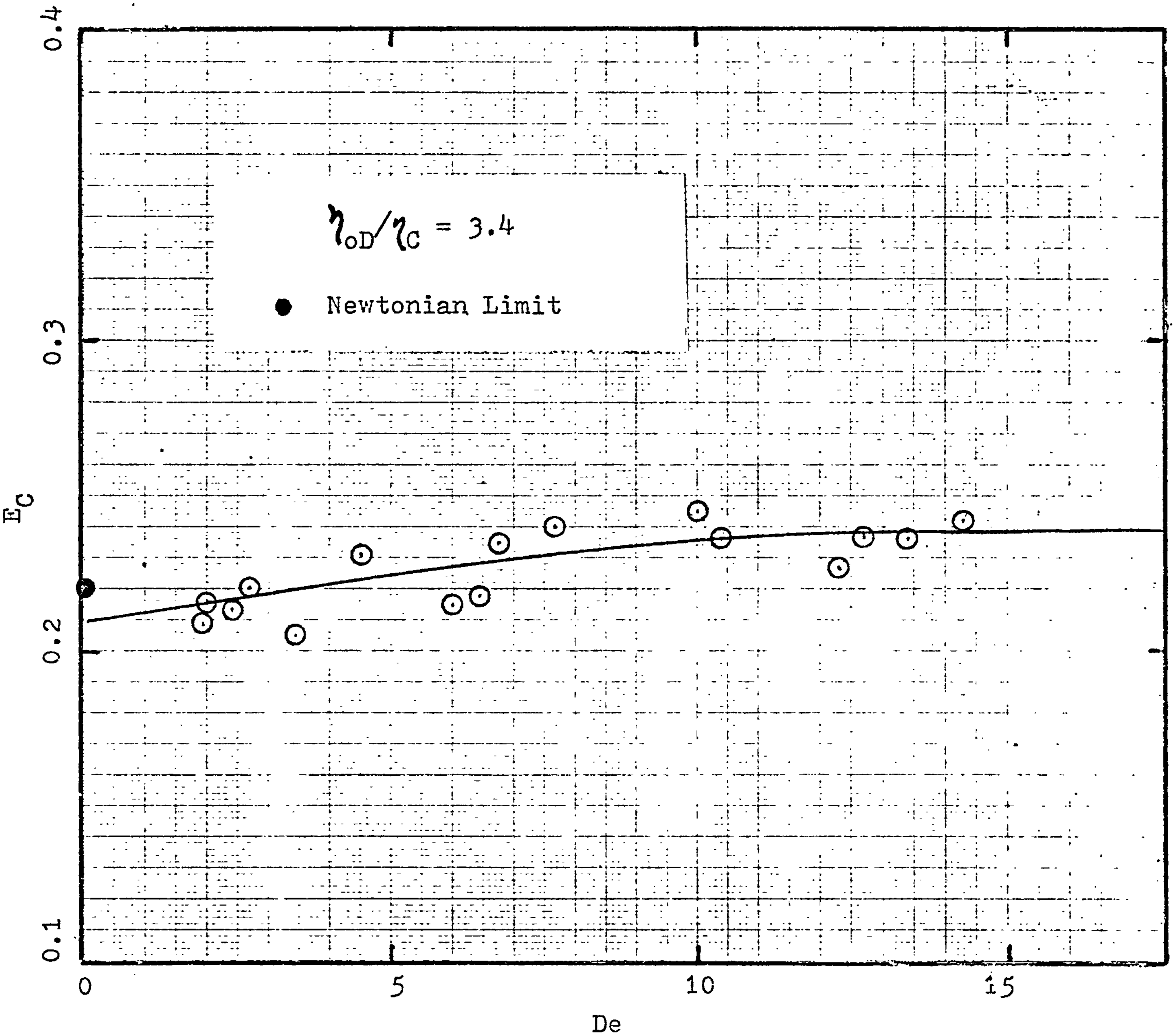


Figure 4-18. Effect of Deborah Number on $E_C$ Required for Breakup of 1.5% Sep AP 30 Drop - Silicone Oil

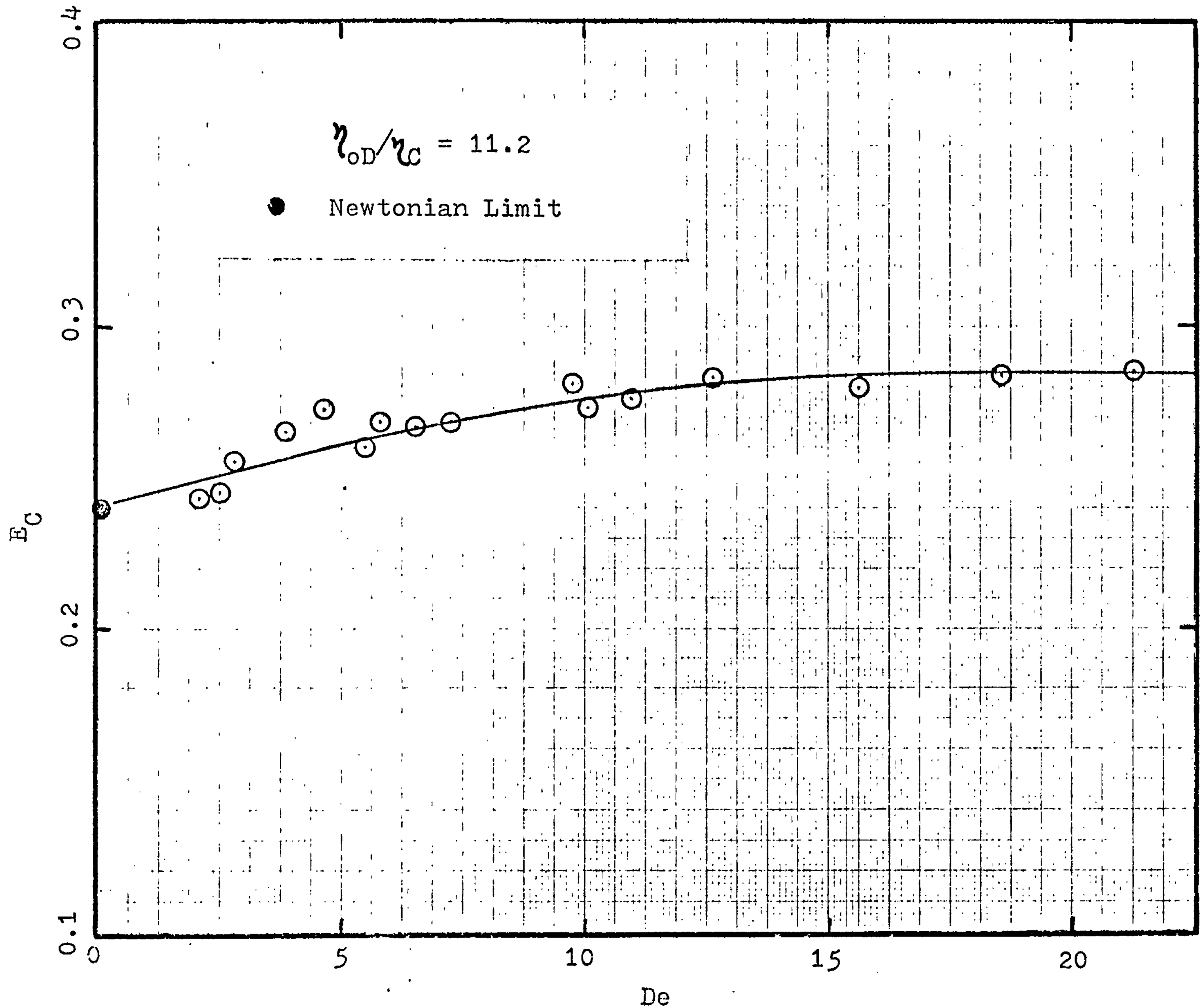


Figure 4-19. Effect of Deborah Number on $E_C$ Required for Drop Breakup of 2.0% Sep AP 30 Drop - Silicone Oil

2.0% Sep AP 30 agree fairly well with the corresponding $E_c$ in Newtonian system with $\lambda = \eta_{\infty}/\eta_c$, but about 10% deviation were observed for 0.75% and 1.0% Sep AP 30 solutions.

# CHAPTER 5

# THE INSTABILITY OF LIQUID THREADS IMMERSED IN ANOTHER LIQUID PHASE

## 5-1. Introduction

The breakup of liquid drops in viscous systems consists of two distinct machanisms: 1) the breakup of the liquid drops into a cylindrical liquid thread, and 2) the breakup of the liquid thread into a number of smaller droplets. The former process depends on the ratio of the viscous and interfacial forces for a given Newtonian fluid system as shown in previous chapters; the latter process depends on the stability of the thread to interfacial wavy disturbances caused by certain external factors such as the mechanical vibration in the apparatus and fluctuation of pressure in the ambient fluid.

The breakup of liquid threads or jets has attracted the attention of scientists for over a century, and is one of the most important problems in capillary hydrodynamics. Practically, such problems are encountered in fiber spinning operations, internal combustion engines, and many emulsification and dispersion processes.

From considerations of minimum surface area (or surface potential energy), Plateau (23) in 1873 established that a cylindrical liquid thread subject to surface tension will become unstable if its length exceeds its circumference. By considering the stability of the disturbance wave imposed upon the thread surface, Lord Rayleigh (25) reached a similar conclusion in 1879, i.e., the disturbancewave will be unstable if $\lambda_w > 2\pi a$. This can also be revealed quite easily by considering the variation in capillary pressure due to the wavy motion on a cylindrical interface. Imagine an axisymmetrical capillary wave with length $\lambda_w$ in the surface of a stationary thread (see figure 5-1).

$$\delta = \delta_0 \cos(2\pi x/\lambda_w) \qquad (5\text{-}1\text{-}1)$$

Then the pressure due to surface tension $\sigma$ for an undistorted thread is:

$$P_0 = \sigma(1/a) \qquad (5\text{-}1\text{-}2)$$

and the pressure for the surface with axisymmetrical distortion $\delta$ as described by Eq. (5-1-1) is:

$$P = \sigma\left[\frac{1}{a+\delta} - \frac{d^2\delta}{d^2x}\right] \cong \sigma\left[\frac{1}{a} - \frac{\delta}{a^2} - \frac{d^2\delta}{d^2x}\right] \qquad (5\text{-}1\text{-}3)$$

Hence the change of pressure due to distortion, after using Eq. (5-1-1) is:

$$\Delta P = P - P_0 = -\frac{\sigma\delta}{a^2}\left[1 - \left(\frac{2\pi a}{\lambda_w}\right)^2\right] \qquad (5\text{-}1\text{-}4)$$

Now it is obvious that a wavelength greater than the perimeter of undistorted thread will produce an increase in pressure in the nodes ( $\delta < 0$) and a decrease in the peaks ( $\delta > 0$). Consequently this will lead to an increasing distortion and finally to the breakup of the thread when $\delta_0 = a$. When $\lambda_w$ is less than $2\pi a$, the wave disappears according to Eq. (5-1-4).

Since viscosity can be considered a damping factor for the amplitude growth, the capillary breakup process will occur more rapidly in liquids of low viscosity; this will be confirmed by experimental breakup data in Section 5-4.

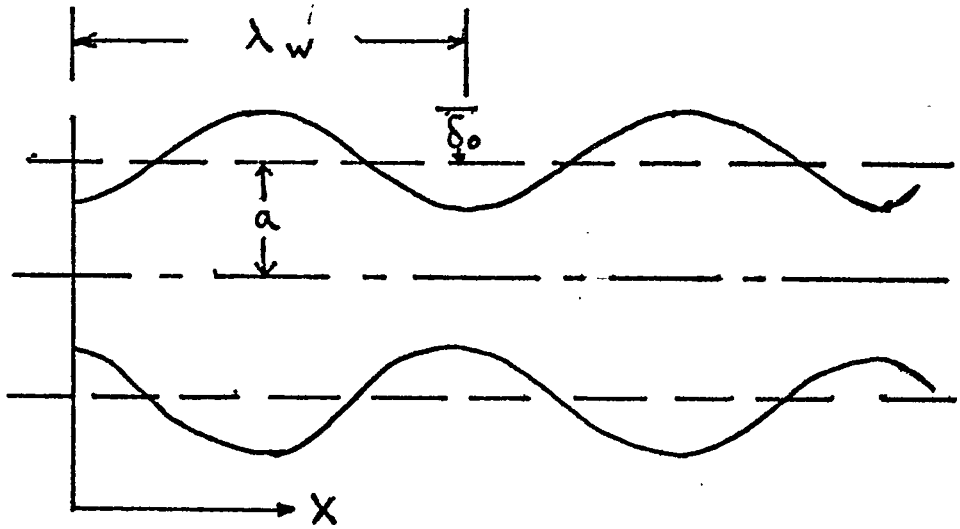


Figure 5-1. Parameters of Surface Varicosity on liquid Threads

Most of the previous theoretical studies of this problem were restricted to different limiting situations by either eliminating viscous effects or inertial effects in the continuous or disperse phase. In 1935 Tomotika, using linearized stability theory, obtained a relation which included the viscous and inertial effects in both fluid media. The previous works of Rayleigh ( 26, 27) and the later work of Christiansen ( 6 ) are limiting cases of Tomotika's general solution. The complete solution structure of such problems in terms of the characteristic dimensionless parameters has recently been given by Lee (20). W. K. Lee and Flumerfelt has reconsidered this problem and obtained a more goneral relation in terms of dimensionless growth rate, wave number, density ratio, viscosity ratio, and Ohnesorge number. From this the different limiting cases considered previously by Rayleigh, Weber, and Christiansen were also derived. Unfortunately they did not select the applicability criterion in terms of the independent dimensionless variables for the limiting equations.

In the present work, we present a brief review of this work, with particular emphasis on the approach used by Lee. In addition, the applicable ranges of various limiting equations are obtained as well as some experimental results on the breakup phenomena associated with stationary and extending threads. A historic survey of this problem can be found in Lee's Ph. D. dissertation (20).

## 5-2. Basic Equations— A Stationary Viscous Thread In Another Viscous Fluid

By following Lee, the equation of motion for the axisymmetric wave can be written in vectoral form as:

$$\frac{\partial \bar{V}}{\partial t} = -\frac{1}{\rho}\nabla P + \nu \nabla^2 \bar{V} \qquad (5\text{-}2\text{-}1)$$

Here cylindrical co-ordinates (r, θ, z) are used, and $\bar{V} = (U, 0, W)$. Note that the non-linear inertial effects and body force effects have been neglected.

By introducing the stream function $\psi$ and by eliminating pressure terms, Equation (5-2-1) can be combined into one differential equation as:

$$\left(\mathcal{D} - \frac{1}{\nu}\frac{\partial}{\partial t}\right)\mathcal{D}\psi = 0 \qquad (5\text{-}2\text{-}2)$$

where $\mathcal{D} = \left(\frac{\partial^2}{\partial r^2} - \frac{1}{r}\frac{\partial}{\partial r} + \frac{\partial^2}{\partial z^2}\right)$

As shown by Tomotika, the above equation can be satisfied by the following relation:

$$\psi = R_e\left\{\left[A r I_1(kr) + B r K_1(kr) + C r I_1(nr) + D r K_1(nr)\right]\exp(\alpha t + ikz)\right\} \qquad (5\text{-}2\text{-}3)$$

Where $\alpha$ is the wave growth rate; k is the wave number; n is defined as $(k^2+\alpha/\gamma)^{\frac{1}{2}}$, $I_p$ and $k_p$ are Bessel and modified Bessel functions of order p, and A, B, C, D, are arbitrary constants to be determined by the boundary conditions.

The finiteness of physical motions at r = 0 and r = $\infty$ gives the following stream functions for the inside and outside fluids, respectively.

$$\psi_D = \left[A_D r I_1(kr) + C_D r I_1(\ell r)\right] \exp(\alpha t + ikz) \qquad (5\text{-}2\text{-}4)$$

and $$\psi_c = \left[B_c r K_1(kr) + D_c r K_1(mr)\right] \exp(\alpha t + ikz) \qquad (5\text{-}2\text{-}5)$$

where $\ell = (k^2+\alpha/\gamma_D)^{\frac{1}{2}}$ and $m = (k^2+\alpha/\gamma_c)^{\frac{1}{2}}$

The boundary conditions at the interface between the two phases are:

(1) The velocity is continuous at the interface,

$$\left(u_D = u_c\right)_{r=a}, \quad \left[W_D = W_c\right]_{r=a} \qquad (5\text{-}2\text{-}6a,\ b)$$

(2) The shear stress is continuous at the interface,

$$\left[(\tau_{rz})_D = (\tau_{rz})_c\right]_{r=a} \qquad (5\text{-}2\text{-}7)$$

(3) The difference in the normal stress across the interface is due to the interfacial tension,

$$\left[(\tau_{rr})_c - (\tau_{rr})_D\right]_{r=a} = \sigma\left[\frac{1}{R_1}+\frac{1}{R_2}\right] = \frac{\sigma\delta(k^2a^2-1)}{a^2} \qquad (5\text{-}2\text{-}8)$$

Where $R_1$ and $R_2$ are the principal radii of curvature at the interface.

These boundary conditions give four linear homogeneous algebraic equations in terms of $A_D$, $B_C$, $C_D$, $D_C$. Nontrivial solutions exist only if the determinant of the coefficient matrix vanishes and thus we obtain the frequency equation as

$$\begin{vmatrix} I_1 & \bar{I}_1 & K_1 & \bar{K}_1 \\ XI_0 & X_D\bar{I}_0 & -XK_0 & -X_C\bar{K}_0 \\ 2UX^2I_1 & U(X_D^2+X^2)\bar{I}_1 & 2X^2K_1 & (X_C^2+X^2)\bar{K}_1 \\ F_1 & F_2 & F_3 & F_4 \end{vmatrix} = 0 \qquad (5\text{-}2\text{-}9)$$

with $F_1 = 2\,\Pi_{1D}X(XI_o - I_1) + \Pi_{2D}I_D + X(X^2-1)I_1$

$F_2 = 2\,\Pi_{1D}X(X_D\bar{I}_D - \bar{I}_1) + X(X^2-1)\bar{I}_1$

$F_3 = -\,2\,\Pi_{1C}X(XK_o + K_1) + \Pi_{2C}K_o$

$F_4 = -\,2\,\Pi_{1C}X(X_C\bar{K}_o + \bar{K}_1)$

Where $X = ka$, $\quad U = \eta_D/\eta_C$

$X_D = \ell a = \left(X^2 + \dfrac{a^2\rho_D}{\theta\,\eta_D}S\right)^{\frac{1}{2}}$, $\quad X_c = ma = \left(X^2 + \dfrac{a^2\rho_C}{\theta\,\eta_C}S\right)^{\frac{1}{2}}$

$I_p = I_p(X)$, $\quad \bar{I}_p = I_p(X_D)$, $\quad K_p = K_p(X)$, $\quad \bar{K}_p = K_p(X_C)$

$\Pi_{2D} = \left(\dfrac{a^3\rho_D}{\theta^2\sigma}\right)S^2$, $\quad \Pi_{2C} = \left(\dfrac{a^3\rho_C}{\theta^2\sigma}\right)S^2$, $\quad \Pi_{1D} = \left(\dfrac{a\,\eta_D}{\theta\,\sigma}\right)S$, $\quad \Pi_{1C} = \left(\dfrac{a\,\eta_C}{\theta\,\sigma}\right)S$

Here a characteristic time $\theta$ is used to define the dimensionless growth rate $S = \alpha\theta$.

The above equation gives the relationship between X and S.

For various characteristic times, it can be expressed in terms of the following dimensionless groups: the viscosity ratio U, the density ratio G $(=\rho_D/\rho_C)$, the ohnesorge numbers defined as $Oh_D=(a\sigma\rho_D)^{\frac{1}{2}}/\eta_D$ and $Oh_C=(a\sigma\rho_C)^{\frac{1}{2}}/\eta_C$, the dimensionless growth rate S, and the wavenumber X.

In order to obtain a complete solution structure, it is necessary to define a number of different characteristic times ( see Lee (20)). These characteristic times are listed in Table 5-1 along with the various dimensionless groups which can arise in the problem.

Table 5-1. The Characteristic Times and the Dimensionless Parameters

| $\pi$ \ $\theta$ | $\theta_{ID}=\left(\frac{a^3\rho_D}{\sigma}\right)^{1/2}$ | $\theta_{IC}=\left(\frac{a^3\rho_C}{\sigma}\right)^{1/2}$ | $\theta_{VD}=\left(\frac{a\eta_D}{\sigma}\right)$ | $\theta_{VC}=\left(\frac{a\eta_C}{\sigma}\right)$ |
|---|---|---|---|---|
| $\frac{a^3\rho_D}{\theta^2\sigma}$ | 1 | G | $Oh_D^2$ | $U^2Oh_D^2$ |
| $\frac{a^3\rho_C}{\theta^2\sigma}$ | $1/G$ | 1 | $Oh_D^2/G$ | $Oh_C^2$ |
| $\frac{a\eta_D}{\theta\sigma}$ | $1/Oh_D$ | $U/Oh_C$ | 1 | U |
| $\frac{a\eta_C}{\theta\sigma}$ | $1/UOh_D$ | $1/Oh_C$ | $1/U$ | 1 |
| $\frac{a^2\rho_D}{\theta\eta_D}$ | $Oh_D$ | $G^{1/2}Oh_D$ | $Oh_D^2$ | $UOh_D^2$ |
| $\frac{a^2\rho_C}{\theta\eta_C}$ | $Oh_C/G^{1/2}$ | $Oh_C$ | $Oh_C^2/U$ | $Oh_C^2$ |

Note that the relation between the two Ohnesorge numbers is

$$G^{\frac{1}{2}} Oh_C = U\ Oh_D \qquad (5\text{-}2\text{-}10)$$

Now it is clear that the whole problem can be expressed in terms of any three combinations of the quantities, U, G, $Oh_D$, and $Oh_C$ with S and X as dependent variables.

## 5-3. Limiting Cases and Bounds of Applicability

In this section various limiting cases of Equation (5-2-9) will be cited and criteria for their applicability will be indicated.

The important characteristics of thread breakup are the rate of the breakup process and the size of the droplets formed after breakup. Experimentally, the maximum wave growth rate, $S^*$, and the corresponding wave number, $X^*$, are the direct measurements of these two characteristics. The selection of a criterion of applicability in each limiting case is obtained by considering the variation of $S^*$ and $X^*$ with the independent dimensionless parameters as they approach the limiting values.

### (A) Dominant Inertial Effects

Two cases can be considered in this category.

(A-1) $Oh_C \rightarrow \infty$ , $G^{\frac{1}{2}} Oh_D \rightarrow \infty$ , $G \rightarrow 0$ (Implicit: $U \rightarrow 0$)

By using $\theta_{IC} = \left(\frac{a^3 \rho_c}{\sigma}\right)^{\frac{1}{2}}$ as the characteristic time and referring to Table 5-1, we found that a dominant inertial effect implies $Oh_C \longrightarrow \infty$ and $G^{\frac{1}{2}} Oh_D \longrightarrow \infty$.

With $Oh_c \to \infty$ , $G^{\frac{1}{2}}Oh_D \to \infty$ , $G \to 0$, Lee has derived the limiting equation as

$$S_{IC}^2 = X(1-x^2)K_1/K_o \qquad (5\text{-}3\text{-}1)$$

with $S_{IC}^* = 0.819$ and $X^* = 0.485$ being the maximum growth rate and the corresponding wave number, respectively.

Note that $U = GOh_c/Oh_D G^{\frac{1}{2}}$, i.e., U is equivalent to $1/G^{\frac{1}{2}}Oh_D$ for given values of G and $Oh_C$. By substituting various values of $Oh_c$, G, U (corresponding to $G^{\frac{1}{2}}Oh_D$) into Equation (5-2-9) and numerically solving for $S^*$ and $X^*$, it is possible to determine the effects of $Oh_c$, G, and $G^{\frac{1}{2}}Oh_D$ near the limit. i.e., $Oh_C \to \infty$, $G^{\frac{1}{2}}Oh_D \to \infty$ , and $G \to 0$.

These numerical results are shown in Figures (5-2) ~ (5-5) for this particular case. Figure (5-2) shows generally the effect of G, $Oh_c$, and $G^{\frac{1}{2}}Oh_D$ on $S^*$. Figures (5-3) ~ (5-5) show the individual effect of each parameter on $S^*$ and $X^*$ with the other two being fixed at various values close to the limiting values. It is clear from these results that the effects of G and $Oh_c$ on $S^*$ and $X^*$ are quite strong and that of $G^{\frac{1}{2}}Oh_D$ is quite small when close to the limit.

Expanding $S^*$ (or $X^*$) in terms of G, $1/Oh_c$, $1/G^{\frac{1}{2}}Oh_D$ arrround the limit point (0, 0, 0), we obtain the following expression of $S^*$ (or $X^*$),

$$S^* = S^*(0,0,0) + \left(\frac{\partial S^*}{\partial X_1}\right)_0 X_1 + \left(\frac{\partial S^*}{\partial X_2}\right)_0 X_2 + \left(\frac{\partial S^*}{\partial X_3}\right)_0 X_3 + \text{Higher order terms}$$

or $$S^*(0,0,0)\left[\frac{S^* - S^*(0,0,0)}{S^*(0,0,0)}\right] = \left(\frac{\partial S^*}{\partial X_1}\right)_0 X_1 + \left(\frac{\partial S^*}{\partial X_2}\right)_0 X_2 + \left(\frac{\partial S^*}{\partial X_3}\right)_0 X_3 + \text{Higher order terms.}$$

Where $X_1 = G$, $X_2 = 1/Oh_C$, $X_3 = 1/G^{\frac{1}{2}}Oh_D$.

An approximate conservative criterion for 5% deviation in $S^*$ (or $X^*$) can be defined as

$$S^*(0,0,0)(5\%) \geqslant K_1X_1 + K_2X_2 + K_3X_3$$

where $K_i = \left[(\partial S^*/\partial X_i)_0 / (\partial S^*/\partial X_i)_0 \right] \mathrm{Sup}\left|\frac{\partial S^*}{\partial X_i}\right|$ within (0, 0, 0) and ($X_1$, $X_2$, $X_3$)

for 5% deviation.

Since $X_3$ has the smallest effect on $S^*$ (or $X^*$), we choose $\mathrm{Sup}(|\frac{\partial S^*}{\partial X_1}|)$ and $\mathrm{Sup}(|\frac{\partial S^*}{\partial X_2}|)$ in ($X_1$, $X_2$, 0.0005) as in Figures 5-3 and 5-4.

Based on this approach, for 5% deviation in $S^*$ and $X^*$, Equation (5-3-1) is limited to the following conditions,

$$74.4G + 30.0/Oh_c + 7.3/G^{1/2}Oh_D < 1 \qquad \text{For } S^* \qquad (5\text{-}3\text{-}1a)$$

$$|115.6G - 44.8/Oh_c + 10.3/G^{1/2}Oh_D| < 1 \qquad \text{For } X^* \qquad (5\text{-}3\text{-}1b)$$

Also for 5% deviation in $S^*$, Meister and Scheele (21) obtained

$$Oh_c > 36$$

as the restriction on Equation (5-3-1) for the case of a gas jet in a low viscosity liquid by simply neglecting the effects of G and $1/G^{\frac{1}{2}}Oh_D$.

However, with typical values of 0.005 g/c.c. for gas and 1.0 g/c.c. for aqueous liquids, and with negligible effect of $G^{\frac{1}{2}}Oh_D$, Equation (5-3-1a) requires that

$$Oh_c > 48$$

Therefore, simply neglecting the effect of G even in the case of gas jets in low viscosity liquids is not strictly correct.

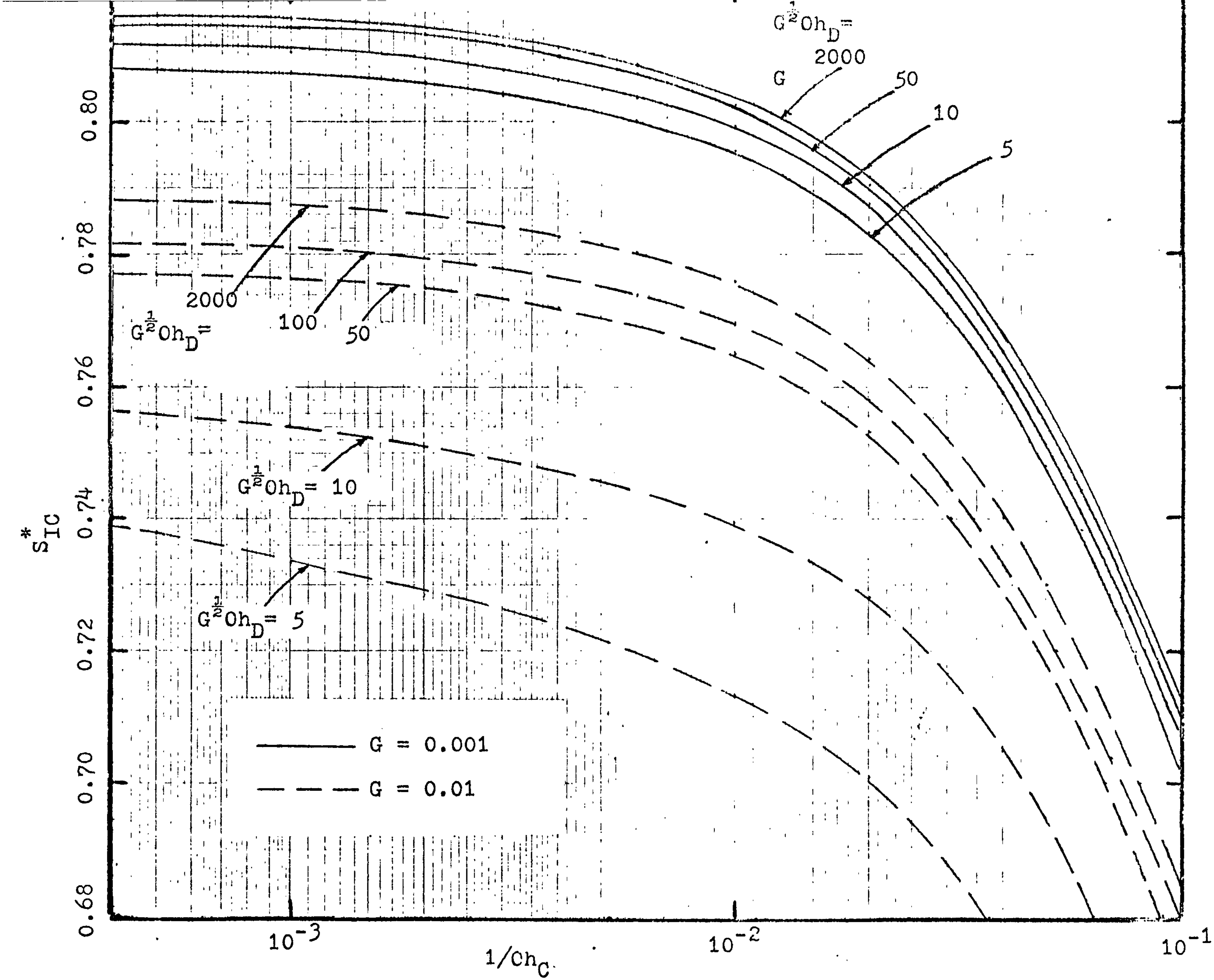


Figure 5-2. The Variation of $S^*$ with G, $1/Oh_C$, and $1/G^{\frac{1}{2}}Oh_D$ in The Case of (A-1)

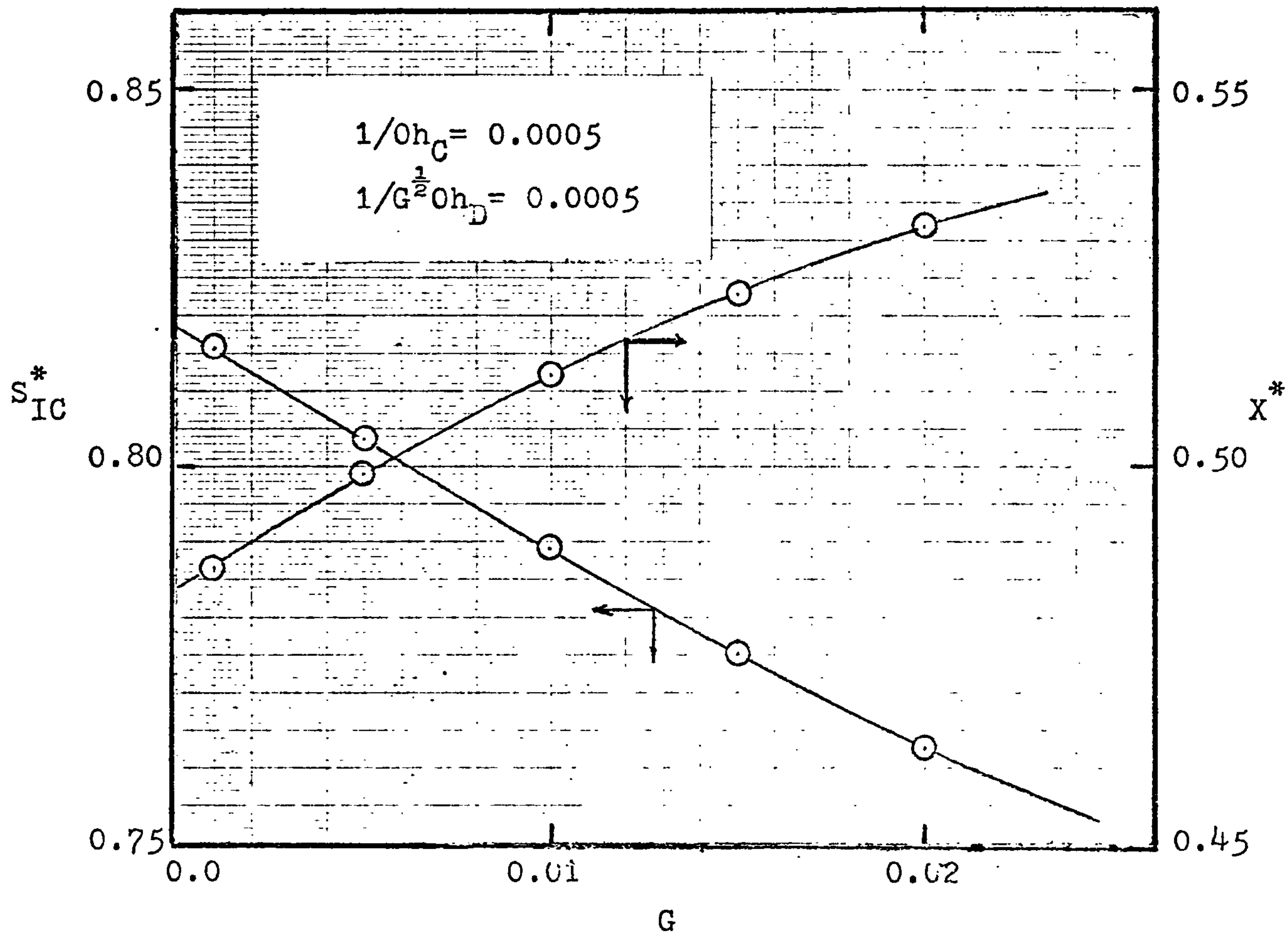


Figure 5-3. Variations of $S^*_{IC}$ and $X^*$ with G

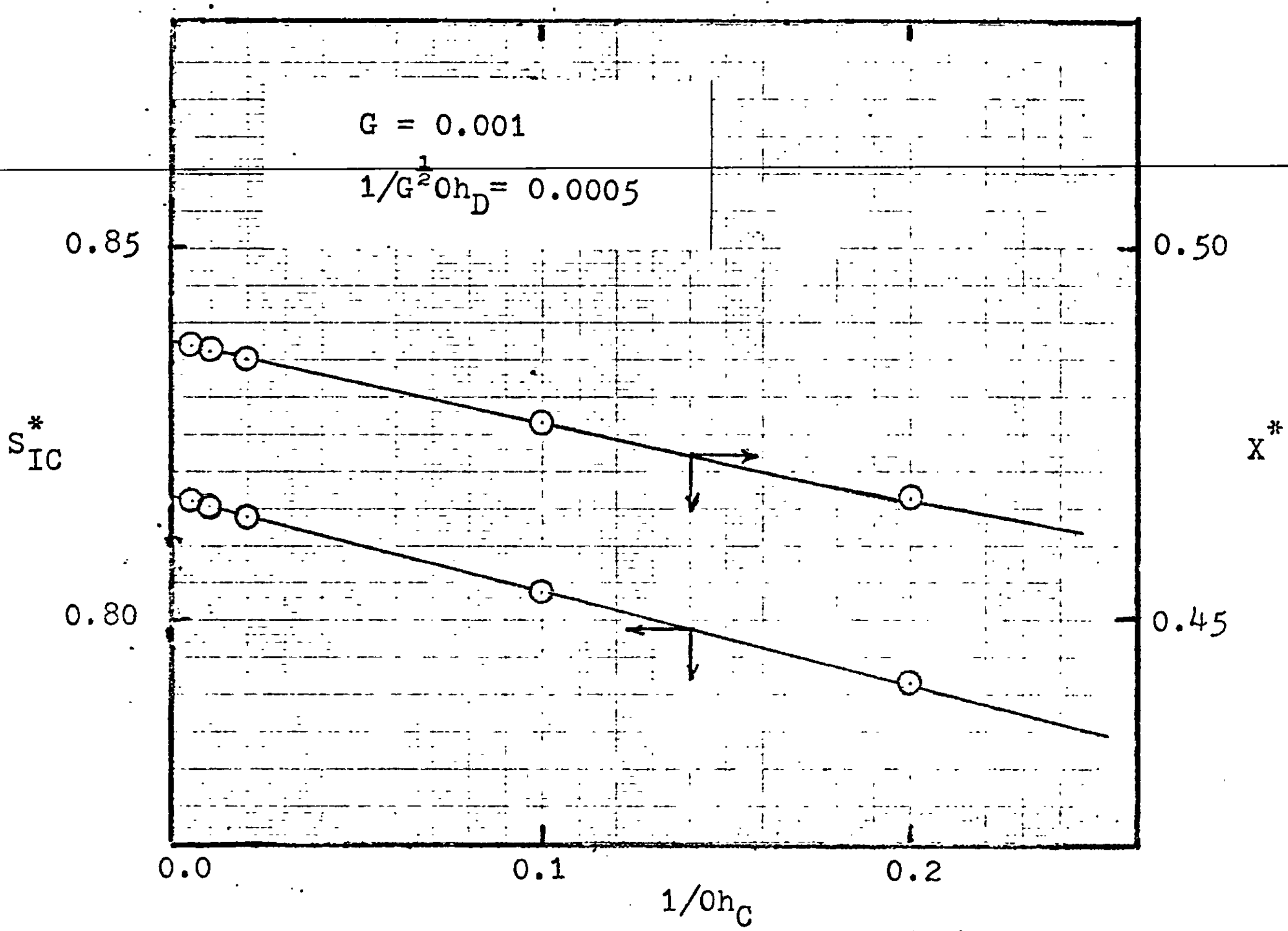


Figure 5-4. Variations of $S^*_{IC}$ and $X^*$ with $1/Oh_C$

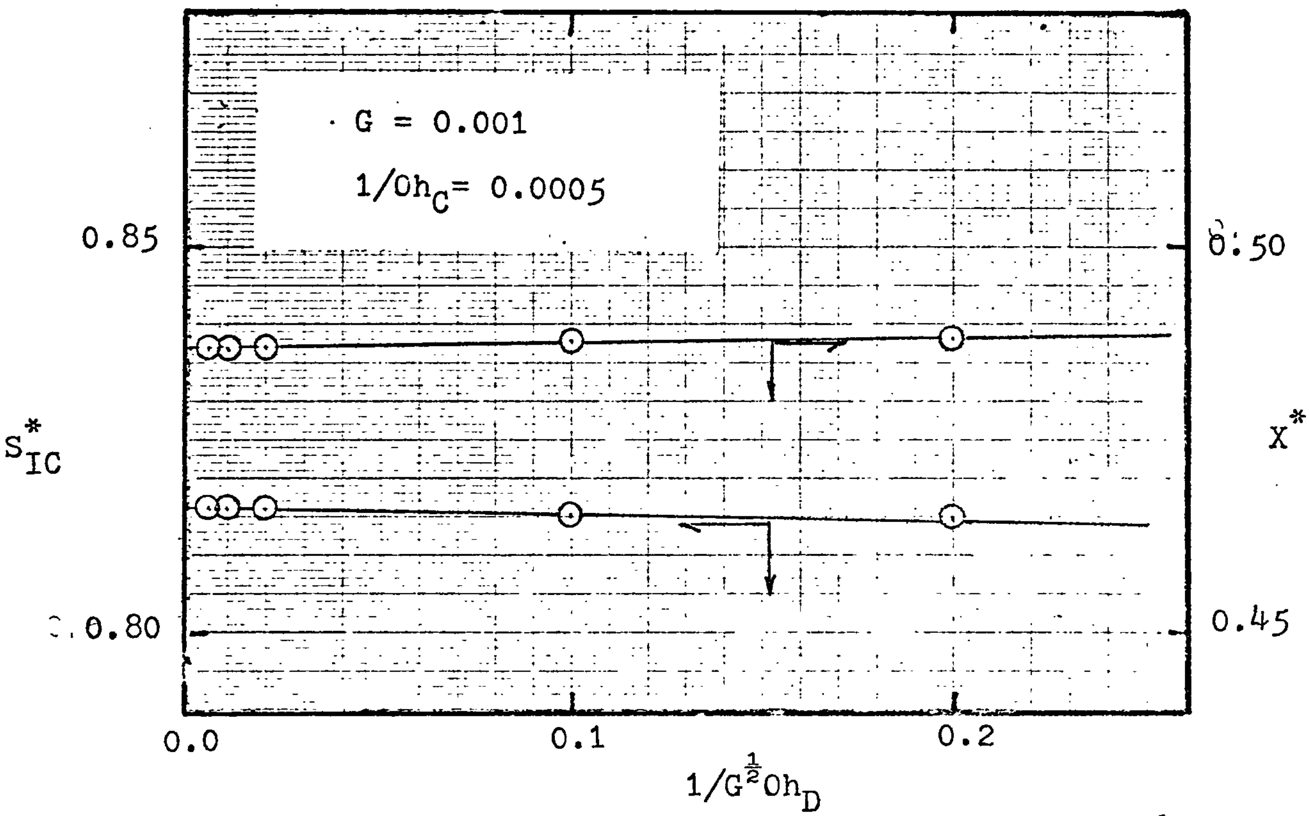


Figure 5-5. Variation of $S^*_{IC}$ and $X^*$ with $1/G^{\frac{1}{2}}Oh_D$

(A-2). $Oh_D \to \infty$, $Oh_C/G^{\frac{1}{2}} \to \infty$, $G \to \infty$ (Implicit $U \to \infty$).

By taking $\theta_{ID}$ as the characteristic time, it can be seen that dominant inertial effects imply that $Oh_D \to \infty$ and $Oh_C/G^{\frac{1}{2}} \to \infty$. Note also here that U is equivalent to $Oh_C/G^{\frac{1}{2}}$ for given $Oh_D$ and G.

The limiting equation is:

$$S_{ID} = X(1-X^2)I_1/I_o \tag{5-3-2}$$

with $S^*_{oo} = 0.344$, $X^*_o = 0.696$ as the critical growth rate and wave-number.

The most sensitive parameter in this case turns out to be $Oh_D$. For 5% deviation in $S^*_{ID}$ and $X^*$; Equation (5-3-2) is limited to conditions where

For $S^*_{ID}$: $$38.8/Oh_D + 4.08/G + 1.54(G^{\frac{1}{2}}/Oh_C) < 1 \tag{5-3-2a}$$

For $X^*$ : $$20.3/Oh_D + 0.86/G + 0.12(G^{\frac{1}{2}}/Oh_C) < 1 \tag{5-3-2b}$$

Using the same typical values of density for gas and aqueous solutions, we found that errors in $S^*$ and $X^*$ assiciated with G and $G^{\frac{1}{2}}/Oh_C$ are almost negligible. Therefore, for a low viscosity liquid jet in a gas, the restrictions can be rewritten as:

For $S^*_{ID}$ $$Oh_D > 39 \tag{5-3-2a'}$$

For $X^*$ $$Oh_D > 20 \tag{5-3-2b'}$$

(B). Negligible Inertial Effects as Compared with Viscous Effects

In this case we have

$$U \leq 1, \quad Oh_C^2 \to 0, \quad U\,Oh_D^2 \to 0,$$

and $$U > 1, \quad Oh_D^2 \to 0, \quad Oh_C^2/U \to 0.$$

By expanding the functions in the second and fourth column of Equation (5-2-9) in ascending powers of $Oh_c$ and $UOh_D^2$ (or $Oh_D$ and $Oh_c^2/U$ for $U > 1$), and then letting these two parameters pass to zero, we can obtain Tomotika's special equation corresponding to negligible inertial effects as

$$\begin{vmatrix} I_1 & XI_o - I_1 & K_1 & -XK_o - K_1 \\ I_0 & XI_1 - I_o & -K_o & XK_1 - K_o \\ UI_1 & UXI_o & K_1 & -XK_o \\ G_1 & G_2 & G_3 & G_4 \end{vmatrix} = 0 \qquad (5\text{-}3\text{-}3)$$

where $G_1 = UI_1'S + \dfrac{(X^2 - 1)I_1}{2X\left(\dfrac{a\eta_c}{\theta\sigma}\right)}$

$G_2 = U(I_1' + XI_1'' - I_o)S + \dfrac{(X^2 - 1)I_1}{2\left(\dfrac{a\eta_c}{\theta\sigma}\right)}$

$G_3 = K_1' S$

$G_4 = (K_1' + XK_1'' + K_o)S$

Here $\theta_{VD}$ was used for the case $U > 1$ and $\theta_{VC}$ used for $U \leq 1$. We will not consider the bound criterion for this equation, since it is still quite complicated and not convenient for simple application. Two limiting equations can be derived from Equation (5-3-3).

(B-1). $U \rightarrow 0$, $Oh_c^2 \rightarrow 0$, $UOh_D^2 \rightarrow 0$

In this case, Equation (5-3-3) can be simplified to

$$S_{VC} = \left[ \frac{(1-X^2)/2}{1+X^2-(XK_o/K_1)^2} \right] \qquad (5\text{-}3\text{-}4)$$

with $S_o^* = 0.5$ and $X_o^* = 0.0$.

The numerical results for this case indicate a dominant dependence of $S^*$ on U, a slight dependence on $Oh_c$, and very little dependence on $UOh_D^2$ (equivalent to G). This situation actually is a result of the assumption that the viscous effect is dominant in this limiting case.

The slope of $S_{VC}^*$ v.s. U with $Oh_C^2$ and $UOh_D^2 \longrightarrow 0$ increases quickly as $U \rightarrow 0$. As an approximation, an average slope was chosen to set up the criterion. The restriction in this case for 5% deviation in $S^*$ is:

---

$$14000U+8.0Oh_C^2+0.08UOh_D^2 < 1 \qquad (5\text{-}3\text{-}4a)$$

The large coefficient of U is quite reasonable since Equation (5-3-4) was derived by Tomotika for the system of a "vacuum" jet in a low density viscous medium.

(B-2). $Oh_D^2 \longrightarrow 0$, $Oh_C^2/U \longrightarrow 0$, $U \longrightarrow \infty$

The limiting equation now becomes (using $\theta_{VD}$ as the characteristic time)

$$S_{VD} = \left[ \frac{(X^2-1)/2}{1+X^2-(XI_o/I_1)^2} \right] \qquad (5\text{-}3\text{-}5)$$

with $S_o^* = 0.166$ and $X_o^* = 0.0$.

The same type of dependence on U, $Oh_D^2$, and $Oh_C^2/U$ was observed as in (B-1). According to the numerical results, the applicability restriction on Equation (5-3-5) is

$$903/U+84.30h_D^2+0.420h_C^2/U < 1 \qquad (5\text{-}3\text{-}5a)$$

This case corresponds to that considered by Rayleigh for a low density viscous jet in a "vacuum" medium.

## 5-4. Experimental Studies

In his experimental studies on the breakup of a liquid drop in an extending flow field in 1934, G. I. Taylor came across two interesting and essential observations which initiated two papers by Tomotika (35,36) concerning the instability of stationary and extending threads. G. I. Taylor observed that when a drop of black lubricating oil was surrounding by syrup, the thread formed by continuously stretching out of the deformed drop did not at once break up into small drops but remained cylindrical for some time and finally broke up into many tiny droplets after being stretched into a quite thin thread. On the other hand, if the flow field was abruptly stopped at some stage, the thread gradually broke into a number of small drops spaced at nearly regular intervals, although it had seemed quite stable while the surrounding fluid was in motion.

As mentioned by Tomotika, the base flow in the surrounding fluid may have a stabilizing effect which suppresses the breakup of the thread. This can be visualized in the following way. As the thread is draw out by the motion of the surrounding fluid, any varicosity formed at the interface would have its wavelength increased. That is, even though a disturbance wave at the interface of the thread might have the tendency to amplify, the base flow associated with the thread diminishes this effect by "stretching out" the wave and as a result delays the ultimate breakup.

The formation of liquid threads in other liquid media is quite important in the formation and extrusion of synthetic fibres. In particular, such processes are encountered in wet spinning processes where the liquid polymer thread is extruded and drawn in a liquid bath.

Experimental data on thread breakup under both conditions, stationary and extending, will be presented in this section and compared with Tomotika's theory of stationary liquid threads in liquid media.

### 5-4-1. Experiments on the Instability of Stationary Liquid Threads

The experiments were conducted in the four-roll apparatus described previously and the conditions similar to those employed in the study of deformation and breakup of liquid drops. Stationary liquid threads were obtained by instantly stopping the flow field which had pulled the liquid drops into cylindrical threads. The whole process was photographed with a movie camera and then the dominant wavenumber $X^* = 2\pi a/\lambda_W$ was calculated by measuring the thread diameter and wavelength $\lambda_W$.

Silicone oil F510 ($\eta_C$= 300 poise) was used as the continuous phase and different syrup, molasses, glycerol solutions, and several polymer solutions as the dispersed phases covering $\eta_D/\eta_C$ from 0.008 to 10.

The key dimensionless parameters in case of polymer threads can be expressed as, according to Lee's analysis,

$$S = S(X,\ U,\ G,\ \alpha_1,\ T = \frac{\sigma \lambda_1}{d_{TH} \eta_{oD}}) \qquad (5\text{-}4\text{-}1)$$

therefore, the dominant wavenumber, $X^*$, is:

$$X^* = X^*(U,\ G,\ \alpha_1,\ T = \frac{\sigma \lambda_1}{d_{TH} \eta_{oD}}) \qquad (5\text{-}4\text{-}2)$$

Here the effects of $Oh_D$ and $Oh_C$ have been neglected, since in the case of a liquid thread immersed in a liquid medium these two parameters are usually very small. Moreover the density ratio can also be considered as a minor factor and neglected.

The measured data on the dominant wavenumber, $X^*$, are plotted on Figure 5-6 (including some data points for extending threads) with $= \eta_D/\eta_C$ as abscissa. Data for the polymer threads were specified with the corresponding values of $\alpha_1$, and $\frac{\sigma \lambda_1}{d_{TH} \eta_{oD}}$. The numerical results for Tomotika's theoretical equation for negligible inertial effects, i.e., Equation (5-3-3), are also shown in Fig. 5-6.

The experimental results are in fairly good agreement with the theoretical curve from Equation (5-3-3), except possible for those data with $\lambda = 0.0083$ which show some deviation from the theoretical curve. This might be expected, however, since the inertial effect of the thread phase, neglected in Equation (5-3-3), is getting more and more important as $\lambda$ becomes smaller and smaller. The numerical results from Equation (5-2-9) were added for $\lambda = 0.0083$. Wavenumber data, $X^*$, for four polymer solutions are also plotted in Figure 5-6. The results with $\lambda \leq 3.4$ (0.75%, 1%, and 1.5% Sep AP 30 solutions) were below the curve for Newtonian threads, and those with $\lambda = 11.2$ (2% Sep AP 30 solution) were a little bit higher. This trend agrees qualitatively with the numerical results of Lee's theory (Figure 3-15 in his dissertation).

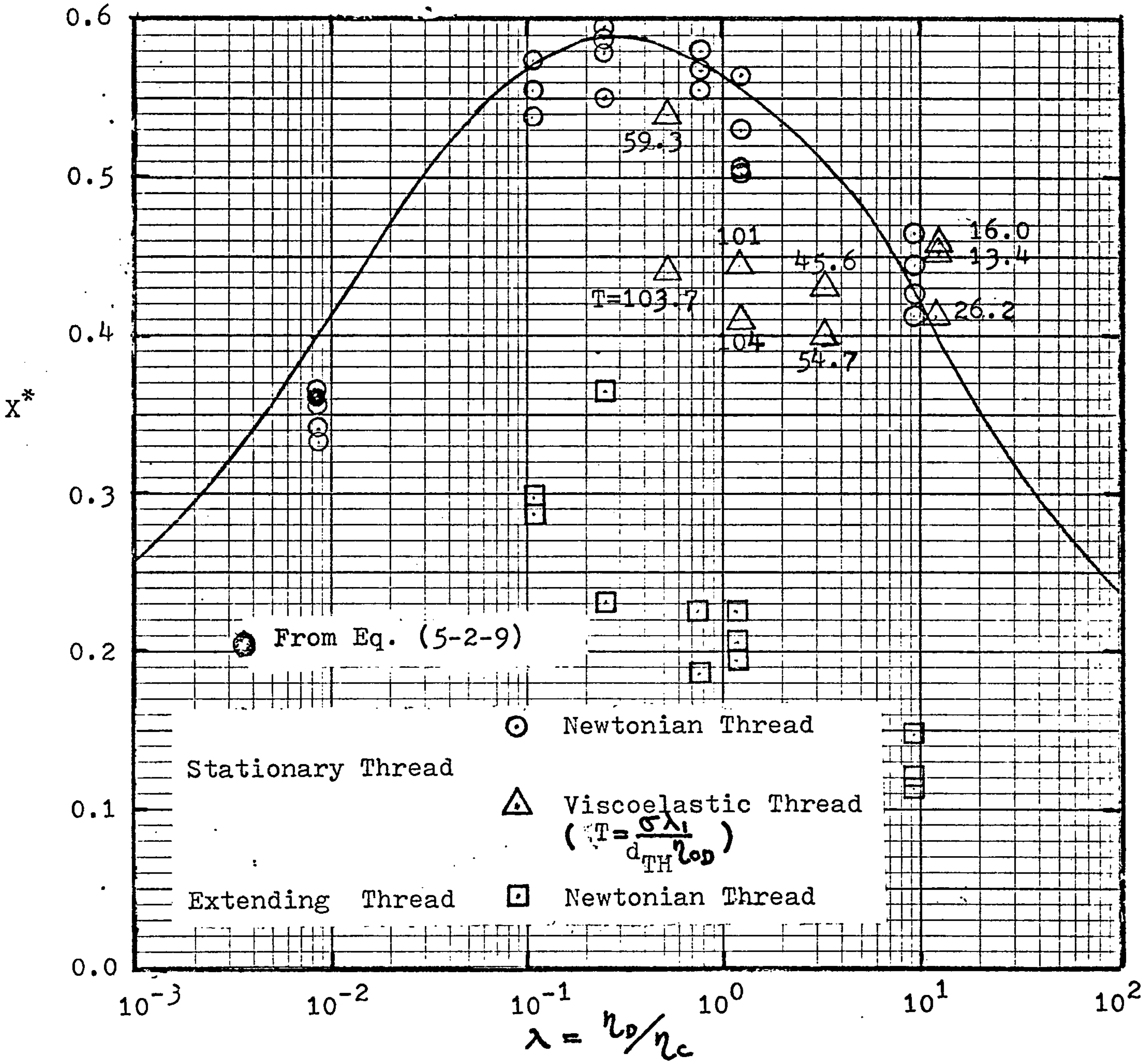


Figure 5-6. The effect of $\lambda$ on the Dominant Wavenumber for Liquid Threads in Liquid Media

It is interesting to note that systems with high viscosity ratios always take longer periods of time to show unstable varicosities at the interface than those with smaller viscosity ratios. This may reveal that the viscosity of the dispersed phase may have a damping effect on the growth of unstable waves.

In order to compare the relative instability between Newtonian threads and viscoelastic threads, the amplitude of the varicosity, $\delta$ , at various times before breakup were measured on two individual systems with same viscosity ratios, one for a Newtonian system, and one for a viscoelastic system. The fluid systems are indicated on Fiqure 5-7. The results are plotted on a semi-log scale paper with $\delta/a$ and t as the co-ordinates, as shown in Figure 5-7. Here $\delta/a = 1$ corresponds to the breakup point and t corresponds to the time before the breakup point. The comparison here shows that a viscoelastic thread is more unstable than a Newtonian thread except possibly for a short period before the breakup point. The almost linear relation for the Newtonian thread agrees with Tomotika's linear instability theory.

In most of the experiments here the breakup pattern was quite regular with the thread being broken into almost equal size droplets at equal intervals with some smaller satellite droplets between them. The ratio of diameters of the final main droplets and that of the thread ranged from 2.0 to 2.6 as shown in Appendix II (C-1). In some case, superimposed waves were observed during the breakup process; this might be due to some external mechanical vibration in the apparatus or due to a non-uniform interfacial tension distri-

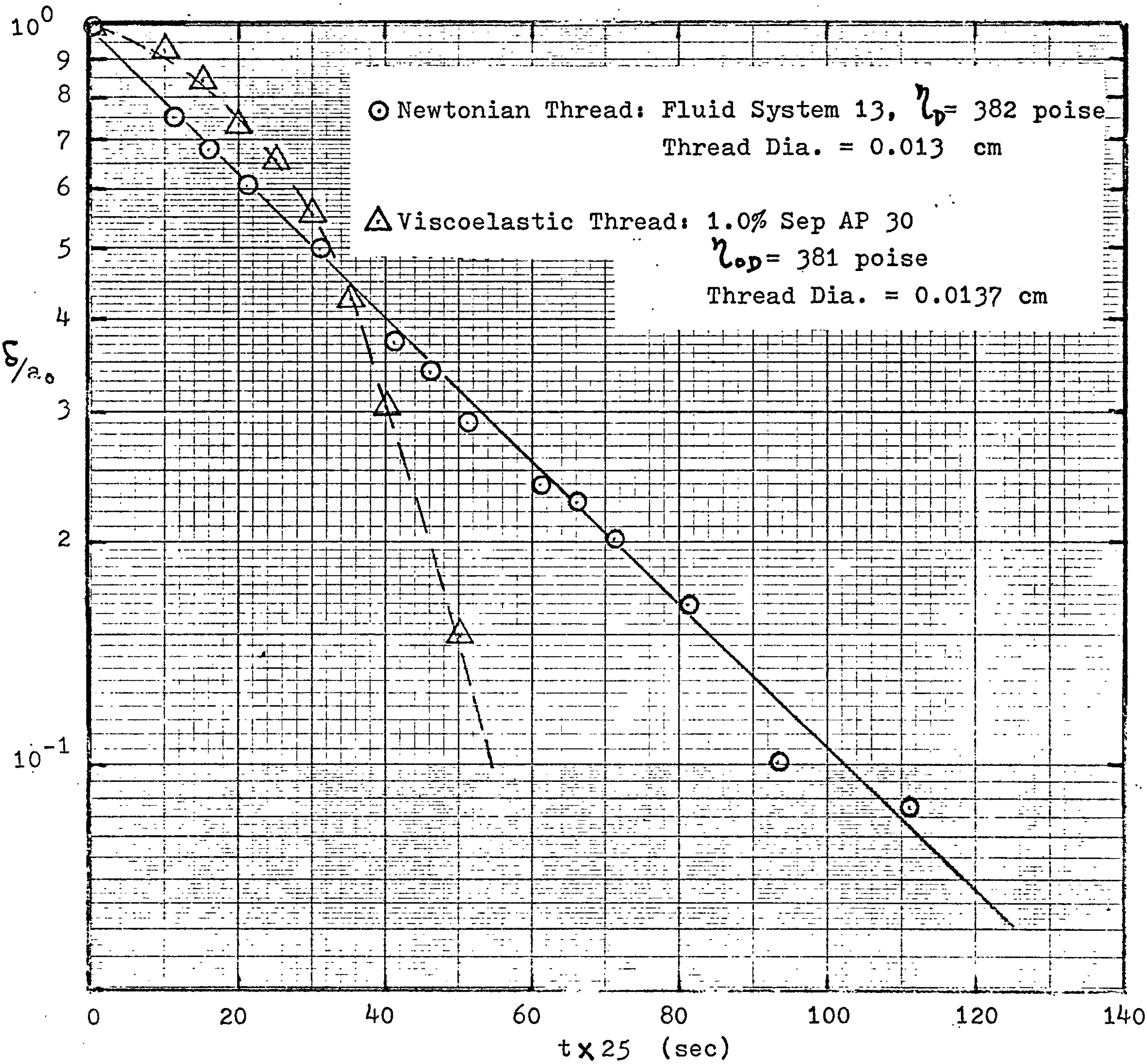


Figure 5-7. The relative Amplitude, $\delta/a_o$, vs. Time for Stationary Threads

bution caused by the impurity absorbed at the interface.

5-4-2. Experiments of the Breakup of a Liquid Thread under Extension

In this section some experimental results are presented on the breakup of an extending thread; that is a thread being continuously stretching out by the outside base flow field until breakup occurs. G. I. Taylor first reported that the sizes of droplets formed by an extending thread were much smaller than those formed by a stationary thread. Later in 1936 Tomotika developed a theoretical analysis of this phenomenon and found that the extension of the thread has a stabilizing effect in constraining the increase of any initial disturbance to a finite value. Besides this, the disturbances could occur at various stages during the elongation and it was shown that these wave disturbances could increase in very different proportions.

In order to reveal what these results imply, let us consider the mechanism for breakup problem. Here there are two main forces counteracting each other, i.e., the viscous stretching force tending to stablize the disturbances and the interfacial force tending to promote the disturbances. In our experiments, we maintain a constant stretching rate, $C = \overline{G}/2$, and start with a thread of somewhat larger diameter than that which finally exists at the point of breakup. As time goes on, the thread diameter decreased and since the interfacial tension force is inversely proportional to the diameter, the interfacial forces increase and eventually dominate the viscous forces - breakup then occurs. This suggests that there exists a critical thread diameter associated with each given extension rate, $C = \bar{G}/2$. Therefore, an experimental correlation for this problem can be expressed as

$$d_{TH} = d_{TH}(\eta_C, \eta_D, \rho_C, \rho_D, \sigma, C) \qquad (5\text{-}4\text{-}1)$$

where $d_{TH}$ is the critical thread diameter. Based on dimensional considerations, this relation can be transformed into the following dimensionless form:

$$E_{THC} = C d_{TH} \eta_C / \sigma = E_{TH}(\eta_D/\eta_C, \rho_D/\rho_C, Oh_D = (d_{TH}\rho_D \sigma)^{\frac{1}{2}}/\eta_D) \qquad (5\text{-}4\text{-}2)$$

In this study, all the fluid systems were with $\rho_D/\rho_C = 1$ and small $Oh_D$, and therefore Equation (5-4-2) can be simplified to

$$C d_{TH} \eta_C / \sigma = E_{THC}(\eta_D/\eta_C) \qquad (5\text{-}4\text{-}3a)$$

Assuming that the main droplet diameters and the thread diameter are in a nearly constant ratio, we can have

$$C d_{DP} \eta_C / \sigma = E_{DPC}(\eta_D/\eta_C) \qquad (5\text{-}4\text{-}3b)$$

Equation (5-4-3b) is used to analyze the experimental data, since the measurement of the final main drop diameter is easier and more definitive than the thread diameter. Here $d_{DP}$ is the final droplet diameter.

The same viscoelastic fluid systems studied in the stationary thread case were also tested here. The correlation function, similar to that in viscoelastic drop breakup, is

$$\eta_c d_{DP} C/\sigma = E_{DPC}(\eta_{oD}/\eta_C, \ De = C\lambda_1, \ \alpha_1) \qquad (5\text{-}4\text{-}4)$$

Before presenting any experimental data on extending threads, we have to establish the relation between the actual extension rate of the thread and that of the external flow field ($\bar{G}/2$). For this purpose, the change of thread diameter with time for three cases ( one Newtonian thread and two viscoelastic threads) were measured. The instantaneous axial extension rate of the thread was calculated from the instantaneous diameter $d_{TH}$ from

$$C = \frac{1}{L}\frac{dL}{dt} = -2\frac{1}{d_{TH}}\frac{d(d_{TH})}{dt} \qquad (5\text{-}4\text{-}5)$$

The above equation was derived with the condition of constant thread volume for an incompressible fluid. In particular, for a long thread, the volume is

$$V = \frac{\pi d_{TH}^2}{4} L = \text{constant}$$

and
$$\frac{dV}{dt} = \frac{\pi}{2} L d_{TH} \frac{d(d_{TH})}{dt} + \frac{\pi d_{TH}^2}{4}\frac{dL}{dt} = 0$$

Dividing the above equation by $\frac{\pi L d_{TH}^2}{4}$, we obtain Equation (5-4-5).

The measurements of $d_{TH}$ as a function of time for the three systems studied are plotted in Figure 5-8. The data reveal that the threads were extending at a constant rate, defined as $C = \frac{dL}{Ldt}$, and the extension rates as calculated by Equation (5-4-5) were quite close to those for the basic flow field calculated by Eq. (3-3a). This observation seems to imply that for the systems studied, the viscous forces in the thread which resist the extension are small compared with the forces of the continuous phase

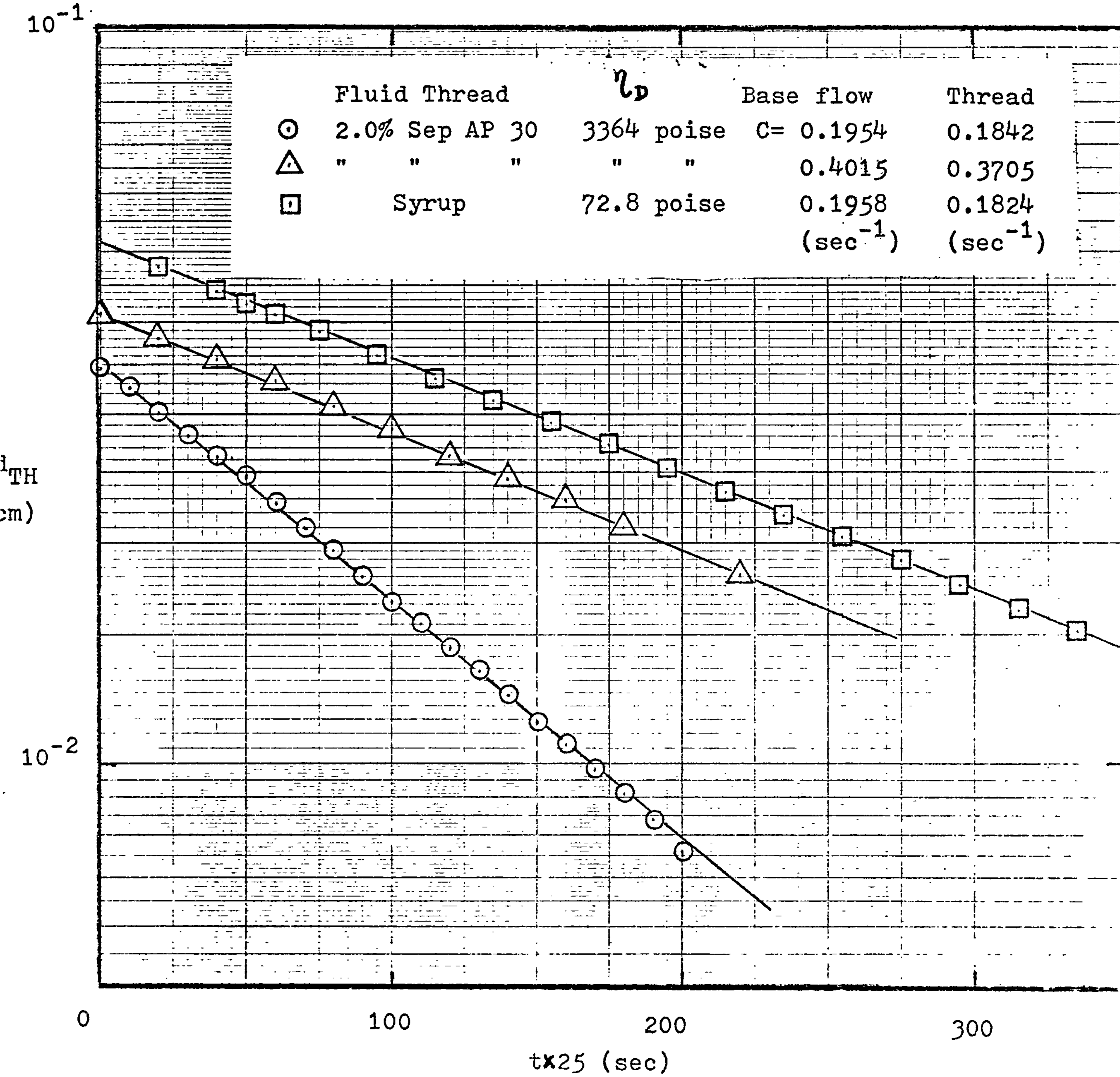


Figure 5-8. Variation of Thread Diameter with Time

which act at the thread surface and cause the extension of the thread.

If the extending threads are allowed to continually extend at a given rate, they will eventually breakup. This breakup process was photographed with a movie camera, the conditions being the same as before ( $T = 24.5^{o}C$ ). In addition to measurements of $E_{DPC}$, we also measured the critical wavenumber, $X^{*}$. The results are shown in Figure 5-6. Here we found that all of the data fell below the curve of a stationary thread. This seems contrary to what Lee reported in his dissertation that the extending critical wavenumbers are similar to those in the case of a stationary thread. However most of his data were also below the curve of the stationary case (refer to Fig. 4-5 in his dissertation).

The data of $E_{DPC}$ on Newtonian threads are plotted, according to Eq. (5-4-3b), on Figure 5-9 with viscosity ratio, $\lambda$, ranging from 0.008 to 10. It is seen that the value of $E_{DPC}$ increases as the viscosity ratio decreases; and the slope is higher and higher as $\lambda$ becomes smaller and smaller. This implies that the higher the viscosity relative to the surrounding media, the smaller the diameter of the thread before breakup occurs. In other words, we can obtain smaller drops and finer dispersions in such systems than with systems with smaller viscosity ratios, all other conditions being the same.

In Figure 5-10, we plotted the values of $(E_{DPC})_{VE}$ in term of $De = \bar{G}\lambda_1/2$, for three Sep AP 30 solutions according to Eq. (5-4-4). In all cases, the values of $(E_{DPC})_{VE}$ increase more or less linearly

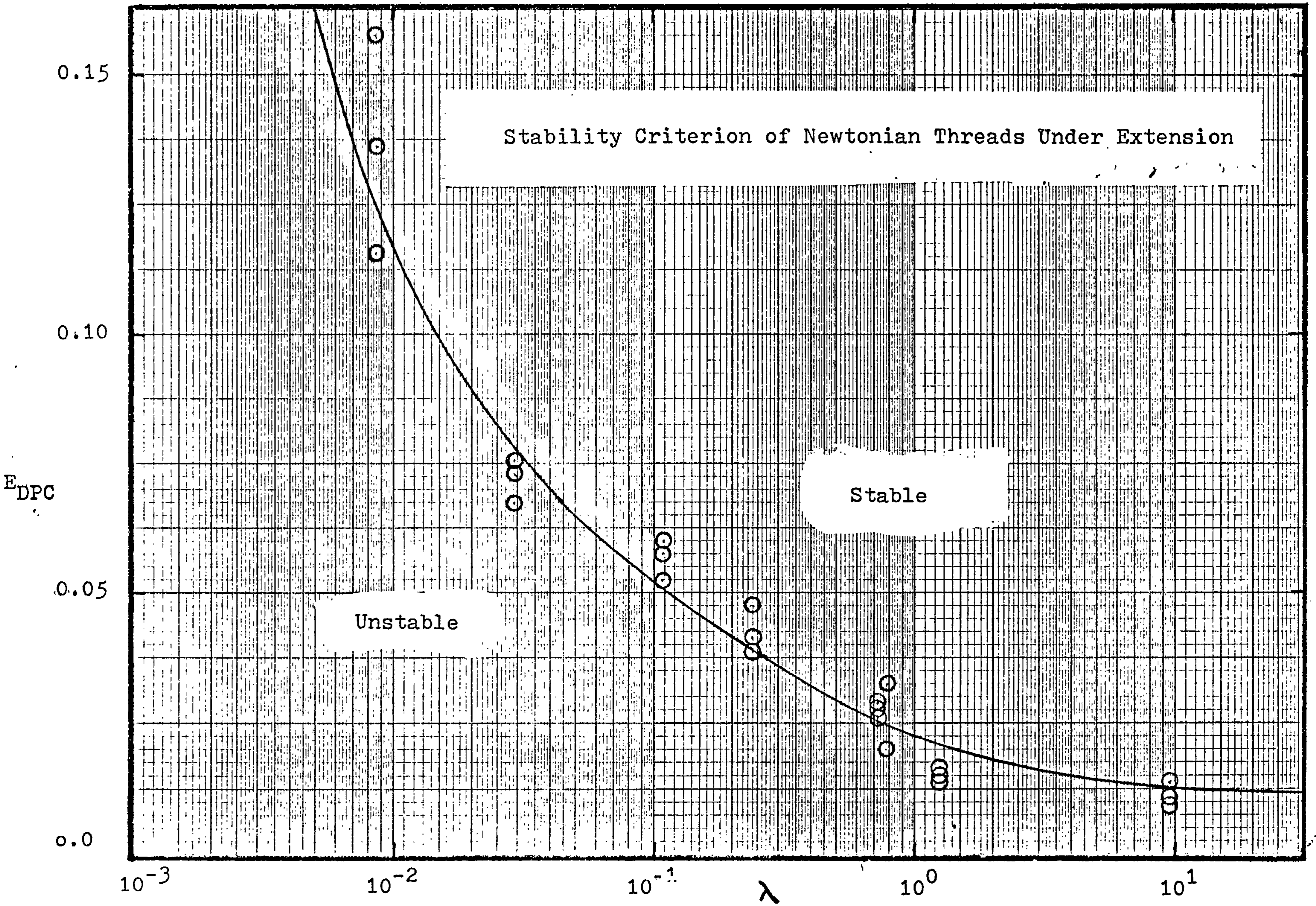


Figure 5- 9 . The effect of $\lambda$ on $E_{DPC}$ for Newtonian Threads Under Extension

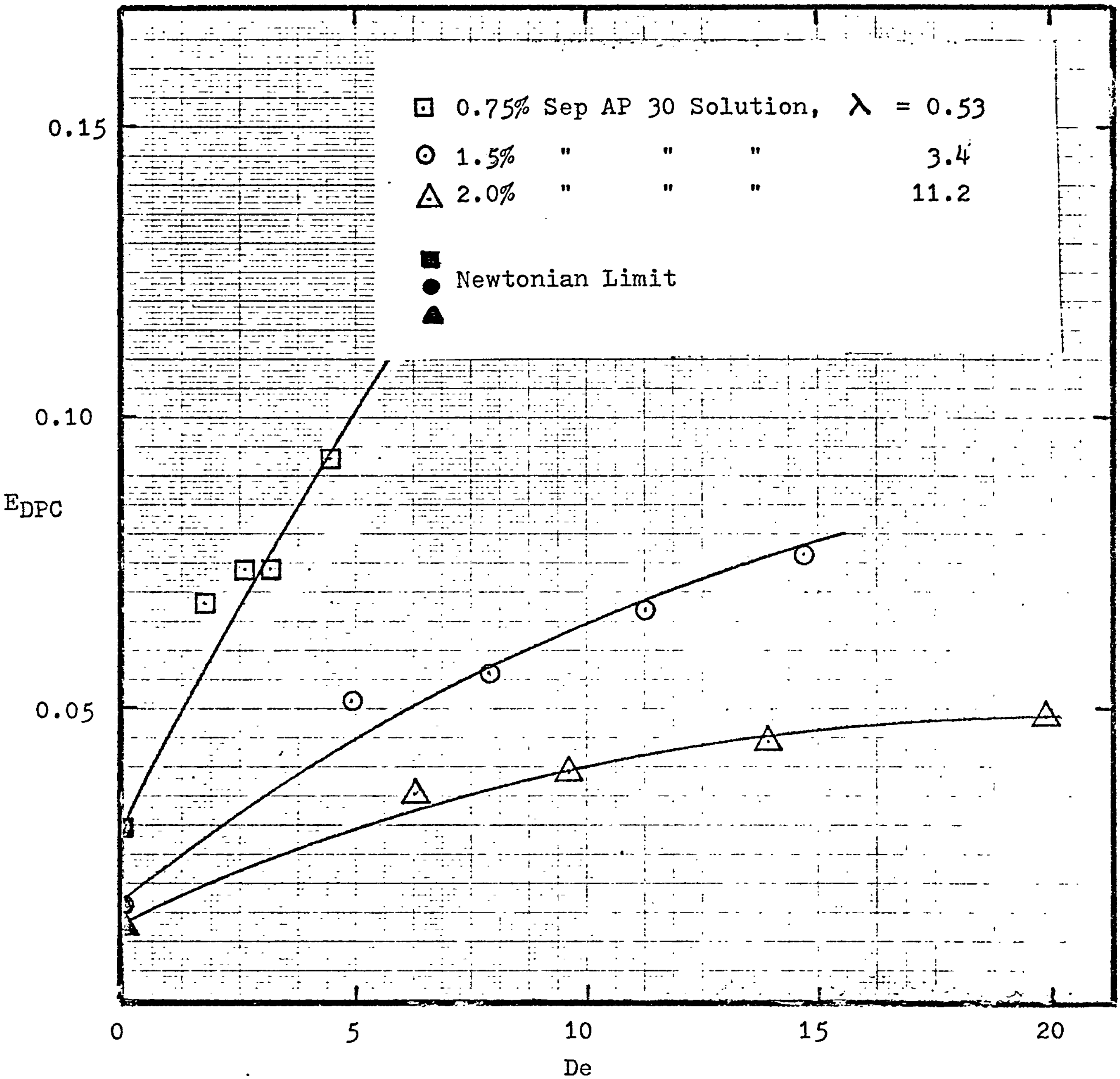


Figure 5-10. The effect of Deborah Number on $E_{DPC}$ for Viscoelastic Threads Under Extension

with De. The corresponding values of $E_{DPC}$ for Newtonian cases are also shown on Figure 5-10. In all three cases, $(E_{DPC})_{VE}/(E_{DPC})_N$ are always greater than 1, under similar conditions. If we consider the same values of $\sigma$, C, and $\eta_C$ for the comparable systems, the ratio, $(E_{DPC})_{VE}/(E_{DPC})_N$, would be equivalent to the ratio of the broken main droplet sizes. This seems to imply that the extending threads of polymer solution are more unstable than the corresponding Newtonian threads under similar kinematic conditions.

In order to substantiate this, the measurements of $\delta(t)/a(t)$ at various times up to breakup were taken on two comparable systems with the same extension rate, C. The Newtonian thread, used here, with lower viscosity and higher interfacial tension than the polymer thread should be more unstable than a Newtonian thread with same values of $\eta_D$ and $\sigma$ as the polymer thread. But the results shown on Figure 5-11 still indicate the the Newtonian extending thread is more stable than the polymer extending thread, when both threads are extending at the same rate.

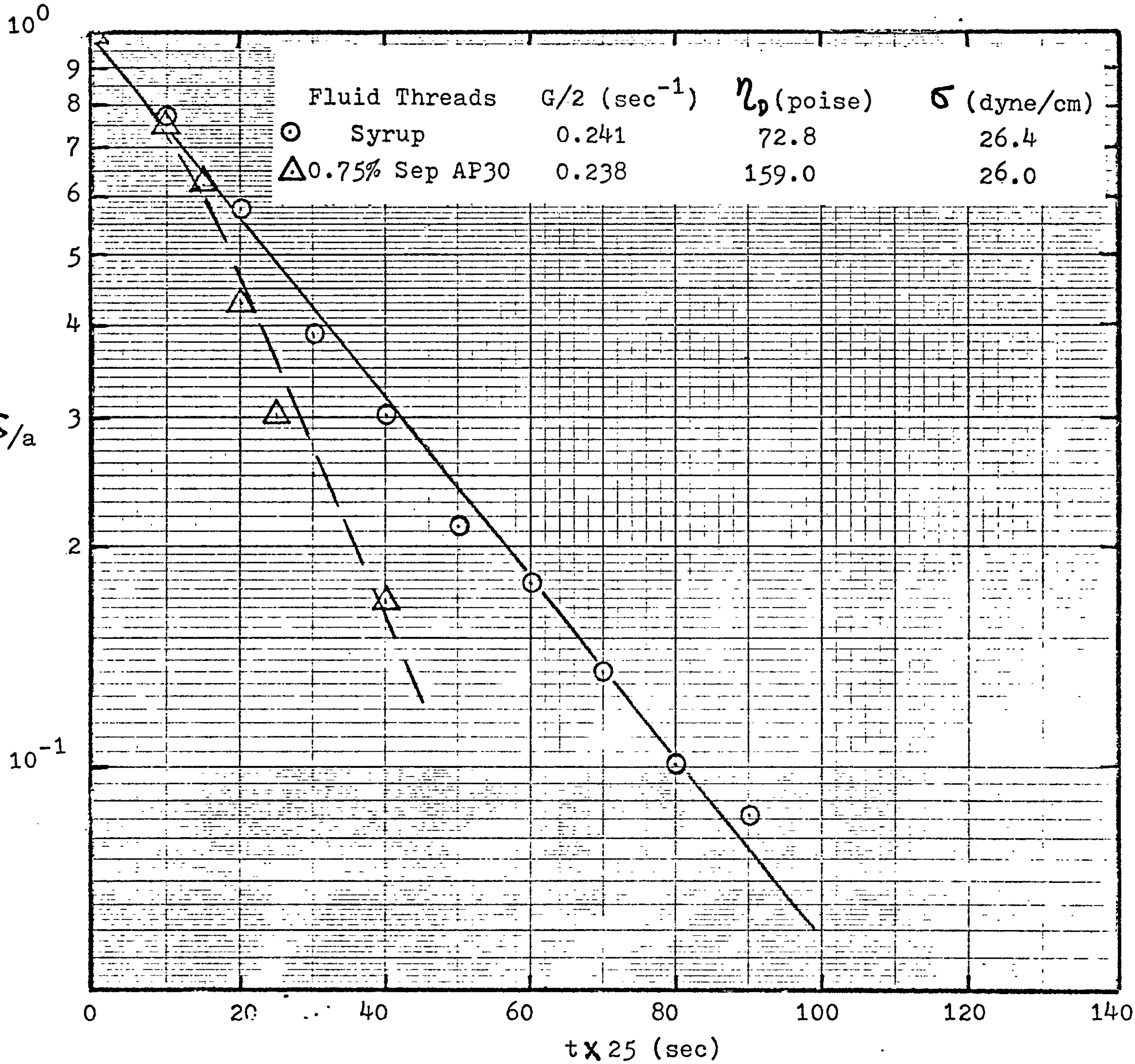


Figure 5-11 The Relative Amplitude, $\delta/a(t)$, vs. Time for Extending Threads

# CHPATER 6

## CONCLUSIONS

The drop deformation and breakup as well as the instability of liquid threads (both Newtonian and viscoelastic fluids) have been studied experimentally in this thesis. Here, we summarize the main conclusions in this work as follows:

I. The second order theory developed by Chaffey and Brenner does not seem to provide a better approximation than the first order theory of Taylor in predicting the drop deformation in Newtonian systems. Taylor's theory (Eq. (2-10)) works fairly well as $D = (L-B)/(L+B)$ goes up to about 0.2 for $\lambda (= \eta_D/\eta_C) = 3.42$ and about 0.35 for $\lambda = 0.006$. Where L and B are the major and minor axes of the deformed drop, and $\eta_D$ and $\eta_C$ are the dispersed phase and the continuous phase viscosities. Barthes and Acrivos' theory is quite good when $\lambda \geq 0.7$, but fails to describe the deformation for systems with small $\lambda$. The drop breakup occurs approximately when $D = 0.35 \sim 0.55$ for $\lambda$ changing from 0.0189 to 3.42, and about $0.6 \sim 0.7$ for $\lambda = 0.006$. Therefore, the value $D_C = 0.5$ which was estimated by Taylor is approximately correct.

II. The range of viscosity ratio within which the drop breakup can occur in a plane hyperbolic flow field is wider than that in a simple shear flow field. The system with $\lambda$ between about 1 and 2 seems to be the most favorable system for dispersion processes. The ratio of $E_C = \bar{G}_C a \eta_C/\sigma$ (where

$\bar{G}_C$ is the rate of strain at burst, a is the drop radius, and $\sigma$ is the interfacial tension) obtained here to that in a simple shear flow field is only about 1/3 at $\lambda = 1$, and becomes even smaller as the viscosity ratio takes values different from 1. Thus, for the same value of $\bar{G}$, the plane hyperbolic flow field seems to be more effective in drop breakup and dispersion than the simple shear flow field.

III. In the case of viscoelastic drops, $E_C$ increases with Deborah number up to about 10, and then goes gradually into an asymptotic constant value as De increases further.

IV. The applicable range of four limiting equations derived from Tomotika's general theory for stationary liquid threads have been obtained and expressed in terms of appropriate dimensionless groups, i.e., density ratio, viscosity ratio, $Oh_c = (d_{TH} \rho_C \sigma)^{\frac{1}{2}} / \eta_C$, and $Oh_D = (d_{TH} \rho_D \sigma)^{\frac{1}{2}} / \eta_D$, where $d_{TH}$ is the thread diameter. These bounds have been shown to provide more general criteria for the applicability of the limiting equations of Rayleigh and Tomotika.

V. The experimental critical wavenumbers, $X^* = \pi d_{TH} / \lambda_w$ (where $\lambda_w$ is the wave length), for Newtonian threads are found to agree fairly well with Tomotika's linearized stability theory for a stationary liquid thread, and those for viscoelastic stationary threads deviate from the Newtonian systems in a way which seems to confirm qualitatively Lee's theory, that is, $(X^*)_{VE} < (X^*)_N$ when $\lambda < 1$ and $(X^*)_{VE} > (X^*)_N$ when $\lambda > 1$.

VI. An extensional base flow has a stabilizing effect on the instability of an extending liquid thread, therefore threads of very small diameter can be maintained before the final breakup occurs. The system with low viscosity ratio is more unstable than a system with higher viscosity ratio.

VII. The value of $E_{DPC} = Cd_{DP}\eta_C/\sigma$ (where $d_{DP}$ is the broken drop diameter) in viscoelastic threads is again found to increase almost linearly with Deborah number and the slope depends on the viscosity ratio, $\eta_{oD}/\eta_C$; the smaller the viscosity ratio, the steeper the slope. The ratio of $(E_{DPC})_{VE}/(E_{DPC})_N$ is always greater than 1 for systems with the same viscosity ratio, that is, an extending viscoelastic thread will result in larger broken droplets than an extending Newtonian thread.

VIII. Measurements on the relative varicosity amplitude, $\delta/a$, at various times before breakup indicate that the viscoelastic thread (both stationary and extending) is more unstable than the Newtonian thread with the same viscosity ratio, interfacial properties, and kinematic conditions.

# BIBLIOGRAPHY


1. Bartok, W. and S. G. Mason, J. Colloid Sci., 13, 293 (1958)
2. Bartok, W. and S. G. Mason, ibid, 14, 13 (1959)
3. Bird, R. B. and P. J. Carreau, Chem. Eng. Sci., 23, 427 (1968)
4. Carreau, P. J., I. F. Macdonald, R. B. Bird, Chem. Eng. Sci., 23, 901 (1968)
5. Chaffey, C. E. and H. Brenner, J. Colloid Interface Sci., 24, 258 (1967)
6. Christiansen, R. M., A. N. Hixson, Ind. Eng. Chem., 49, 1017 (1957)
7. Cox, R. G., J. Fluid Mech., 37, 601 (1969)
8. Barthes, B. D. and A. Acrivos, 1972 (to appear)
9. Eirich, F. R., "Rheology, Theory and Applications", Volume 2 & 4, Academic Press, N. Y. and London
10. Flumerfelt, R. W., I. E. C. Fund., 11, 312 (1972)
11. Fordam, S., Proc. Roy. Soc. (London), A194, 1 (1948)
12. Frankel, N. A. and A. Acrivos, J. Fluid Mech., 44, 65 (1970)
13. Fredricksen, A. G., "Principle and Applications of Rheology" Prentice-Hall, New Jersey, (1964)
14. Goldin, M, J., Yerushalmi, R. Pfeffer, R. Shinnar, J. Fluid Mech., 38, 689 (1969)
15. Grace, H. P., 3rd Engineering Foun. Research Conference on Mixing, Andover, N. H., Aug. 1971
16. Grant, R. P., S. Middleman, A.I.Che.E. J., 12, 669 (1966)
17. Hinze, J. O., A.I.Che.E. J., 1, 289 (1955)
18. Karam, H. J., J. C. Bellinger, I. E. C. Fund., 7, 576 (1968)
19. Krosser, F. W. and S. Middleman, A.I.Che.E. J., 15, 383 (1969)
20. Lee, W. K., Ph. D. Dissertation, University of Houston, (1972)
21. Meister, B. J., G. F. Scheele, A.I.Che.E. J., 13, 682 (1967)
22. Middleman, S., Chem. Eng. Sci., 20, 1037 (1965)

23. Plateau, M., "Statique des liquides", Gauthier-Villars, Paris (1873)

24. Rayleigh, Lord, Proc. London Math. Soc., 10, 4 (1879)

25. Rayleigh, Lord, Proc. Roy. Soc. (London), 29, 71 (1879)

26. Rayleigh, Lord, Phil. Mag., 34, 145 (1892)

27. Rayleigh, Lord, ibid, 34, 177 (1892)

28. Rumscheidt, F. D., and S. G. Mason, J. Colloid Sci., 16, 210, 238 (1961)

29. Spriggs, T. W., Chem. Eng. Sci., 20, 931 (1965)

30. Stauffer, C. E., J. Phys. Chem., 69, 1933 (1965)

31. Sutterby, J. L., Trans. Soc. Rheo., 17, 559 (1973)

32. Tavgaç, Tunç , Ph. D. Dissertation, University of Houston, (1972)

33. Taylor, G. I., Proc. Roy. Soc. (London), A138, 41 (1932)

34. Taylor, G. I., ibid, A146, 501 (1934)

35. Tomotika, S., Proc. Roy. Soc. (London) A150, 322 (1935)

36. Tomotika, S., ibid, A153, 302 (1936)

37. Torza S., R. G. Cox, S. G. Mason, J. Colloid Interface Sci., 38, 395 (1972)

38. Turner, B. M. and Chaffey, C. E., Trans. Soc. Rheo., 13, 411 (1969)

39. Weber, C., Z.A.M.M., 11, 136 (1931)

NOMENCLATURE

| | |
|---|---|
| $a$ | radius of the undeformed liquid drop |
| $a_i$, $b_i$, and $c_i$ | coefficients defined in Appendix I |
| $B$ | length of minor axis of a deformed drop |
| $C$ | extension rate in plane hyperbolic flow field |
| $D$ | apparent deformation (= $(L-B)/(L+B)$) |
| $D_I$ | deformation parameter defined in Eq. (2-10) |
| $\bar{D}$ $D_{1111}$ | defined in Eq. (2-14) |
| $\mathcal{D}$ | differential operator defoned in Equation (5-2-2) |
| De | Deborah number (= $C\lambda_1$ or $\bar{G}\lambda_1/2$) |
| $d_{DP}$ | diameter of the broken droplets from extending (or stationary) liquid threads |
| $d_{TH}$ | critical diameter of extending liquids threads, or diameter of stationary liquid threads |
| $E$ , $E'$ | dimensionless group defined as $\bar{G} a \eta_c/\sigma$ ($E' = E/2$) |
| $E_{DP}$ | dimensionless breakup group for extending threads $(C d_{DP} \eta_c/\sigma)$ |
| $E_{TH}$ | dimensionless breakup group for extending threads $(C d_{TH} \eta_c/\sigma)$ |
| $F_1$, $F_2$, $F_3$, $F_4$ | Functions defined in Equation (5-2-9) |
| $F_{11}$, $F_{22}$ | tensors defined in Equation (2-13) |
| $F_{1111}$ $F_{2222}$ | tensors defined in Equation (2-13) |
| $\bar{G}$ | strain rate |
| $\bar{G}_C$ | critical strain rate for drop breakup |
| $G$ | density ratio $(\rho_D/\rho_c)$ |

$g^{ij}, g_{ij}$ contravariant and covariant components of the metric tensor

$H', H$ functions defined in Equation (2-11)

$G_1, G_2, G_3, G_4$ functions defined in Equation (5-3-3)

$I_p(x)$, $K_p(x)$ modified Bessel functions of order p with argument x

$I'_p, I''_p, K'_p, K''_p$ derivatives of $I_p(x)$ and $K_p(x)$ with respect to x

$\bar{I}_p$ $= I_p(X_D)$

$i$ $= (-1)^{\frac{1}{2}}$

$II(t)$ second invariant of the rate of strain tensor

$\bar{K}_p$ $= K_p(X_C)$

$k$ wave number

$L$ lengths of the major axis of a deformed drop

$\ell$ $= (k^2 + \alpha/\gamma_D)^{\frac{1}{2}}$

$m$ $= (k^2 + \alpha/\gamma_C)^{\frac{1}{2}}$

$\vec{m}$ memory function defined in Equation (2-17)

Oh Ohnesorge number $(a \rho \sigma)^{\frac{1}{2}}/\eta$

$P'_{rr}, P_{rr}$ normal stresses in the dispersed and continuous phases

$\Delta P_N$ pressure differences generated by normal stresses

$R_1, R_2$ principal radii of curvature

$(R, \theta, Z)$ cylindrical coordinates

Re( ) real part of ( )

| | |
|---|---|
| $S$ | dimensionless growth rate ( $= \alpha\theta$ ) |
| $\bar{S}$ | function defined in Equation (2-14) |
| $T$ | Deborah Group, $\frac{\lambda_1 \sigma}{a \eta_{o}}$ , for viscoelastic drops (or $\frac{\lambda_1 \sigma}{d_{TH} \eta_{oD}}$ for stationary threads) |
| $t'$, $t$ | time, present time |
| $u$ | velocity in X-direction |
| $U$ | viscosity ratio |
| $v$ | velocity in Y-direction |
| $w$ | velocity in Z-direction |
| $x_i$, $x_i'$ | material coordinate of fluid element at time t and t' |
| $X$, $X^*$ | wavenumber and critical wavenumber |
| $X_D$, $X_C$ | modified wavenumber defined in (5-2-9) |
| $(X,Y,Z)$ | the cartesian coordinates |

SUBSCRIPTS

| | |
|---|---|
| C | quantities in the continuous phase |
| D | quantities in the dispersed phase |
| I | inertial effect |
| V | viscous effect |

GREEKS

| | |
|---|---|
| $\alpha$ | dimensional growth rate |
| $\alpha_1, \alpha_2$ | slope parameters in Bird-Carreau Model |
| $\dot{\gamma}$ | shear rate |
| $\delta$ | amplitude of interfacial varicosity |

| | |
|---|---|
| $\eta$ | viscosity |
| $\eta_o$ | zero shear viscosity |
| $\theta$ | characteristic time defined in Table 5-1 |
| $\lambda$ | viscosity ratio (equivalent to U) |
| $\lambda_1, \lambda_2$ | characteristic time in B-C model |
| $\lambda_{1p}, \lambda_{2p}$ | characteristic time defined in Equation (2-20) |
| $\nu$ | kinematic viscosity |
| $\pi$ | dimensionless groups in Table 5-1 |
| $\rho$ | density |
| $\sigma$ | interfacial tension |
| $\tau_{ij}$ | shear stress |
| $\phi, \phi'$ | polar angle in X-Y, X'-Y' coordinate system |
| $\psi$ | stream function |
| $\Gamma_{ij}, \bar{\Gamma}_{ij}$ | strain tensor defined in Equations (2-18) and (2-19) |
| $\epsilon$ | a small parameter represent the magnitude order of drop deformation |
| $\xi$ | twice the ratio $(\tau_{22}-\tau_{33})/(\tau_{11}-\tau_{22})$ in steady simple shear flow |

## Appendix I

The coefficients $a_i$, $b_i$, and $c_i$ in Equations (2-14) and (2-15) are all rational functions of $\lambda$ which, as shown by Barthes-Biesel (1972), are given by

$$a_0=\frac{5}{3(2\lambda+3)}$$

$$a_1=\frac{-40(\lambda+1)}{(2\lambda+3)(19\lambda+16)}$$

$$a_2=\frac{10(4\lambda-9)}{7(2\lambda+3)^2}$$

$$a_3=\frac{288(137\lambda^3+624\lambda^2+741\lambda+248)}{7(2\lambda+3)^2(19\lambda+16)}$$

$$a_4=\frac{-2(11172\lambda^4+18336\lambda^3+17440\lambda^2+3499\lambda-7572)}{49(2\lambda+3)^3(19\lambda+16)}$$

$$a_5=\frac{-2(\lambda-1)(22344\lambda^3+52768\lambda^2+45532\lambda+19356)}{49(2\lambda+3)^3(19\lambda+16)}$$

$$a_6=\frac{-48P(\lambda)}{49(2\lambda+3)^3(19\lambda+16)^3(10\lambda+11)(17\lambda+16)}$$

$$a_7=\frac{48(\lambda-1)(2793\lambda^3+7961\lambda^2+8474\lambda+3522)}{49(2\lambda+3)^3(19\lambda+16)}$$

$$a_8=\frac{-400(43\lambda^2+79\lambda+53)}{3(2\lambda+3)^2(19\lambda+16)}$$

$$a_9=\frac{80Q(\lambda)}{(2\lambda+3)^2(19\lambda+16)^2(10\lambda+11)(17\lambda+16)}$$

where

$$P(\lambda)=2127976\lambda^7-16341920\lambda^6-38494964\lambda^5+122942551\lambda^4$$
$$+474068311\lambda^3+591515680\lambda^2+332123136\lambda+71700480,$$

$$Q(\lambda)= 405260\,\lambda^5+2366960\,\lambda^4+9142173\,\lambda^3+8595967\,\lambda^2+3334160\,\lambda$$
$$+693760,$$

$$b_o=\frac{-360(\lambda+1)}{(17\lambda+16)(10\lambda+11)},$$

$$b_1=\frac{1}{7(2\lambda+3)},$$

$$b_2=\frac{16(-14\lambda^3+207\lambda^2+431\lambda+192)}{21(2\lambda+3)(19\lambda+16)(17\lambda+16)(10\lambda+11)},$$

and

$$c_1= a_4-\frac{39}{35}\frac{a_8b_2}{b_o}-\frac{3}{14}\frac{a_9b_1}{b_o},$$

$$c_2= -\frac{3}{70}\frac{a_8b_1}{b_o},$$

$$c_3= a_6-\frac{54}{35}\frac{a_9b_2}{b_o},$$

$$c_4= a_5-3\frac{a_8b_2}{b_o}-\frac{3}{70}\frac{a_9b_1}{b_o},$$

$$c_5= -\frac{3}{14}\frac{a_8b_1}{b_o},$$

$$c_6= a_7+\frac{36}{7}\frac{a_8b_2}{b_o}-\frac{18}{7}\frac{a_9b_1}{b_o},$$

$$c_7= -\frac{18}{7}\frac{a_8b_1}{b_0}.$$

# APPENDIX II

# EXPERIMENTAL DATA

## A. Deformation Data

### A-1. Newtonian drops in Newtonian Continuous Phase

Fluid System 2 ($\lambda$=3.42)

| Drop Diameter (cm) | $\bar{G}a\eta_c$ (cm/dyne) | Deformation |
|---|---|---|
| 0.1045 | 4.813 | 0.162 |
| 0.770 | 3.674 | 0.113 |
| 0.0576 | 2.771 | 0.092 |
| 0.0665 | 3.186 | 0.108 |
| 0.0720 | 3.463 | 0.116 |
| 0.1176 | 5.703 | 0.217 |
| 0.0940 | 4.633 | 0.148 |
| 0.0924 | 4.409 | 0.1422 |
| 0.1117 | 5.373 | 0.179 |
| 0.0758 | 3.724 | 0.128 |
| 0.1103 | 5.392 | 0.181 |
| 0.1270 | 6.204 | 0.227 |
| 0.1150 | 5.768 | 0.207 |
| 0.1469 | 7.363 | 0.277 |
| 0.1345 | 6.798 | 0.236 |
| 0.1533 | 7.882 | 0.138 |
| 0.1363 | 6.948 | 0.262 |
| 0.0919 | 4.685 | 0.1621 |

Fluid System 4 ($\lambda$= 0.707)

| Drop Diameter (cm) | $\bar{G}a\eta_c$ (cm/dyne) | Deformation |
|---|---|---|
| 0.0822 | 4.069 | 0.132 |
| 0.1104 | 5.397 | 0.194 |
| 0.1154 | 5.688 | 0.198 |
| 0.0718 | 3.584 | 0.116 |
| 0.0782 | 3.871 | 0.127 |

Fluid System 4 ($\lambda = 0.707$)

| Drop Diameter (cm) | $\bar{G}a\eta_c$ (cm/dyne) | Deformation |
|---|---|---|
| 0.0645 | 3.179 | 0.100 |
| 0.0510 | 2.567 | 0.082 |
| 0.0960 | 4.822 | 0.161 |
| 0.1059 | 5.422 | 0.185 |
| 0.1294 | 6.7111 | 0.263 |
| 0.1038 | 5.159 | 0.174 |
| 0.1330 | 6.828 | 0.270 |
| 0.1460 | 7.256 | 0.280 |
| 0.1530 | 7.573 | 0.282 |
| 0.1320 | 6.680 | 0.244 |

Fluid System 7 ($\lambda = 0.085$)

| Drop Diameter (cm) | $\bar{G}a\eta_c$ (cm/dyne) | Deformation |
|---|---|---|
| 0.1568 | 8.350 | 0.281 |
| 0.1056 | 5.476 | 0.177 |
| 0.0879 | 4.639 | 0.139 |
| 0.0781 | 3.787 | 0.117 |
| 0.0635 | 3.293 | 0.103 |
| 0.0635 | 3.293 | 0.103 |
| 0.0599 | 2.880 | 0.086 |
| 0.1016 | 5.109 | 0.160 |
| 0.1045 | 5.345 | 0.166 |
| 0.1070 | 5.602 | 0.180 |
| 0.1346 | 6.951 | 0.226 |
| 0.1684 | 8.734 | 0.311 |
| 0.0611 | 3.225 | 0.101 |
| 0.1394 | 7.457 | 0.247 |
| 0.1273 | 6.720 | 0.211 |
| 0.1052 | 5.456 | 0.1672 |
| 0.1562 | 8.318 | 0.295 |
| 0.1382 | 7.850 | 0.248 |
| 0.1344 | 7.937 | 0.256 |
| 0.1900 | 9.604 | 0.386 |

Fluid System 8 ($\lambda$= 0.033)

| Drop Diameter (cm) | $\overline{Ga}\eta_c$ (cm/dyne) | Deformation |
|---|---|---|
| 0.1757 | 8.451 | 0.2760 |
| 0.1007 | 4.824 | 0.160 |
| 0.0705 | 3.460 | 0.109 |
| 0.0841 | 4.145 | 0.131 |
| 0.0841 | 4.215 | 0.134 |
| 0.0477 | 2.422 | 0.082 |
| 0.0821 | 4.064 | 0.123 |
| 0.0782 | 3.919 | 0.123 |
| 0.0568 | 2.823 | 0.093 |
| 0.0560 | 2.783 | 0.093 |
| 0.1010 | 4.938 | 0.153 |
| 0.1283 | 6.3241 | 0.198 |
| 0.1690 | 8.330 | 0.285 |
| 0.1500 | 7.333 | 0.239 |
| 0.1233 | 6.028 | 0.185 |
| 0.1386 | 6.860 | 0.216 |
| 0.1025 | 5.032 | 0.156 |

Fluid System 10($\lambda$= 0.018)

| Drop Diameter (cm) | $\overline{Ga}\eta_c$ (cm/dyne) | Deformation |
|---|---|---|
| 0.1071 | 5.413 | 0.194 |
| 0.0705 | 3.635 | 0.124 |
| 0.0950 | 4.822 | 0.169 |
| 0.0658 | 3.354 | 0.123 |
| 0.0458 | 2.335 | 0.089 |
| 0.1087 | 5.560 | 0.206 |
| 0.1266 | 6.566 | 0.253 |
| 0.1429 | 7.073 | 0.264 |
| 0.1248 | 6.329 | 0.222 |
| 0.1375 | 7.009 | 0.257 |
| 0.1428 | 7.248 | 0.274 |
| 0.0609 | 3.105 | 0.099 |
| 0.2063 | 10.737 | 0.438 |
| 0.1584 | 8.144 | 0.306 |
| 0.0930 | 4.757 | 0.164 |

Fluid System 11 ($\lambda = 0.006$)

| Drop Diameter (cm) | $\overline{G}a\eta_c$ (cm/dyne) | Deformation |
|---|---|---|
| 0.0779 | 4.005 | 0.151 |
| 0.0918 | 4.563 | 0.159 |
| 0.1195 | 5.939 | 0.212 |
| 0.1168 | 5.781 | 0.211 |
| 0.1329 | 6.984 | 0.277 |
| 0.1524 | 7.769 | 0.311 |
| 0.1425 | 7.172 | 0.275 |
| 0.1404 | 7.127 | 0.278 |
| 0.0503 | 2.573 | 0.105 |
| 0.1760 | 9.088 | 0.371 |
| 0.1243 | 6.589 | 0.257 |
| 0.1195 | 6.040 | 0.237 |
| 0.0871 | 4.478 | 0.178 |
| 0.1482 | 7.587 | 0.311 |
| 0.1625 | 8.178 | 0.333 |
| 0.2350 | 11.632 | 0.499 |
| 0.0450 | 2.255 | 0.093 |

A-2. Viscoelastic Drops in Newtonian Continuous Phase

Continuous Phase: Silicone Oil, $\eta_c$ = 300 poise

Drop Phase: 0.75% Sep Ap 30 Solution

$T = \frac{\sigma \lambda_1}{a \eta_c} = 13.45$

| $\bar{G}/2$ (sec$^{-1}$) | Deformation |
|---|---|
| 0.0296 | 0.060 |
| 0.0388 | 0.083 |
| 0.0505 | 0.112 |
| 0.0623 | 0.148 |
| 0.0741 | 0.184 |
| 0.0834 | 0.218 |
| 0.0952 | 0.263 |
| 0.1047 | 0.315 |
| 0.1165 | 0.434 |

$T = \frac{\sigma \lambda_1}{a \eta_c} = 6.95$

| $\bar{G}/2$ (sec$^{-1}$) | Deformation |
|---|---|
| 0.0180 | 0.075 |
| 0.0249 | 0.107 |
| 0.0320 | 0.144 |
| 0.0367 | 0.175 |
| 0.0437 | 0.221 |
| 0.0505 | 0.280 |
| 0.0531 | 0.319 |
| 0.0555 | 0.377 |
| 0.0581 | 0.543 |

Drop Phase: 1.0% Sep AP 30 Solution

$T = \frac{\sigma \lambda_1}{a \eta_c} = 30.48$

| $\bar{G}/2$ (sec$^{-1}$) | Deformation |
|---|---|
| 0.0320 | 0.061 |
| 0.0390 | 0.076 |
| 0.0507 | 0.105 |
| 0.0603 | 0.128 |
| 0.0721 | 0.163 |
| 0.0836 | 0.201 |
| 0.0906 | 0.219 |
| 0.0976 | 0.251 |
| 0.1139 | 0.329 |
| 0.1266 | 0.412 |

$T = \frac{\sigma \lambda_1}{a \eta_c} = 12.37$

| $\bar{G}/2$ (sec$^{-1}$) | Deformation |
|---|---|
| 0.0178 | 0.089 |
| 0.0249 | 0.127 |
| 0.0294 | 0.161 |
| 0.0341 | 0.191 |
| 0.0387 | 0.221 |
| 0.0434 | 0.258 |
| 0.0506 | 0.341 |
| 0.0550 | 0.505 |

Continuous Phase: Silicone Oil, $\eta_c$ = 300 poise

Drop Phase: 2.0% Sep AP 30 Solution ($\lambda$= 11.2)

| $T = \frac{\sigma \lambda_1}{a \eta_c} = 52.50$ | | $T = \frac{\sigma \lambda_1}{a \eta_c} = 23.86$ | |
|---|---|---|---|
| $\bar{G}/2$ ($sec^{-1}$) | Deformation | $\bar{G}/2$ ($sec^{-1}$) | Deformation |
| 0.0298 | 0.064 | 0.0152 | 0.083 |
| 0.0391 | 0.087 | 0.0199 | 0.111 |
| 0.0506 | 0.114 | 0.0247 | 0.143 |
| 0.0646 | 0.153 | 0.0295 | 0.171 |
| 0.0789 | 0.188 | 0.0342 | 0.205 |
| 0.0905 | 0.234 | 0.0413 | 0.263 |
| 0.1005 | 0.276 | 0.0504 | 0.367 |
| 0.1096 | 0.307 | 0.0553 | 0.455 |
| 0.1189 | 0.401 | | |

B. Drop Breakup Data

B-1. Newtonian Drops in Newtonian Continuous Phase

| Fluid System 2 ($\lambda$= 3.42) | | Fluid System 1 ($\lambda$=27.46) | |
|---|---|---|---|
| Drop Diameter(cm) | $E_C$ | Drop Diameter(cm) | $E_C$ |
| 0.1090 | 0.2505 | 0.1421 | 0.2676 |
| 0.1263 | 0.2459 | 0.1249 | 0.2728 |
| 0.1371 | 0.2363 | 0.1181 | 0.2650 |
| 0.1230 | 0.2355 | 0.1005 | 0.2573 |
| 0.1222 | 0.2366 | 0.0997 | 0.2593 |
| 0.1455 | 0.2411 | 0.1210 | 0.2542 |

Fluid System 3 ($\lambda$=2.25)

| Drop Diameter (cm) | $E_C$ |
|---|---|
| 0.0742 | 0.2204 |
| 0.1091 | 0.2265 |
| 0.1432 | 0.2384 |
| 0.1287 | 0.2365 |
| 0.1267 | 0.2484 |
| 0.1315 | 0.2320 |
| 0.1305 | 0.2374 |
| 0.1109 | 0.2249 |
| 0.1125 | 0.2308 |

Fluid System 4 ($\lambda$= 0.707)

| Drop Diameter (cm) | $E_C$ |
|---|---|
| 0.1479 | 0.2627 |
| 0.1584 | 0.2535 |
| 0.1368 | 0.2464 |
| 0.1318 | 0.2423 |
| 0.1231 | 0.2434 |
| 0.1177 | 0.2528 |

Fluid System 5 ($\lambda$= 0.413)

| Drop Diameter (cm) | $E_C$ |
|---|---|
| 0.1484 | 0.2341 |
| 0.1412 | 0.2406 |
| 0.1468 | 0.2371 |
| 0.1665 | 0.2478 |
| 0.1249 | 0.2323 |
| 0.1245 | 0.2331 |
| 0.1362 | 0.2351 |
| 0.1428 | 0.2351 |

Fluid System 6 ($\lambda$= 0.298)

| Drop Diameter (cm) | $E_C$ |
|---|---|
| 0.1633 | 0.2579 |
| 0.1507 | 0.2430 |
| 0.1674 | 0.2409 |
| 0.1605 | 0.2417 |
| 0.1492 | 0.2416 |
| 0.1835 | 0.2506 |
| 0.1261 | 0.2369 |
| 0.1167 | 0.2334 |

Fluid System 7 ($\lambda$= 0.085)

| Drop Diameter (cm) | $E_C$ |
|---|---|
| 0.1475 | 0.3390 |
| 0.1407 | 0.3275 |
| 0.1545 | 0.3216 |
| 0.1528 | 0.3237 |
| 0.1504 | 0.3268 |
| 0.1238 | 0.3174 |

Fluid System 8 ($\lambda$= 0.033)

| Drop Diameter (cm) | $E_C$ |
|---|---|
| 0.1726 | 0.3631 |
| 0.1750 | 0.3689 |
| 0.1642 | 0.3687 |
| 0.1471 | 0.3673 |
| 0.1387 | 0.3578 |
| 0.1723 | 0.3490 |

Fluid System 9 ($\lambda = 0.025$)

| Drop Diameter (cm) | $E_C$ |
|---|---|
| 0.1475 | 0.4409 |
| 0.1714 | 0.4269 |
| 0.1180 | 0.4378 |
| 0.1570 | 0.4380 |
| 0.1790 | 0.4255 |
| 0.1462 | 0.4470 |
| 0.1912 | 0.4304 |
| 0.1731 | 0.3958 |

Fluid System 10 ($\lambda = 0.018$)

| Drop Diameter (cm) | $E_C$ |
|---|---|
| 0.1621 | 0.4384 |
| 0.1529 | 0.4490 |
| 0.1401 | 0.4404 |
| 0.1804 | 0.4326 |
| 0.1600 | 0.4568 |
| 0.1301 | 0.4547 |

Fluid System 11 ($\lambda = 0.006$)

| Drop Diameter (cm) | $E_C$ |
|---|---|
| 0.1502 | 0.4884 |
| 0.1317 | 0.4833 |
| 0.2152 | 0.4909 |
| 0.1286 | 0.5036 |
| 0.1540 | 0.4985 |
| 0.1413 | 0.4918 |

B-2. Viscoelastic Drops in Newtonian Continuous Phase

Continuous Phase: Silicone Oil, $\eta_c$ = 300 poise

Drop Phase: 0.75% Sep AP 30 Solution ($\lambda = 0.53$)

| Drop Diameter (cm) | $\bar{G}_c/2$ ($sec^{-1}$) |
|---|---|
| 0.2439 | 0.0669 |
| 0.1746 | 0.0956 |
| 0.1260 | 0.1343 |
| 0.1200 | 0.1412 |
| 0.0702 | 0.2454 |
| 0.0540 | 0.3194 |
| 0.0935 | 0.1874 |
| 0.0457 | 0.3829 |
| 0.1350 | 0.1283 |
| 0.0742 | 0.2278 |
| 0.0576 | 0.3024 |
| 0.1937 | 0.0886 |
| 0.1380 | 0.1226 |
| 0.2770 | 0.0594 |

Drop Phase: 1.0% Sep Ap 30 Solution ($\lambda$= 1.27)

| Drop Diameter (cm) | $\overline{G}_C/2$ ($sec^{-1}$) |
|---|---|
| 0.2270 | 0.0675 |
| 0.1904 | 0.0794 |
| 0.1310 | 0.1217 |
| 0.0878 | 0.1825 |
| 0.0532 | 0.3154 |
| 0.0425 | 0.3979 |
| 0.1000 | 0.1596 |
| 0.0890 | 0.1813 |
| 0.0650 | 0.2512 |
| 0.0450 | 0.3744 |
| 0.1140 | 0.1441 |
| 0.2470 | 0.0633 |
| 0.2828 | 0.0550 |
| 0.1148 | 0.1397 |

Drop Phase: 1.5% Sep AP 30 Solution ($\lambda$= 3.4)

| Drop Diameter (cm) | $\overline{G}_C/2$ ($sec^{-1}$) |
|---|---|
| 0.2360 | 0.0676 |
| 0.2844 | 0.0550 |
| 0.1574 | 0.0974 |
| 0.2196 | 0.0755 |
| 0.0942 | 0.1704 |
| 0.0832 | 0.2166 |
| 0.0449 | 0.4031 |
| 0.0930 | 0.1898 |
| 0.0656 | 0.2799 |
| 0.0900 | 0.1816 |
| 0.2916 | 0.0556 |
| 0.0600 | 0.2950 |
| 0.0470 | 0.3773 |
| 0.0496 | 0.3578 |
| 0.0634 | 0.2872 |
| 0.1354 | 0.1280 |
| 0.0500 | 0.3400 |

Drop Phase: 2.0% Sep AP 30 Solution ($\lambda$= 11.2)

| Drop Diameter (cm) | $\overline{G}_C/2$ ($sec^{-1}$) |
|---|---|
| 0.1430 | 0.1120 |
| 0.8740 | 0.1984 |
| 0.2894 | 0.0523 |
| 0.1224 | 0.1346 |
| 0.3522 | 0.0426 |
| 0.0820 | 0.2054 |
| 0.0404 | 0.4352 |
| 0.0762 | 0.2235 |
| 0.0676 | 0.2580 |
| 0.0542 | 0.3184 |
| 0.0462 | 0.3787 |
| 0.1400 | 0.1183 |
| 0.1114 | 0.1485 |
| 0.2738 | 0.0574 |
| 0.2059 | 0.0794 |
| 0.1760 | 0.0956 |

## C. Breakup Data of Liquid Threads

### C-1. Stationary Liquid Threads

#### C-1-1. Newtonian Threads in Newtonian Continuous Phase

| Fluid System | $d_{TH}$ (cm) | $\lambda_W$ (cm) | $d_{DP}$ (cm) | $d_{DP}/d_{TH}$ |
|---|---|---|---|---|
| 12 | 0.0088 | 0.0600 | 0.0193 | 2.19 |
| " | 0.0208 | 0.1470 | 0.0430 | 2.06 |
| " | 0.0109 | 0.0810 | 0.0253 | 2.32 |
| " | 0.0092 | 0.0701 | 0.0215 | 2.34 |
| 13 | 0.0098 | 0.0608 | 0.0216 | 2.20 |
| " | 0.0079 | 0.0493 | 0.0178 | 2.26 |
| " | 0.0129 | 0.0721 | 0.0274 | 2.12 |
| 1" | 0.0244 | 0.1446 | 0.0515 | 2.11 |
| 14 | 0.0103 | 0.0580 | 0.0205 | 1.99 |
| " | 0.0109 | 0.0608 | 0.0217 | 1.99 |
| " | 0.0178 | 0.0962 | 0.0385 | 2.16 |
| 15 | 0.0125 | 0.0666 | 0.0245 | 1.96 |
| " | 0.0167 | 0.0903 | 0.0331 | 1.98 |
| " | 0.0118 | 0.0632 | 0.0238 | 2.02 |
| 16 | 0.0198 | 0.1089 | 0.0411 | 2.07 |
| " | 0.0138 | 0.0808 | 0.0276 | 2.00 |
| " | 0.0170 | 0.0966 | 0.0355 | 2.09 |
| 18 | 0.0171 | 0.1576 | 0.0408 | 2.38 |
| " | 0.0246 | 0.2169 | 0.0661 | 2.69 |
| " | 0.0127 | 0.1204 | 0.0307 | 2.41 |
| " | 0.0239 | 0.2051 | 0.0611 | 2.56 |

### C-1-2. Viscoelastic Threads in Newtonian Continuous Phase

Continuous Phase: Silicone Oil, $\eta_C$ = 300 poise

| % of Sep AP 30 | $d_{TH}$ (cm) | $X^*$ | $d_{DP}$ (cm) | $d_{DP}/d_{TH}$ |
|---|---|---|---|---|
| 0.75 | 0.0306 | 0.542 | 0.0624 | 2.04 |
| " | 0.0175 | 0.440 | 0.0371 | 2.13 |
| 1.0 | 0.0133 | 0.410 | 0.0284 | 2.13 |
| " | 0.0137 | 0.449 | 0.0322 | 2.35 |
| 1.5 | 0.0173 | 0.432 | 0.0367 | 2.12 |
| " | 0.0144 | 0.398 | 0.0321 | 2.23 |
| 2.0 | 0.0171 | 0.459 | 0.0361 | 2.11 |
| " | 0.0104 | 0.415 | 0.0226 | 2.17 |
| " | 0.0202 | 0.453 | 0.0425 | 2.20 |

## C-2. Breakup Data of Extending Liquid Threads

### C-2-1. Newtonian Threads in Newtonian Continuous Phase

| Fluid System | G/2 ($sec^{-1}$) | $d_{TH}$ (cm) | $X^*$ | $d_{DP}$(cm) | $d_{DP}/d_{TH}$ |
|---|---|---|---|---|---|
| 12 | 0.1983 | 0.0026 | 0.118 | 0.0061 | 2.34 |
| " | 0.2928 | 0.0013 | 0.148 | 0.0033 | 2.54 |
| " | 0.1432 | 0.0032 | 0.135 | 0.0070 | 2.19 |
| 13 | 0.2120 | 0.0036 | 0.224 | 0.0069 | 1.92 |
| " | 0.1640 | 0.0046 | 0.203 | 0.0083 | 1.80 |
| " | 0.2492 | 0.0042 | 0.194 | 0.0064 | 1.52 |
| 14 | 0.2262 | 0.0064 | 0.227 | 0.0138 | 2.15 |
| " | 0.2790 | 0.0025 | 0.183 | 0.0070 | 2.80 |
| 15 | 0.1958 | 0.0102 | 0.233 | 0.0214 | 2.49 |
| " | 0.2410 | 0.0075 | 0.366 | 0.0151 | 2.01 |
| " | 0.2668 | - | - | 0.0138 | - |
| 16 | 0.2830 | 0.0087 | 0.288 | 0.0183 | 2.10 |
| " | 0.2497 | 0.0079 | 0.296 | 0.0182 | 2.30 |
| " | 0.1640 | - | - | 0.0303 | - |
| 17 | 0.3604 | - | - | 0.0184 | - |
| " | 0.2668 | - | - | 0.0271 | - |
| " | 0.2668 | - | - | 0.0278 | - |
| 18 | 0.2311 | - | - | 0.0345 | - |
| " | 0.3178 | - | - | 0.0342 | - |
| " | 0.2115 | - | - | 0.0444 | - |

C-2-2. Viscoelastic Threads in Newtonian Continuous Phase

Continuous Phase: Silicone Oil, $\eta_C$ = 300 poise

| % of Sep AP 30 | $\bar{G}/2$ (sec$^{-1}$) | $d_{TH}$ (cm) | $X^*$ | $d_{DP}$ (cm) | $d_{DP}/d_{TH}$ |
|---|---|---|---|---|---|
| 0.75 | 0.2380 | 0.0114 | - | 0.0269 | 2.36 |
| " | 0.1620 | 0.0152 | 0.204 | 0.0363 | 2.38 |
| " | 0.4015 | 0.0076 | 0.224 | 0.0201 | 2.64 |
| " | 0.2888 | 0.0102 | 0.265 | 0.0221 | 2.16 |
| 1.5 | 0.1381 | 0.0125 | 0.182 | 0.0278 | 2.22 |
| " | 0.2208 | 0.0088 | 0.198 | 0.0190 | 2.16 |
| " | 0.3180 | 0.0069 | 0.186 | 0.0155 | 2.26 |
| " | 0.4145 | 0.0057 | 0.226 | 0.0138 | 2.42 |
| 2.0 | 0.1268 | 0.0073 | 0.2325 | 0.0172 | 2.35 |
| " | 0.2815 | 0.0050 | 0.1653 | 0.0114 | 2.28 |
| " | 0.1954 | 0.0072 | - | 0.0144 | 2.00 |
| " | 0.4015 | 0.0036 | 0.2304 | 0.0087 | 2.45 |

D. Experimental Data of The Apparatus Flow Field

Diameter of Rollers = 1.5"

$u = \bar{G}X/2, \quad v = -\bar{G}Y/2, \quad w = 0$

$$\bar{G}/2 = \ln(X_2/X_1)/(t_2-t_1) \quad (\text{sec}^{-1}) \qquad (D-1)$$

or

$$\bar{G}/2 = -\ln(Y_2/Y_1)/(t_2-t_1) \quad (\text{sec}^{-1}) \qquad (D-2)$$

| Roller Speed(RPM) | $\bar{G}/2$ from (D-1) | $\bar{G}/2$ from (D-2) |
|---|---|---|
| (Glycerine Solution) | | |
| 9.8 | 0.2556 | 0.2589 |
| 13.2 | 0.3211 | - |
| 14.1 | 0.3525 | 0.3625 |
| 15,7 | 0.3821 | - |
| 18.0 | 0.4402 | 0.4429 |
| 20.8 | 0.4926 | 0.5036 |
| 24.0 | 0.5530 | 0.5608 |
| 27.2 | 0.6079 | - |
| 2.4 | 0.0585 | - |
| 5.1 | 0.1351 | 0.1341 |
| 7.5 | 0.1798 | 0.1832 |
| (Silicone Oil) | | |
| 5.5 | 0.1442 | - |
| 8.9 | 0.2419 | - |
| 13.8 | 0.3839 | - |
| 14.7 | 0.4150 | - |
| 27.0 | 0.7348 | - |
| 34.5 | 0.9460 | - |
| 37.5 | 1.0803 | - |
| 43.6 | 1.2468 | - |
| 50.0 | 1.4430 | - |